DEVELOPMENT OF AUTONOMOUS AMPHIBIOUS VEHICLE MANEUVERING SYSTEM USING WHEEL-BASED GUIDED PROPULSION APPROACH

TEE YU HON

MASTER OF ENGINEERING SCIENCE

FACULTYOF ENGINEERING AND SCIENCE
UNIVERSITI TUNKU ABDUL RAHMAN
JULY 2013

DEVELOPMENT OF AUTONOMOUS AMPHIBIOUS VEHICLE MANEUVERING SYSTEM USING WHEEL-BASED GUIDED PROPULSION APPROACH

By

TEE YU HON

A dissertation submitted to the
Department of Mechatronics and BioMedical Engineering
Faculty of Engineering and Science
Universiti Tunku Abdul Rahman
in partial fulfillment of the requirements for the degree of
Master of Engineering Science
July 2013

ABSTRACT

DEVELOPMENT OF AUTONOMOUS AMPHIBIOUS VEHICLE MANEUVERING SYSTEM USING WHEEL-BASED GUIDED PROPULSION APPROACH

Tee Yu Hon

This research focuses on developing the appropriate locomotion mechanism for use in confined areas. CAD modeling and CFD simulation were conducted to improve the wheeled-vehicle efficiency in amphibious application. Centrifugal wheel pump, called the Centripellor, is employed as an active moving mechanism to generate a guided propulsive force to generate the motion characteristic of zero radius turn and proportional directional differential drive to facilitate both land and water maneuvering. iAAV-1 platform is developed as a test bed for autonomous experiments using developed FPGA hardware and Quartus II program as control system in order to analyze its motion performances based on kinematics and dynamics model. With Centripellor built on iAAV-1 as an auxiliary propulsion device, the developed prototype leads to a flexible single drive maneuvering control with an increase water speed of up to three times compared to an ordinary wheel-based propulsion.

ACKNOWLEDGEMENTS

I wish to express my sincerest appreciation to my supervisors, Dr. Tan Yong Chai and Dr. Than Cheok Fah for giving me the opportunity to do my post-graduate studies in UTAR. I would like to thank both for their guidance, advice and inspiration that helped sustained me through the years of my research work have been the greatest help in this research. I gratefully acknowledge Dr. Tan Ching Seong for providing me the research fund that enables me to pursue this research. He gave his outstanding and deep insight in technical support, great work and patience through the years in this research.

I thankfully acknowledge the cooperation with project partners: Teoh Chee Way and Peter Chan Kim Chon for their unlimited help during various stages of the research work. Special thanks to Thoo Wei Ning for her love, support and understanding throughout the research. My thanks also go to UTAR for providing the research funding and facilities which enabled me to carry out my research work. I also wish to thank my Workplace Mates for the great environment and joyful atmosphere while carrying out this research. Besides, I thank anyone who have been Associated with this project and made it a worthwhile experience. It is my pleasure to work with you all. Last, but certainly not least, the continual encouragement and support from my Family have been the most influential during the whole course of my education. I would like to dedicate this work to them, and with a heartfelt gratitude, I express my sincere "THANKS!"

FACULTY OF ENGINEERING AND SCIENCE

UNIVERSITI TUNKU ABDUL RAHMAN

Date: 12th July 2013

SUBMISSION OF DISSERTATION/THESIS

It is hereby certified that TEE YU HON (ID No: 09UEM09107) has completed this dissertation/ thesis entitled "DEVELOPMENT OF AUTONOMOUS AMPHIBIOUS VEHICLE MANEUVERING SYSTEM USING WHEEL-BASED GUIDED PROPULSION APPROACH" under the supervision of Dr. TAN YONG CHAI (Supervisor) from the Department of Mechatronics and BioMedical Engineering, Faculty of Engineering and Science, and Dr. THAN CHEOK FAH (Co-Supervisor) from the Department of Mechanical and Material Engineering, Faculty of Engineering and Science.

I understand that University will upload softcopy of my dissertation/ thesis in pdf format into UTAR Institutional Repository, which may be made accessible to UTAR community and public.

Yours truly,

_____

TEE YU HON

APPROVAL SHEET

This dissertation/thesis entitled "**DEVELOPMENT OF AUTONOMOUS AMPHIBIOUS VEHICLE MANEUVERING SYSTEM USING WHEEL-BASED GUIDED PROPULSION APPROACH"** was prepared by TEE YU HON and submitted as partial fulfillment of the requirements for the degree of Master of Engineering Science at Universiti Tunku Abdul Rahman.

Approved by:

_____

(Dr. TAN YONG CHAI) Date: 12th July 2013
Assistant Professor/Supervisor
Department of Mechatronics and BioMedical Engineering
Faculty of Engineering and Science
Universiti Tunku Abdul Rahman

_____

(Dr. THAN CHEOK FAH) Date: 12th July 2013
Associate Professor/Co-supervisor
Department of Mechanical and Material Engineering
Faculty of Engineering and Science
Universiti Tunku Abdul Rahman

DECLARATION

I hereby declare that the dissertation is based on my original work except for quotations and citations which have been duly acknowledged. I also declare that it has not been previously or concurrently submitted for any other degree at UTAR or other institutions.

Name : TEE YU HON

Date : 12th JULY 2013

TABLE OF CONTENTS

LIST OF TABLES

LIST OF FIGURES

LIST OF ABBREVIATIONS

A	Distance from left wheel to centerline
AATV	Amphibious All-Terrain Vehicle
AAV	Autonomous Amphibious Vehicle
ABS	Anti-lock Braking System
B	Distance from right wheel to centerline
BLDC	Brushless Direct-Current Motor
C	Axle to rear wheel pivot distance
CFD	Computational Fluid Dynamics
CG	Center of gravity
CT	Vehicle center of zero radius turning
D	Axle to center of gravity
d_L/d_R	Distance travelled for left wheel
DTSS	Deep Tunnel Sewerage System
EV	Electric Vehicle
f	Frequency
FPGA	Field Programmable Gate Array
G	Gear ratio
GPS	Global Positioning System
I	Current
J_L	Rotor inertia
LSV	Low-Speed Vehicle
M	Motor load
N_{wheel}	Number of wheels on vehicle
P	Power
PWM	Pulse-width Modulator
r_a	Left prime mover wheel radius
r_b	Right prime mover wheel radius
$r_c = r_d$	Left/Right steering wheel radius
RCS	Real-time Control System
R_{icc}	Instantaneous center of curvature radius
R_L/R_R	Instantaneous center of curvature left/right wheel radius
t	Time
T	Torque
T_L/T_R	Encoder tick counts for left/right wheel
T_{res}	Encoder resolution
V_v	Speed of vehicle
(V_x, V_y)	vehicle component velocities in y-axis and x-axis
W	Width of vehicle
$W_{vehicle}$	Vehicle weight
α	Acceleration
β_L/β_R	Left/Right rear wheel heading angle
ρ	Density
φ	Heading angle

$\dot{\varphi} = \dot{\theta}$	Turning rate
ω_L / ω_R	Rotation angle of left/right wheel
$\dot{\omega}_L / \dot{\omega}_R = v_L / v_R$	Left/Right wheel speed
$\hat{u}_x$	Amplitude
μ	Coefficient of friction
θ_L / θ_R	Instantaneous center of curvature angle left/right wheel
(x_o, y_o)	Instant center
(x_c, y_c)	Center position of vehicle

Chapter 4

A	Cross-section area
b	Blade height
h_i	Head rise
$\dot{m}$	Mass flow rate
P	Power generated/transferred
Q	Volumetric flow rate
r	Impeller radius
T	Thrust generated
U	Tangential blade velocity
v	Fluid velocity at cross-section area
V	Absolute blade velocity
V_r	Relative absolute velocity
V_θ	Tangential absolute velocity
W	Relative blade velocity
ω	Rotational speed

CHAPTER 1

INTRODUCTION

1.1 Research Motivation

Global warming has been linked to many environmental issues and while it is difficult to ascertain the causality relationship, there have been a number of nature disasters over the years that have affected millions of people and led to billions of dollars in property damages. The Tohoku earthquake and tsunami that hit Japan in 2011, the catastrophic Haiti of 2010, the Hurricane Katrina which hits the southern coast of the US in 2005, and the 9.0 magnitude quake that led to the devastating Tsunami in the Indian Ocean in 2004 are some of the more significant examples. Destruction to the communities also negatively affect the efforts to assist those affected. The aftermath of the disaster is often dire and rescuers risk their lives trying to reach the missing or stranded victims, and it is not uncommon to have rescuers falling victims themselves trapped as they scramble through rubbles looking for survivals. Breakthroughs in aerial surveying technologies have allowed rescuers to obtain clear overall view of the disaster area. However, due to the proximity, the images obtaining from the ground are more detailed compared to images obtained from an aircraft and can be the key between life and death. In fact, rescuers are often sent out on foot to listen for sounds or sending dogs to locate survival. However, some disaster areas have proven to be simply too

dangerous for the rescue team to enter. Many of the disasters involve huge area submerged in water and hence an autonomous amphibious vehicle (AAV) is the most suitable development to complement the rescue's team effort to identify the location of the victims in those hazardous conditions. It allows the rescue operation to be carried out at a lower risk and a higher efficiency without the need of any onboard operator, and can help capture the images of the disaster area.

Autonomous Amphibious Vehicle (AAV) - AAV is a driverless land/water transport capable of navigating itself using an intelligent control system. Some of the earliest amphibious vehicles were used as carriages as early as the 17th century. One of the most notable early inventions dates back to 1805, when Oliver Evans invented the first high-pressure steam engine amphibian vehicle, the Oruktor Amphibolos (Wikipedia, 2011a), to solve the problem of dredging and cleaning the city's dockyards. However, it was only a century later, during the Industrial Revolution, that numerous of amphibian concepts were created for a broad range of applications, including military, search and rescue, planetary exploration, mining, environment monitory, surveillance, and disaster recovery. Despite the progress, major car manufacturers seem reluctant to embrace this area and instead focused only on the on-road automobile development. Prior to this, many existing amphibious vehicle in the market still lack many key amphibious technology, especially when it comes to flexibility and ease of incorporating complex autonomous capability. Numerous studies were carried out using amphibious vehicle

currently available in the market (Tran et. al., 2007) but most proved to be unreliable in terms of performance and all-round capability.

Autonomous Vehicle - As it stands today, autonomous vehicles only served as supplementary devices to the driver while the driverless system are only starting to trickle into standard road-going vehicles. Autonomous vehicle control has been overlooked in off-road terrain and it is still constrained to performing experiments and data collection. Working under unpredictable situation meant that autonomous vehicle have to be designed to adapt and behave according to the environment while completing tasks such as avoiding obstacles including rocks, tree and holes that can dampen the rescue operation. These integrated autonomous modules require other modules to operate the AAV, some of the systems include mechanical module, sensor fusion module, positioning module, map computation module, and motion generation module (Lacroix et al., 2002). The development and implementation of various processing control algorithms are crucial for AAV to have quantifiable and measureable maneuverability during navigation.

1.2 Problem Statement

There were many existing amphibious vehicles where their steering mechanism and mechanical linkages relied upon at least a pair of individual controls (Adams, 1999) to control two or more individual transmission or transaxles for land and water maneuvering (Tran et. al., 2007). However, these mechanisms were found to be complex and present challenges, especially in

the area of autonomous control. These autonomous amphibious vehicle platforms need to be further simplified in terms of mechanical design and modularity design. The need for a simpler, more exacting steering mechanism that can deliver turn capability in coordination, packaged in an amphibious vehicle is required to cover both the land and water transportation.

1.3 Scope of Research

Aim of Research:

- To develop an autonomous amphibious vehicle with suitable single locomotion mechanisms to allow the vehicle to navigate effectively on both land and water.

The **research objectives** are as follows:

1. To develop an amphibious vehicle for confined and narrow areas using suitable steering configuration and maneuvering system.
2. To improve the efficiency of water propulsion for wheel-based vehicle by optimizing its water thruster design by cutting down the extra load for a separate thruster drive.
3. To integrate various vehicle system for amphibious application using developed FPGA technology as a functional module control for an Electrical Vehicle (EV).
4. To perform experiments on the prototype and evaluate the maneuverability and performance of the autonomous amphibious vehicle.

1.4 Research Claims

The significance of the research work can be claimed as follows:

1. The Methodology of iAAV-1 control architecture is equipped with electric vehicle design to replace petroleum as transportation fuels benefitted the turn move towards greener environment and an improved sustainability of the transportation energy sector. The iAAV-1 compact vehicular design is modelled with flexible steering configuration. The method of applying Ackerman and differential drive steering in iAAV-1 is used as a tool to analyze the properties of the steering geometries that involved zero radius turn for path navigation. The iAAV-1 low level controls are implemented using developed FPGA as the control unit has made the autonomous mode more manageable compared with other autonomous vehicle platform using gasoline engine to drive or multiple CPUs to operate.

2. A new and novel wheel-based water thruster design has made improvement on the actual effectiveness and performance capabilities of an amphibious wheeled vehicle. The design helped to cut down the extra design and system payload for a separate thruster drive. It is also indicated that the Centripellor was practical and potentially useful when incorporated in the iAAV-1 wheel propulsion design.

CHAPTER 2

LITERATURE REVIEW

2.1 Historical Perspective

Given the rapid increases in vehicular technology, one may reasonably ask, “Where are the promised amphibious vehicles for land-water?” Many companies were founded in the 1960s, most notably, the ARGO company, to manufacture and commercialize the amphibious all-terrain vehicles (AATV)(Wikipedia, 2012). However, due to the oil crisis of 1973, poor quality product have resulted in a rapid decline in this type of AATVs, only a small number of manufacturers remain today (Wikipedia, 2011b). From the latter part of 1980s, amphibious vehicles exist only for military, research, hobby, and educational use. Today, the use of these amphibious vehicles have been recognized as important logistic tools by the US marine as a single vehicle support line over land and water operations (Gonzales et. al, 2007). However, the wait for a promising unmanned amphibious vehicle has proven to be an unexpected long and difficult one. The exponential increase in computer processing capability and other advancements have not led to improvements of general solutions to the machine vision, robotic sensory, and the ability to navigate autonomously (Gage, 1997). In the other comments (Hu et. al., 1997) stated that: “To date, many mobile robots have been built worldwide for outdoor navigation, some of which worked, some fewer of

which appear to have worked well, and far fewer of which were actually transferred into regular use. Therefore, to achieve a routine deployment of autonomous robots for outdoor applications remains a great challenge."

2.2 Application and Environment Challenges

Recent efforts by the Malaysian government in acquiring the "Amphibious Sealegs" (Figure 2.1) for use to assist persons or property in potential or actual distress (The Star, 2009) is a sign of the increasing importance of amphibious vehicles. The "Sealegs" is a modified high-tech boat made to be functional both in water and on land. It meets the needs for the flood rescue and civil defense-type applications in tropical countries like Malaysia.

Figure 2.1: A mock sea rescue operation using "Sealegs" (The Star, 2009)

Sealegs' unique amphibious ability allows rapid deployment of boats, equipment and rescue personnel which is crucial in any such missions. An amphibious vehicle usually comprises of a boat-like body to increase buoyancy and maneuverability in water. A majority of these also consist of six wheels with the rear wheel providing the driving force to propel the vehicle on

land and in water. Unfortunately, Sealegs were not meant for autonomous application; they were not designed to function without human operator to provide for the initial medical or other need. Urban terrain and sub-sea rescue mission comprises difficult terrains and it requires a more intelligent mechanical and control design to adapt to its surrounding.

2.2.1 Search and Rescue Operation

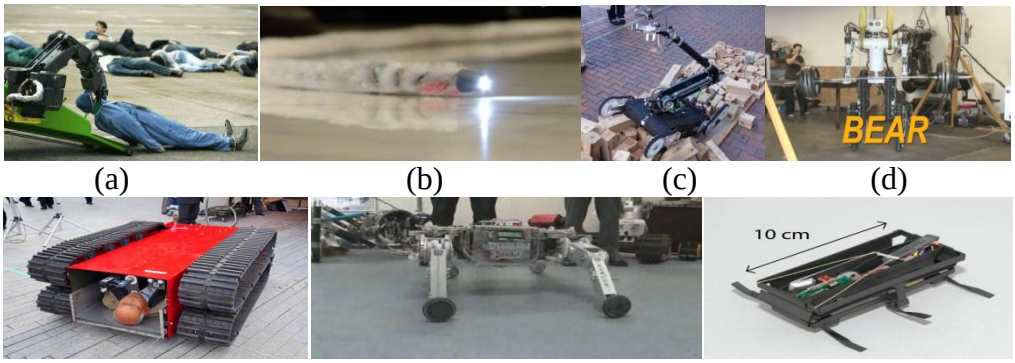

(a) (b) (c) (d)

(e) (f) (g)

Figure 2.2: Various search and rescue robots: (a) RoboCue (Ashcraft, 2009); (b) snakebot (Wang, 2009); (c) Quince (Lee, 2011); (d) BEAR (Hsu, 2009); (e) Robotic crawler (Gizmodo, 2011); (f) Roller-skating rescuer (Black, 2009); (g) RoachBot (Hart, 2010)

Japan, a country prone to recurring earthquakes, had a recent encounter with the disaster in Tohoku. The country happens to be a hotbed for robotics research and a variety of search and rescue robots are put to service in their rescue efforts. However, every robot shown comes with its own limitation to adaptability and the key stumbling block is the machine's intelligence. When the nature environment is un-navigable and dangerous for human search and

rescue teams, some of these robots such as the humanoid rescue-bots are designed to safely replace human, as shown in Figure 2.2, can be placed in good use (Figure 2.2 (d))(Hsu, 2009). The almost indestructible Roachboats (Figure 2.2 (g)) are sent out in a mass quantity to keep rescuers from being in danger and to locate survivors (Hart, 2010).

The RoachBot was inspired by cockroach locomotion which highlighted that the key to effective search robots is not the electronics but the mechanical structure to allow the machine to run like a cockroach and even to climb obstacles. At a cost of less than 1 USD/unit, RoachBot made it possible to release these robots even in mass quantity to locate or map the disaster environment before sending out the rescue team. Another potential search robot in a snake inspired snakebot (Figure 2.2 (b))(Wang, 2009) which uses Active Scope Camera that works by wrapping up its fibre-optic camera in a layer of tiny cilia bristles allowing for millipede-like locomotion. While the Snakebot moves relatively slow at around 2 in/s, it is capable of turning sharp corners, climbing 20° inclines, and squeezing through tiny gaps while its camera captures images inside a disaster zone.

Inspired by roller-skates footwear, the roller-skating rescuer, (Figure 2.2 (f)) uses an ingenious convertible leg that can turn into a wheel when necessary to propel itself (Black, 2009). According to the author, the legs tend to work best when moving over very uneven terrain and the robot can position its leg to land on sturdier steps. But on flat ground, some sort of wheel is preferable as it is faster, requiring much less energy, and a more stable mode

of locomotion. The Quince (Figure 2.2 (c)) is a robots which incorporated sensors to detect human breath and body warmth (Lee, 2011). It is equipped with four sets of wheels driving a tank-like rubber track and powered by six electric motors, enabling the machine to push ahead over bumps and up and down slopes as steep as 82°. Designed for local police/fire department as a rescue machine to locate and transport individuals to safety, RoboCue (Ashcraft, 2009) and Robotic Safety Crawler (Gizmodo, 2011) are two other robots providing carriage and onboard medical support like oxygen canister and sensors to monitor the victim. These robots are designed with powerful onboard motor to carry up to 110 kg; both are capable of using ultrasonic sensors and infrared cameras to locate the victims, and the automated system of loading the injured person onto cart. However, these particular models cannot help multiple victims at a time.

Some guidelines and requirements for a search and rescue robot were described. While there are no restriction to develop technology for the next-generation autonomous rescue vehicle, the capabilities of automotive to work under hazardous areas will require further evaluation of these concepts' effective search and rescue operation.

2.2.2 Terrain Challenges: Swampland

In tropical countries, wide a vast of terrain are covered by large areas of land with shallow bodies of water called swamp. A swampland is a large area of lands which is submerged under shallow bodies of water and generally

consists of a large number of woody vegetation and slow-moving/stagnant waters. The condition of a swampland closely resembles the condition after tropical disaster. In order for autonomous navigation in unstructured terrain to be feasible, a scheme was designed for purpose of detecting ground detection, water body detection and tree trunks detection for rainforest terrain using stereo camera (Teoh, et. al., 2010). However, the developed algorithm has only been tested on image frames from rainforest terrain. Consequently, the author's works open up an interests in developing amphibious vehicle in adopting the system for artificial intelligence and machine vision for vehicle guidance.

2.2.3 Terrain Challenges: Sewerage Tunnel

Another focus and application for amphibious vehicles is for monitoring the Deep Tunnel Sewerage System (DTSS). Beneath the surface of modern cities worldwide lies extensive networks of sewerage tunnels to supply water to all homes and industries. In countries like Singapore, given the small amount of land and territory, the country highly relies on its reclaimed water which makes up 30% of the total water supply in the country (Wikipedia, 2011c). Henceforth, the Singapore government introduces the DTSS project (Wikipedia, 2009), an infrastructure project aimed at providing long term solution to meet the needs in wastewater conveyance, treatment and disposal in Singapore. However, there is a parallel need for an alternative approach to assess the conditions of these underground tunnels. The changing depth of water and unpredictable structural conditions along many kilometres in

confined tunnels imposes difficulty and danger to building or maintenance personnel working in the environment. Based on a case history in Singapore (Zhao et. al, 2007), the authors highlighted a series of problems at the 12.6 km Kranji tunnel, including tunnel face instability, and the excavation face was significantly contorted during tunnelling using an earth pressure balance (EPB) tunnel boring machine (TBM) at site. Although tunnelling has been improved with modification, the magnitude change to the tunnel face was certainly not anticipated. In order to ensure that DTSS operates in a safe and uninterrupted manner, routine monitoring and investigating the whole route is a must. In those confined sewerage tunnels, an autonomous amphibious vehicle can be put into good use in checking and monitoring its conditions.

2.3 Autonomous Amphibious Vehicle

With the introduction of autonomy, more conceptual amphibious vehicles need to be added to supplement the search and rescue operations, and designs that are able to traverse aquatic and terrestrial environment while offering payload capacity are crucial. These AAV can be much smaller and of lower aspect ratio than those used in military, thereby enhancing stability, mobility and accessibility. As a designer, one may ask, "Will it be possible to implement autonomy in these readily available amphibious vehicles on the market?"

2.3.1 Early Works

Amphibious petrol powered carriages are some of the earliest documented amphibians (Richmond, 1905), including a boat-like hull with vehicle frame (Pohl, 1998), and a three-wheeler amphibian using a single front-wheel to provide direction using a three-cylinder petrol combustion engine to power its oversized rear wheels to provide propulsion in water (Wikipedia, 2011d). A remarkable ‘land-water’ boat was invented in 1931 by Peter Prell and the boat basically comprised of a boat-like hull with integrated tracks. It not only travels on rivers and lakes but also in the sea and did not require firm ground to enter or exit the water (Popular Science, 1931).

2.3.2 Concept of Autonomy

The autonomous switching process requires actuators that mechanically drive a control system. In this case, joint motors in the throttle are often used to respond to error signals from a process in feedback to correct the time-varying behaviour. In particular, motors that drive the throttle using position, speed, and perhaps load torque measurements and armature current or field current in feedback, to achieve a specified motion trajectory are called servomotors. In terms of actuator, requirements of size, torque/force, power, stroke, speed, resolution, repeatability, duty cycle, and bandwidth can differ significantly depending on the particular amphibious vehicle design and the specific function of the actuator within the control system. Furthermore, the capabilities of an actuator will be affected by the vehicle structural design and

drive configuration. In the amphibious vehicle itself, the gear box and the connector make the size of the vehicle large and heavy. The connection of the system is complex and highly similar to those found in cars. Although the vehicle is a good carrier, the vehicle is large, heavy, while the gearbox and the connector takes up valuable space. Most importantly, they are too large to move in narrow places and the fuel engine complicates the autonomous application; parallel controls on gear transmission, engine control, and braking requires more platforms and additional programs for characterization and autonomy.

2.3.3 Vehicular Control

With real-time control system (RCS) becoming a popular methodology employed in autonomous vehicles (Chan et. al., 2010), the amphibious vehicle design has to readily integrate real-time intelligent control system models. Operating a battery electric vehicle (EV) in autonomous mode is mechanically simple compared to the internal combustion engine (Tran et. al, 2007) when modelling the vehicle driveline. The EV eliminates the complicated actuator design to control the engine. Although the EV uses more motors to control compared to a gasoline engine, each motor performs only a simple set of task and can be controlled independently thus making it easier for a computer to take over controls for more effective maneuverability. The choice of electric motor also provides greater flexibility and allows for more compact packing that help eases arrangement difficulty. Efficient packing is made possible

because the vehicle is powered by a single drive system located on both sides of the vehicle; fitting direct drive for both amphibious modes.

2.3.4 Water Thrusters

Amphibious vehicles are usually powered by two water-jets at a maximum waterborne speed of 13 km/hr to satisfy floatation requirements during their water operation (Helvacioglu, et. al., 2011). Amphibious vehicle designers are often faced with the conflicting design criteria of road use and water borne stability (Davis & Cornwell, 2005). Amphibious vehicle design specifically for land operation, limited to shallow water operation, often had their floatability and stability requirements ignored. Focus is required primarily to examine the amphibious vehicle on land operation to enhance amphibian capability by means of floatability, stability, and propulsion considerations. These land operation AAVs, eg., the ARGO series (Tran et. al, 2007) relies heavily on their land-driven wheels to propel them in water. The reported ARGO AAV wheel-based propulsion can achieve a speed of up to 3 km/hr on water surface. However, the recorded speed is ineffective and result to clumsiness when afloat. The methodology using an existing ARGO also reveals that the wheel propulsion performance works at its best only when using new tires. The problem is due to the wheel-based propulsion's reliance on the tire threads depth to create propelling forces. Other notable varying performance factors for wheel-based propulsion is the tire diameter, and the width of the wheels.

In another investigation (Gonzales et. al., 2007), water-jets and pump-jets integrated as a secondary driven water propulsor which were found to present serious design complications. The author(s) indicated that locating the waterjet and particularly the waterjet intake within the hull form proved to be difficult and inefficient. Waterjets are typically used in ships with a larger than standard boat-type hull. On the other hand, while pumpjets do not require an intake, they cannot vector their thrust as waterjets can. So, rudders are required to be added to the design to provide suitable maneuverability. However, it was determined that rudders should be avoided to reduce complexity to the autonomous design. Besides, they present ground clearance problem when the AAV is on ground.

Some amphibious inventions (Hewitt & Ketchikan, 2011)(Bryham, 2008) differ from others by having the capability to hydraulically retract the position of driving wheels or caterpillar tracks that enables the vehicle to maneuver on water at a high speed by reducing drag. The width of the amphibious vehicle, with tracks mounted along side, presents certain limitations to the use of the vehicle. Regardless of the advantage derived from the retractable assembly and track positions, the lack of capability to reduce the vehicle weight and width limits its usefulness on land and tight places and to perform optimally. The complexity in its configuration not only limits its autonomous potential, it is also more expensive to produce and maintain. A compact design imparting good stability in the amphibious vehicle in a well-spaced skeletal structure for the main hull is especially advantageous in dense forest navigation.

Extensive efforts to investigate various hydro-jets (pump), paddles, and propellers to provide adequate water speed for both tracked and wheeled vehicles were reviewed by Rymiszewski, 1964. The outcome of these added water thrusters provide improved water speed at the cost of added weight, complexity, and cost for a component that is utilized only at necessary water operation. A later effort by Ehrlich et. al (1970) proved that it would be much more practical to utilize the same propulsion system for water operation as for land operation, that is, wheels or tracks. The author(s) observed that wheel propulsion offers the advantages of being able to propel the vehicle at different submergibility level simply by spinning the wheels; just as tracks do, but less efficiently. However, their advantage lies not in their efficiency, but in the fact that they are already equipped for land operations. With the wheels acting as the only auxiliary propulsion device to obtain modest thrust in water operation, the paddle wheels obtained a moderate speeds of 3.2 to 4.8 km/hr when partially submerged. On the other hand, when the wheels are totally submerged, efficiency further drops to an attainable speed between 2.4 to 3.2 km/hr.

Figure 2.3: The wheel-shroud design (Rymiszewski, 1964)

An extensive close-fitting enclosure, as shown in Figure 2.3, called the shrouded-condition around the tires were used to improve the wheel-spin propulsion (Rymiszewski, 1964). This shrouded-condition propulsion can

radically improve the wheeled vehicle water speed when it is properly designed to control, and redirect the axial, radial, and tangential flows of the submerged and rotating the wheels into useful thrust. The author's efforts, though has tried or has yet untried, the design appears to have promise in using the disc portion of the wheel hub as an axial or centrifugal flow pump, to create inboard flow about the wheel. Continual efforts to determine the maneuverability of an amphibious vehicle using wheel propulsion appears to contribute greatly to the autonomy system. However, without a rudder, the vehicle's dynamic and directional stability has to come from a more efficient wheel propeller to improve the turning moment to overcome the large hydrodynamic turning resistance and very large yaw moment of inertial of the vehicle.

2.4 Case Study

This section outlines the work carried out in the area of autonomous, focusing on various amphibious vehicle or related-planetary vehicular design. The contribution and limitations of each approach will be highlighted while the justification of the design and implementation will be reasoned.

2.4.1 Design of DUKW Series

Since 1943, DUKWs (informally known as Duck)(UATM, 2007) were extensively used to move troops, ground vehicles, and supplies across invasion beaches. A later version of DUKW, the LARC (lighter, amphibious, re-supply,

cargo) and BARC (barge, amphibious, resupply, cargo) (Global Security, 2004) were developed in the 1950s. They are large amphibians used in a variety of auxiliary roles to this day, and there are different versions: LARC-V, LARC-XV, and the BARC which was later designated as LARC-LX.

Figure 2.4: The DUKW-21 demo (Gonzales et. al., 2007)

DUKW-21 concept for a single operator or by automatic/unmanned controlled was developed in 2007 to reduce the needs for multiple vessels and focuses on one craft for cargo transfer (Gonzales et. al., 2007)(Flom, 2009). While there have been many focuses on operations on land, sea, or air but with no integration of autonomy operation modes in different terrain, the team mission is to develop DUKW-21 to facilitate ship-to-shore logistics with limited human interaction. As shown in Figure 2.3, DUKW-21 is a tracked vehicle with a high arching cross structure influenced by cargo container requirement. The tracks run along the bottom of each hull for ground propulsion, and an integrated podded propulsor (Kort nozzle) located at the end of each pontoon were meant for water propulsion. These podded integrated motor propulsors are claimed to be ideal because rudders are not required and they are contained in a single pod, outside the hull. These propulsors are retractable using a hydraulic retraction system to gain more ground clearance on land operation.

The autonomy of this DUKW-21 generally consists of (Flom, 2009):

1. A perception interface, which consists of sensors that acquire information about the system's environment, as well as software that converts low-level input signals from the sensors into high-level information.
2. A planner, which is based on the information acquired by the perception interface, as well as knowledge about the system's present state, produces the best high-level plan for the system to complete its mission.
3. An executive, which upon reading a new plan, calculates what the actuators need to do for the system to run the plan, and outputs high-level commands to the actuator interface.
4. An actuator interface, which consists of moveable components, as well as software that converts high-level commands into low-level signals that control the motion of the actuators.

As an approach to amphibious navigation, the problem field was separated into three components; sea, land and transition. Considering as separate tasks, existing algorithms were selected to investigate feasibility in DUKW-21:

1. Optimal sea paths algorithm uses a simplified global path to derive an optimal heading the vehicle should take which has shown to coincide with the actual optimal path (Dolinskaya & Smith, 2008).
2. Algorithm for autonomous ground navigation implemented on Mars Exploration Rovers (Carsten et. al., 2006).

3. For sea-to-ground, the land area of operation is to be treated as sea, where cells with infinite traversal costs are treated as obstacles, until the vehicle beaches, at which point ground navigation would be used to travel to the goal point. For ground-to-sea, the water area of operation is to be treated as ground, where cells either have costs of infinity (for obstacles), or one (lowest difficulty if there are no obstacles), until the vehicle enters the sea, at which point sea navigation would be used to travel to the goal point.

In summary, DUKW-21 has fulfilled the design requirements of being an amphibious vehicle capable for cargo transfer. The 16.05 m length by 7.62 m width by 7.28 m height amphibious vehicle that weighs about 56 tonnes was able to cruise at 27.78 km/hr with a given 1,500 hp output. However, DUKW-21 report does not address the presence of obstacles that may require optimal motion in rotating a non-circular robot for optimal paths; DUKW-21 constraints with an unidentified high maximum turning radius which will pose a problem in tight spaces autonomy navigation.

2.4.2 Design of Surf Rover

Amphibious remote-operated vehicle (ROV)(Figure 2.5) is an effort to function in the coastal region to collect data and make observations in the surf zone (Dally et. al., 1994). Previous works have seen these vehicles to be essentially large tetrahedrons, nominally 9 m wide and 10 m tall, that ride on hydraulically driven tires powered by an engine mounted on top of the vehicle. However, this 8.2 tonnes technology is critically limited by flexibility to

transport and to access areas. A more viable surf zone ROV was established, called the Surf Rover, to solve the mobility in the variety of soil types and access rough terrain. The Surf Rover consists of a structural frame, two front arms and track units, a watertight housing that contains power, hydraulic, and control equipment, and a caster wheel at the tail. Its 5.2 m wide, 6.7 m length frame and 1.36 tonne dry weight structure are built in a tripodal shape to permit enlargement of its base to increase stability. Both front arms are motorized by hydraulic motors mounted at the rear of each track pod. The motors are reversible and independently controlled, so steerage of the ROV is provided by their relative motion. The key features of The Surf Rover is that the vehicle remain fully operational at any position when the vehicle is folded which greatly improves beach access capabilities.

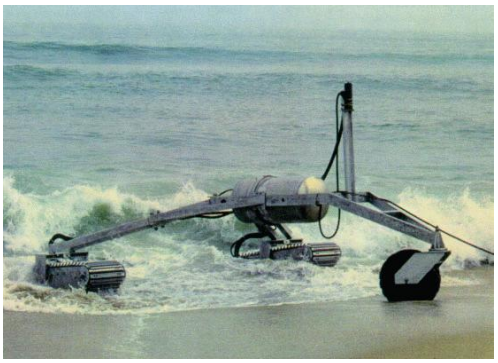

Figure 2.5: The Surf Rover remotely operated vehicle on the beach

(Dally et. al., 1994)

The Surf Rover is not designated to float on the surface water, but it is fully submersible. Hence, the electric motor, pump, and valves are enclosed in a watertight housing that is 0.66 m in diameter and 1.36 m long, and separates into two sections at an O-ring flange. The nominal submerged weight of surf

zone is 860 kg and its electric/hydraulic output of 20 hp can operate the vehicle up to a 1.1 m/s travel speed. The result from field test shows that the navigation of the folded Surf Rover can be difficult with a different pace of two tracks, sideways stability, and the most notable problem encountered is the decreased in vehicle mobility when traction is lacking.

Figure 2.6: The MARC-1 (Wood, 2007)

The position and navigation system for Surf Rover was not mentioned. Another similar work, Modular Amphibious Research Crawler (MARC-1) (Wood, 2006)(Figure 2.6) has been developed without on-board human operator. MARC-1 is a reduced size Surf Rover within a frame size of 3 m length by 2 m wide by 1 m height, and a dry weight of 175 kg. Powered by independent AC electric motors in protected aluminium housing and aluminium tripod. All the electronics are protected from undersea environment by Polyvinylchloride (PVC) pressure housing wrapped in carbon-fibre with clear cast acrylic end plates. The navigational instrumentation on the vehicle consists of inclinometer, with a 3-axis compass, connected to the GPS in order to give the inclination definite distance intervals along with the magnetic

heading. A camera is available to allow a remote operator to see where the vehicle is heading. Different from the Surf Rover track propulsion, MARC-1 composes of two separate AC gear motors that drive the two drive wheels via signals sent down from the information cable.

The MARC-1 ROV has consequently reduced the difficulties of surf zone data acquisition by being able to carry multiple instruments and traverse a variety of subsea terrains. It places the ROV in an advantageous position over other vehicle to float itself out of difficult or impossible condition by being highly maneuverable and able to climb out of difficult condition. Although with its capabilities to travel at most subsea terrains, MARC-1 or Surf Rover is still beyond the capabilities of these vehicles to move over boulders and soft mud. Whereas heavy vehicles face challenges with mobility, vehicles with light submerged weight can easily get washed off in the surf zone. The major challenges remain to incorporate a complete proof-of-concept amphibious on water surface that has high mobility.

2.4.3 Design of ARGO AAV

A commercialized 8 wheels drive ARGO amphibious UTV (Utility Terrain Vehicle) successfully converted into an autonomous platform (Ha et. al., 2005)(Tran et. al, 2007), as shown in Figure 2.7, is now serving as a general framework for automation of tractors used in construction. Powered by an existing 20 hp combustion engine, 8 wheels drive (8x8), on a 3 m length by 1.45 width m by 1.1 m height body that weighs 0.5 ton, the ARGO AAV

can only achieve a sub-par performance of 30 km/hr on land and 3 km/hr on water using wheel-based propulsion. The disadvantage of using wheel-based water propulsion is that the performance reduces as the tread of the ARGO tires wear off. This ARGO platform also adds more complications for having complicated actuators modifications and carrying several heavy computing equipments to achieve autonomy. The use of both electrical energy on computing system, and gasoline energy in combustion engine wasted valuable space and consumed excessive energy because the main objective to generate a reliable autonomous system is based on reusable components to govern the overall system.

Figure 2.7: A commercialized ARGO ATV converted to an AAV

(Tran et. al., 2007)

The paper (Ha et. al., 2005) addresses some control issues of AAV including the vehicle's low-level dynamic equations, development of its braking control system, kinematics in interactions with ground and the slip problem. To derive the wheel speeds, modelling of a gasoline engine driveline including the engine, Continuous Variable Transmission (CVT), gearbox, differential, chains and wheels has been developed using step inputs of throttle and pulses of left and right brakes for straight running and turning of vehicle.

Many of their works were illustrated and simulated using Matlab Simulink for throttle, engine torque and speed, gearbox input speed, left and right brakes and wheel speeds, loads at wheel shafts, gearbox, and engine. The key issue addressed is the braking for vehicle steering. ARGO uses the differential and the brake system to decide the turning of the vehicle. Therefore, the drive configurations involves a highly non-linear control of both hydraulic pressure brake discs and engine piston position, making the vehicle's turning and steering more difficult to control. Although simulation works has verified the newly designed controller which out-performed the current system in terms of robustness, field trials for the implemented controllers have shown that the simulated speeds may look close to the practical development speed at the engines but it is ultimately limited by the gearbox. The difference between trial and simulation results is accounted for by several factors:

1. CVT is modelled as a linear function of speed and load, but in fact, it is highly non-linear.
2. The model did not consider weight and dead zone of the gears in the gearbox, differential, brake discs, and chains.
3. Complicated interactions between vehicle and terrains were not taken into account.

In an unmanned vehicle, hardware resources play an important role for RCS integrity to ensure system stability and performance in real-time environment. As ARGO AAV system is getting more complex, having various actuators and sensors installed on each of the mechanical hardware and the

resulting parallel processing needed to be implemented in the vehicle system will cause a slower response. Hence, the practical real-time performance is not guaranteed. On the other hand, unmanned vehicle does not require humans to be on-board this it can subsequently be smaller and lighter than their manned counterparts. A reduction in mass can be expected to translate into cost effectiveness for smaller capacity amphibious vehicle with compact structural and computational hardware.

Figure 2.8: The ARGO AAV carriage compartment taken in NTU, Singapore

A compact AAV will minimize the system-to-vehicle ratio, making it useful when travelling across a variety of terrains, rainforest, and narrow tunnel. A carriage compartment of an ARGO AAV shown in Figure 2.8 was seen to be fully occupied with on-board control system. A lightweight control system is more desirable as it reduces the vehicle weights significantly so the vehicle can be more agile during navigation.

2.4.4 Design of Planetary Rover

Figure 2.9: The robot Lama (Lacroix et. al., 2002)

In the field of off-road autonomous, Marsokhod model robot Lama, as shown in Figure 2.9, is an autonomous vehicle adaptable in unknown terrains (Lacroix et. al., 2002). The localization and motion generation functionalities for long-range navigation were successfully integrated in the design. All presented functionalities have been individually tested in a more complex integrated experiment with each motion generation algorithm. Multiple tests were carried out to refine the algorithm; it is run until either easy terrain algorithm succeeds again, or until no feasible arcs are found in the elevation map. While another experiment with sub-goal strategy is applied, the result shows reliable results where the rover successfully found its way through various situations. The vehicle performance also suffers from a sub-par performance where the implementation of the algorithms is not optimized and vision algorithms limit the vehicle to a low speed of 0.05 m/s.

The ability of Lama to traverse without human intervention is attributed to the large size mechanical built-up for high obstacle traversability

capacities. The design of its chassis gives flexibility with the passive articulations of the axles, each axle can move independently. Hence, Lama is made with an actively controllable lengthy chassis. The maneuverability of Lama actively depends on its peristaltic locomotion mode (“crawling”) which is especially suited to climbing over steep sandy slopes. The sensors selection equipped/integrated made useable navigation data presented in a logical manner for long-range navigation.

Lama is not designed for all-terrain navigation tasks, specifically the water terrain; Lama is applicable on limited range of dry terrain. The development of Lama has not been clearly defined from a mechanical engineering point of view. However, from descriptions, robot Lama's bulky chassis setup consists of six-wheel, three pairs independently driven wheels and each motor driven by a servo-control board seem to be disadvantages with its dead weight and bulkiness to maneuver in confined or narrow areas. This seems necessary as Lama is not required to carry any human operator or equipped loads. The high-cost autonomous will relatively be unreasonable for various applications. The computing equipment can one area for major improvement in future autonomous development. Four CPUs mounted on Lama will waste lots of space and weight in an area where compact design makes for better flexibility in future designing while imparting good stability in a well-spaced skeletal structure. A simplified design is desirable to reduce energy requirement while offering the benefits of light vehicular-weight especially in dense area navigation for better maneuverability across obstacles.

2.5 Summary

A fundamental question was asked in an autonomous mobile robot design: “What is the ideal mechanical design for an autonomous mobile robot that can perform the defined desired behaviour in an environment in which it will be used?” (Nassiraei & Ishii, 2007). The author admits that the results have contained a myriad of definition with none of them clearly defined. There is no concrete method or approach to actually design an AAV system. Amphibious vehicles were designed and developed to serve as a connection between land and sea. It is very common to find an amphibious vehicle built from existing military truck, modified watercraft/boat, or existing road going vehicle by adding a hull, propeller, and bilge pump system. These vehicles were all intended to be designed for extensive use for their very own subjective purposes or particular environment. Very few actually developed a conceptual amphibious vehicles capable of controllability, flexibility, and a reliable mechanical structure to effectively produce, fabricate or modify for any autonomous agent.

The need for a high mobility amphibious vehicle that is capable of incorporating compact control system with continual effort to improve the maneuverability using wheel propulsion is stressed. The challenges lie in the mechanical system, whose general performance specifications and detailed definition defined the ultimate task of the design needs (Mott, 2006).

CHAPTER 3

MODELLING OF THE iAAV-1 LAND NAVIGATION

3.1 Overview: iAAV-1

The iAAV-1 platform is the main focus in this research. iAAV-1 stands for “first generation interactive autonomous amphibious vehicle”, where the “i” represents one’s self. In this case, a term describing an autonomous amphibious system aimed at allowing for the continuous transfer of information between modules which allows for the use of real-time feedback from a control system. This thesis emphasizes on the iAAV-1 mechanical system, whose general configuration and performance specifications meet the needs of the given task.

The iAAV-1 is intended to perform the search and rescue support operation in tunnel and tropical rainforest terrain. The key elements of this research work includes the development of amphibious vehicle platform that is feasible to traverse both on land and water terrain with suitable navigation techniques, control architecture and the implementation of developed autonomous control using Compact Real-time Control System (CRCS) technique using Field Programmable Gate Array (FPGA) as a control unit.

This chapter begins with a basic engineering design to develop appropriate vehicle architecture for iAAV-1 in realization of an autonomous amphibious vehicle with different degree of mobility and autonomy. The basic engineering design addresses the goal of getting an iAAV-1 platform with an ideal, or redesign locomotion mechanisms. Different wheels and wheel steering configurations are discussed in detail in this chapter. With this knowledge, each different module of the mechanical platform is worked out step by step and the design is slowly refined with the final prototype. As a result, the final mechanical platform, iAAV-1 was developed, as shown in Figure 3.1. The iAAV-1 was developed to demonstrate the value of research work with hardware display and enhance research methodological quality to analyze the autonomy applications. The iAAV-1 will serve as an autonomous platform for experiment and data collection.

Figure 3.1: The iAAV-1 prototype

3.2 AAV Mobility: Land Maneuvering

Based on the literature review in Chapter 2, there is no unified approach or methodology to actually design an autonomous amphibious vehicle system. Given a particular need, an amphibious vehicle would probably require a different configuration. It is very common to find an amphibious vehicle built from an existing military truck, modified watercraft/boat, or existing roadster on road by adding a hull, propeller, and bilge pump system. These vehicles were designed for extensive use for their very own subjective purposes or particular environment. Only a very few developed a conceptual amphibious vehicles that are capable of designing for controllability, flexibility, and a realizable mechanical structure to effectively produce, fabricate or modify for any autonomous agent.

In many applications, it is useful to build a vehicle with higher mobility. The environment surrounding it is adapted to suit the iAAV-1 tasks, while the iAAV-1 have to adapt its behavior to its surroundings. Instead of developing an on-board intelligence to determine the best action to take, the development of the mechanic systems on iAAV-1, which is important to ensure the processing of all kind of sensors information into movement task, is to be delivered effectively while avoiding collisions. In the environment faced, search and rescue operations for nature disaster to co-exists in two very different worlds that require the ability to move from place to place across ground and water terrain. Unlike in rainforest terrain, sewer tunnels pose the needs of a much greater flexibility to perform new and complex tasks. As used

in design context, the iAAV-1 will be given a map as a task to maneuvering from point A to point B, alternatively. The iAAV-1 will use a set of flexible behaviors to decide the route to accomplish them.

The key to an effective autonomous mobile vehicle navigation is accurate self-localization. In order to make an AAV move when needed, the mobility of a vehicle that determines its locomotion mechanism defines how much greater flexibility to perform any given tasks. The drive configurations are fundamental to maneuverability, controllability and stability of an AAV. These can be categorized as follows (Bräunl, 2008):

1. Single-wheel and Three-wheel Drive
2. Differential Drive
3. Continuous Tracks/Crawler/Skid-steer Drive
4. Ackermann Steering
5. Articulated Drive
6. Synchro-Drive
7. Omni-Directional Drive

There are two types of driving configuration terms:

1. Holonomic - also called omni-directional – is a term which simply means the ability to move in any direction. Holonomic vehicles are defined by equal controllable degree of freedom to the total degree of freedom. Holonomic offers full mobility with the same number of degrees of freedom as the environment; making path planning easier because there are no constraints that need to be integrated which can limit the directions in which

the robot can accelerate. However, it is used redundantly in automobile because the nature of mobile vehicles only contain three dimensions which are most commonly thought of as the x, y, and θ. As the global two axes position and global orientation of the vehicle, yet, only two controllable degrees of freedom which are acceleration/braking and the angle of steering wheel.

2. Non-holonomic - vehicles are defined by the controllable degree of freedom which is less than total degree of freedom. In automobile, non holonomic vehicles are most common due to their simplicity and the reduced number of variables to control the favours in implementing autonomous. By nature, non holonomic vehicles have fewer degrees of freedom and these few actuated degrees of freedom are often independently controllable or mechanically decoupled, further simplifying the low-level control of the vehicle. Of course, with fewer degrees of freedom, this makes certain motion planning like parallel parking and u-turn on road difficult.

All of these benefits and detriments are considered part of the research process and all possibilities need to be explored.

3.2.1 Single-wheel and Three-wheel Drive

The single wheel drive is the simplest conceptual design for a mobile vehicle. The vehicle linear velocity and angular velocity are completely decoupled. The front steering wheel directs the orientation and the driving wheels driven at the desired speed, as shown in Figure 3.2 (c), is a static

unstable single wheel drive used in bicycles. Turning on the spot is not possible as the minimal turning radius when the front wheel is set to 90° will rotate about the mid-point between the two rear wheels. So, the minimum turning radius is the distance between the front wheel and the midpoint of the rear wheels. The three-wheeler configuration offers two variants: one wheel driving in the front (Figure 3.2 (a)) or two wheels in the back (Figure 3.2(b)). Having two wheels in the front has improved the aerodynamics, transversal stability, and traction as opposed to having only one wheel. Having one wheel at the front and two in the rear for driving reduces the cost of the steering mechanism, but greatly deteriorates the lateral stability when navigating and braking. Figure 3.2 illustrates the vehicle motion when steering in a curve Figure 3.2 (d), moving in a straight line Figure 3.2 (e), or rotating itself on the spot Figure 3.2 (f).

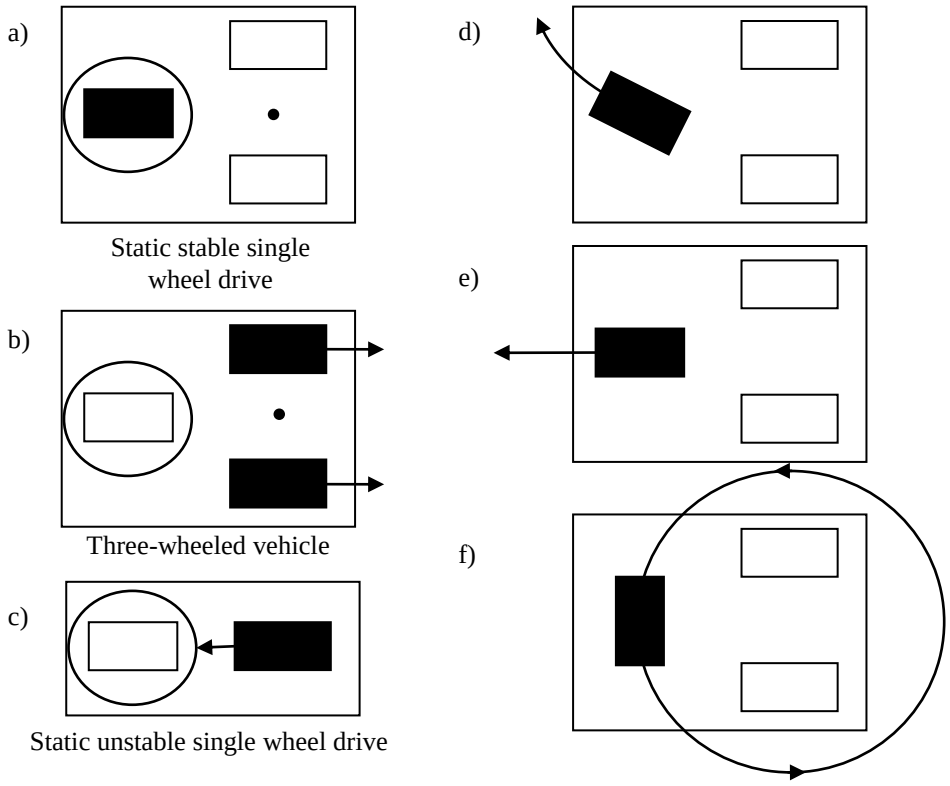

Figure 3.2: Single wheel drive configurations

3.2.2 Differential Drive

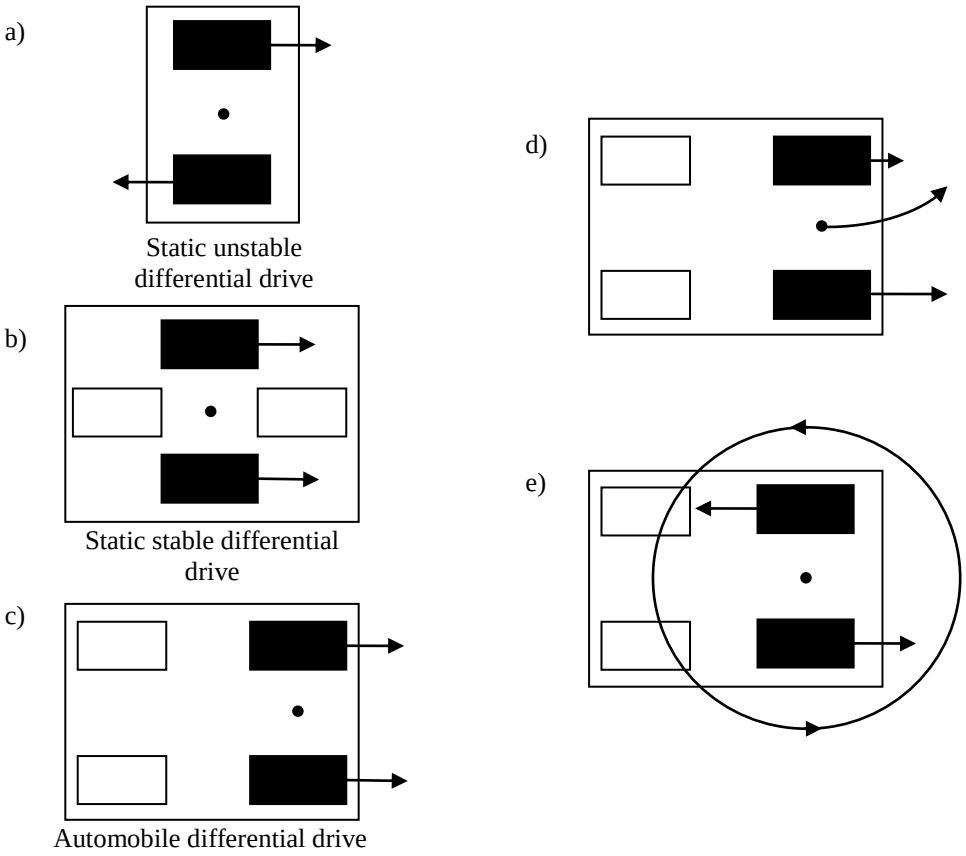

Figure 3.3: Differential drive configurations

Figure 3.3 demonstrates the driving actions of a differential drive. Generally, a minimum of two wheels are for static stability (Figure 3.3 (a)). If two-wheel differential drive is to achieve static stability, it is required to keep the centre of mass below the wheel axle and that requires wheel diameters that are impractically large. Often, one or two castor wheels are necessary for at least three ground contact points.

In differential drive design, two motors are mounted in fixed position on the right and left side of the vehicle, independently driving one wheel each

(Figure 3.3 (b)(c)). The differential drive design is mechanically simpler than the single wheel drive because it does not require rotation of a driven axis. However, the driving control for differential drive is more complex than a single drive because it requires the coordination of two driven wheels. The vehicle will rotate around the off-center midpoint between the two driven wheels, which introduces the surface contact problems. The differential drive motion for moving in a straight line (Figure 3.3 (c)), differential steering (Figure 3.3 (d)) and (Figure 3.3 (e)) satisfied the conditions below:

- Condition for forward driving:

$$v_L = v_R, v_L > 0 \tag{3.1}$$

- Condition for driving in a right curve:

$$v_L > v_R, \tag{3.2}$$

- Condition for rotating on spot in a counter-clockwise rotation:

$$v_L = -v_R \tag{3.3}$$

Unfortunately, the caster wheels can cause problems if the vehicle reverses its direction. Often in the reverse motion, the caster wheels must be rotated against the direction motion. In the process, offset swivel can impart an undesired motion vector to the vehicle, resulting into an undesired heading error. In some robotic design, the differential drive is utilized with minimal turn radius by placing the driving wheels in the middle of the robot. So when turning on the spot, the robot will rotate around the off-centre mid-point between the driven wheels. This design requires two passive wheels to be at both ends, for stability.

Despite the simplicity in implementing the differential drive, the controllability of both motors to move in straight line is rather difficult. Since the drive wheels are independent, if they are not turning at exactly the same rate the vehicle will deviate to one side. Each side of the differential has slight differences in motors, drive trains, transmission, and wheel-ground interface. It is necessary to have a feedback control system to adjust the motor speed very often. It is important to have encoders to provide accurate information on the wheel position. The encoders are normally acting like an anti-lock braking system (ABS) or traction control in automobile that feedback the measurement of rotating wheels and generate control signals to the actuators to correct any output errors, such as a wheel-slippage.

3.2.3 Continuous Tracks/Skid-steer Drive

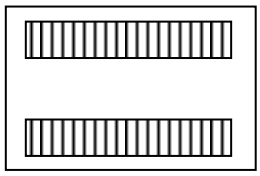

Figure 3.4: Continuous tracks configurations

Vehicles equipped with differentially track steered drive system, configuration is as shown in Figure 3.4, also known as skid steering, are commonly used in small application like robotics, wheel-chair, and house appliances. It is also used in large tracked vehicle in heavy-duty construction such as caterpillar-tracked excavator, crawler, forklift, “Bobcats”, and combat armoured vehicle such as seen in tanks. The wheels/tracks mounted on each

side are independently powered and controlled by different motor, providing both drive and steering function. Both sides of the wheels are engaged in propulsion, acting like a caterpillar endless track while maintaining an all-wheel-drive system to provide power to all the wheels, eliminating the drag from the un-driven free-wheeler while providing much needed power to travel in both land and water. This convenient driving system makes it possible for the amphibious vehicle to move on different terrain. For example, on a muddy terrain, the slippery surface will cause the front wheel directional control to slip. The vehicle will not turn as directed by the wheel. The differential drive can provide more grip and aid in the change of direction. The system uses two different motors to run different sides of the wheels. One motor is used for both the left front and back wheels, while the other is used for the other side. The two motors on each side will rotate in the same direction as the vehicle is moving forward and backward. When the vehicle is required to move to the left or right, the motors will rotate in opposite direction. This system will produce a stronger grip and better turning performance.

Continuous rubber-padded track might provide better maneuverability in rough terrain and the vehicle will benefit from the higher traction due to its tracks and multiple points of contact with the surface. However, the track design build up is complex and contribute to the weight placing enormous strain on segments, and might immobilize the entire vehicle or cause frequent failure. Conventional tires are more suitable and is a safer option to prevent failure during search and rescue mission. Furthermore, it is cost-saving and components are easily obtainable.

3.2.4 Ackermann Steering

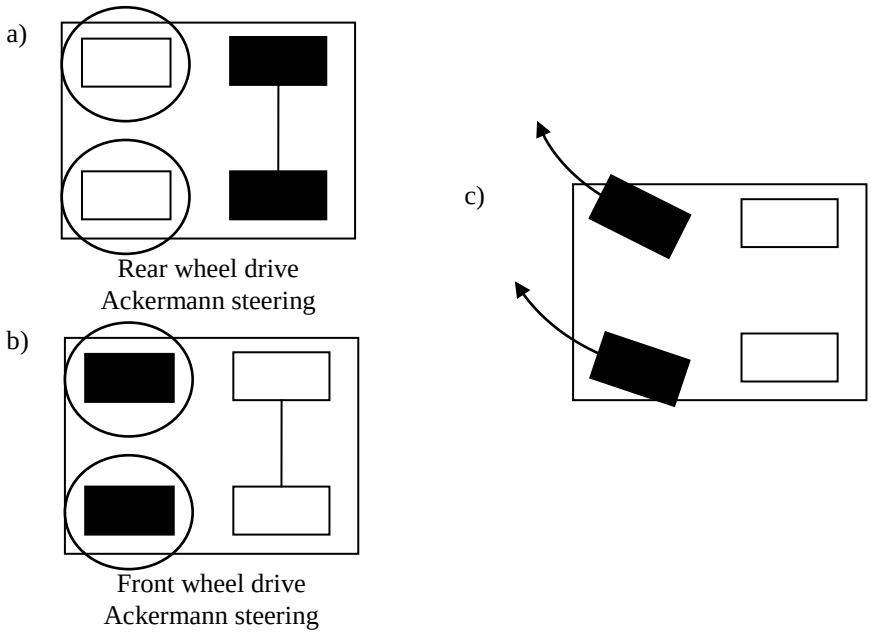

Figure 3.5: Ackermann steering configurations

There are two types of Ackermann steering: front wheel drive (Figure 3.5 (b)) and rear wheel drive (Figure 3.5 (a)). Figure 3.5 (c) illustrates the conventional on-road front wheel drive steering. The rear driving wheels experience a slippage in curves during low speed, while the front driving offers a predictable handling. However, what really separates them is the cost, weight, and fuel efficiency that favors the front wheel steering drive.

The Ackermann steering is a standard drive and steering system used in automobiles. Similar to a three-wheel drive configuration, the Ackermann steering cannot turn on the spot, but requires a certain minimum radius. Since the rear wheels (in some cases, the front wheels drive and rear wheels steer like Forklift truck) are driven via a common axis, this makes it the most

advantageous when driving straight on a highway as it possesses good lateral stability in high-speed turns. The linear velocity and angular velocity are decoupled since they are generated from rear wheel drive train and Ackermann steering.

Arguably, the cheapest way of building an autonomous vehicle is to use a readily available car. Retaining the chassis, motors, servos, and adding a number of sensors and replace the remote control receiver is very much cost effective. However, the construction of an autonomous of this combined drive and steering has great complexity. The limitation manoeuvrability of the Ackermann steering also makes path planning much more difficult in a complicated environment. For such vehicle to move sideways requires repeatable changes in direction forward and backward. A small position error in the turning mechanism can cause large odometry errors.

3.2.5 Articulated Drive

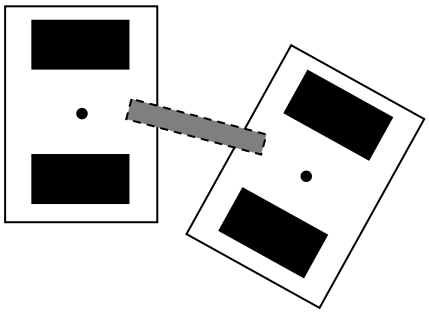

Figure 3.6: Articulated drive configurations

A small-scale AAV (Frejek & Nokleby, 2008) uses articulated drive (Figure 3.6) with deformation mechanism (grey block) to achieve a rotation between segmented bodies of the vehicle to conform to the terrain that it

travels upon. This is an example of non-holonomic system. It can provide the vehicle with a two degree-of-freedom joint that allows pitch as well as roll, as shown in Figure 3.7. The mechanical design uses one motor to drive the wheels and one actuator to change the pivot angle of the chassis. This design is commonly used in construction equipment where differential is used in each segment when required. If multiple wheels are driven and a differential is not used, the wheel slippage will occur. However, in most application for articulated drive, wheel slippage is not an issue because the speeds are slow and the coefficient of friction with the ground is low.

The AAV does gain in mobility with the two degree freedom joint and provide suspension as it incorporates the suspension into the body. This ensures that all wheels are on the ground at all times, providing maximum traction, which is required for navigating on rough terrain and being able to climb over objects when approaching them directly and at an angle.

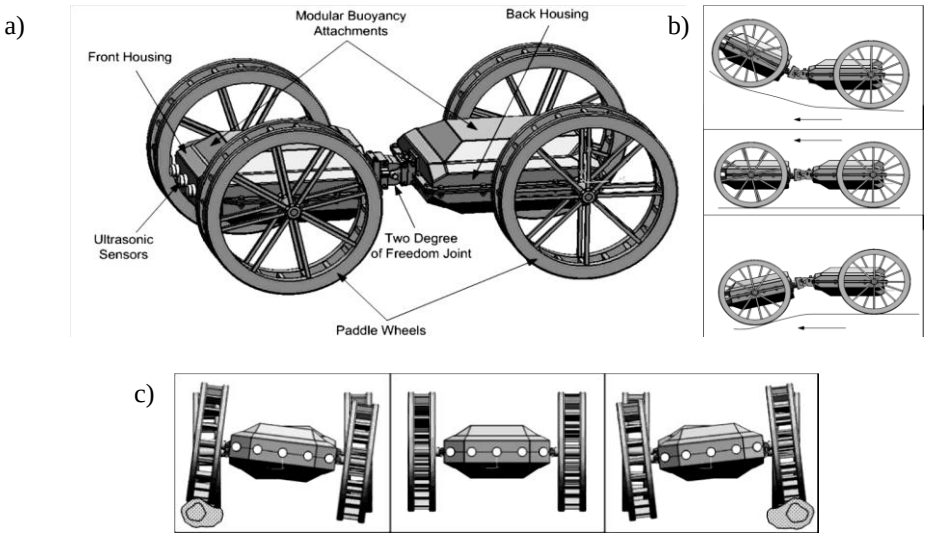

Figure 3.7: An AAV (a) with pitching motion (b) and rolling motion (c) (Frejek & Nokleby, 2008)

3.2.6 Synchro-Drive

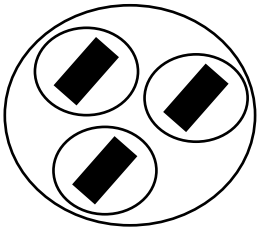

Figure 3.8: Synchro-drive configurations

The synchro-drive (Figure 3.8) is a three wheel (or four wheel to improve stability) configuration system with motor drive configuration where all motor rotates all wheels together to produce motion to change direction, making it advantageous for a complete area coverage in a given environment. The synchro-drive has only two degrees of freedom, and in most cases, its arbitrary motion path is the reason why it usually has cylindrical body shape. The three wheels are always rotated together so they always point in the same driving direction. It is almost a holonomous vehicle, in the sense that it can drive in any desired direction. However, the robot has to stop and realign its wheels when going from driving forward to driving sideways and it cannot drive and rotate at the same time. The mechanical guarantee of straight line motion is a big advantage over the differential drive method. However, its wheel alignment is critical in this drive system. If the wheels are not parallel, the robot will not translate into a straight line. On top of that, the synchro-drive arbitrary can be difficult in all-terrain and its cylindrical shape is difficult to construct to have a good maneuverability on water.

3.2.7 Omni-Directional Drive

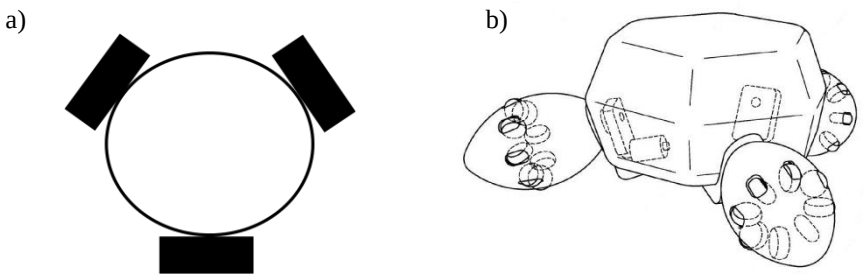

Figure 3.9: (a) Omni-directional configurations, (b) ellipsoidal drive element (Dixon, 2008)

A common approach to design a robot to operate in a narrowly configured operating environment is by using the omni-directional drive (Figure 3.9 (a)). There are a number of different omni-directional wheel variation employed in a holonomic or 3 degree of freedom drive systems. An ellipsoidal drive (Figure 3.9 (b)) is used particularly for all-terrain purpose with a buoyant internal chamber. Each of the roller elements are orientated to provide friction reduced rolling in a main ellipsoid axis direction and traction perpendicular to the main ellipsoid axis direction. The claim of reduced complexity mechanical drive assemblies and undesirable maintenance requirements may be justified, but the cost of high initial drive production may drive potential buyers away. Although the maneuverability of the AAV drive system has been improved, the omni-wheel is heavily built and designed, and it is less robust and tricky to control in autonomous navigation. Compared with other drive configurations, the omni-directional drive usually has less pushing force because the motor-wheel assembly is tightly attached to the vehicle chassis with very minimal clearance.

3.3 Model Development

3.3.1 Design Considerations

The main question to solve before designing a vehicle is: what are the requirements? The challenge is to develop an autonomous amphibious vehicle that is able to maneuver from location to location without colliding with any obstacle. Compared with other search and rescue vehicle, an amphibious vehicle platform needs to have a high level of configurability, able to support the implementation of desirable control system, and modifications for wet and dry terrain. To achieve this goal, the flexibility to control the expendables modules/mechanisms is desired.

To facilitate the vehicle design process, a number of iAAV-1 design requirements were assumed to be able to:

1. Traverse very soft or unstructured ground, eg. mud, beach, and undetectable underneath water obstruction like tree roots in swampland.
2. Climb standard beaches slope of 1:50 gradient.
3. Rain-fall poses no threat to vehicle water proof and visual guidance system.
4. No problem in transition between water and land.

3.3.2 Functional Requirements

The field testing requirements were meant to constraint the design so that iAAV-1 would be able to realistically carry out its functionality of maneuvering from point A to point B:

1. Operate on uneven surface with obstacles in rainforest terrain. To adopt the developed near-range visual guidance system (Teoh et. al., 2010), the vehicle has to satisfy amphibian requirements to travel on-land, on-water, and areas characterized by a combination of the two such as marshes.
2. Deliver up a good low-speed vehicular (LSV) performance of 30 km/hr. In accordance to National Highway Traffic Safety Administration (NHTSA)(IIHS, 2012) safety standards, a LSV must have 4 wheels and able acquired a top speed between 32 - 40 km/hr.
3. Turn and changes direction within 1 meter radius of vehicle space. In accordance to a report (Tai et. al., 2009), the minimal size of conduits to be installed in deep tunnel sewerage vary between 1.1 m to 1.2 m diameter.
4. Cruise at around 3.6 km/hr during water operation. An under-achieving 6 wheeler ARGO ATV wheel-based propulsion recorded 3 km/hr on-water (Tran et. al, 2007).
5. Controlled by either a single man operator or by unmanned control for autonomous implementation.
6. Operate up to 8 hrs without recharging.

Key aspect in the design of iAAV-1 being developed in this project is the provision mobility for AAV to traverse in confined narrow areas and in conjunction of being amphibious to intact with water. The requirements of the iAAV-1 in terms of mobility have been defined as follows:

1. The turning radius of the vehicle should be 0 mm. The search and rescue vehicle should ideally possess zero radius turn for exploration in confined and unstructured spaces.
2. Single drive system for land and water travel. A favourable drive system component with fewer control variables to implement autonomous control.
3. Basic control for navigation: two controllable degree of freedom for moving forward/backward, and turning left/right.
4. Traction control for uneven surface navigation: three degree of freedom for yawing, pitching and rolling.

3.3.3 Locomotion Mechanism

The vehicle plan view shown in Figure 3.10 (a), is a conventional four-wheeler vehicle. The two large front wheels provide drive and steering capability, while the two rear wheels act as a support and steering module. To regain a potential autonomous vehicular without stop-and-steer mechanisms, the iAAV-1 adopts the zero radius turn (Figure 3.10 (b)) with the Ackermann steering for navigation and performs obstacle avoidance. To compensate the zero radius turn, proportional differential directional drive is used as the same mechanism as a prime mover on both land and water travel.

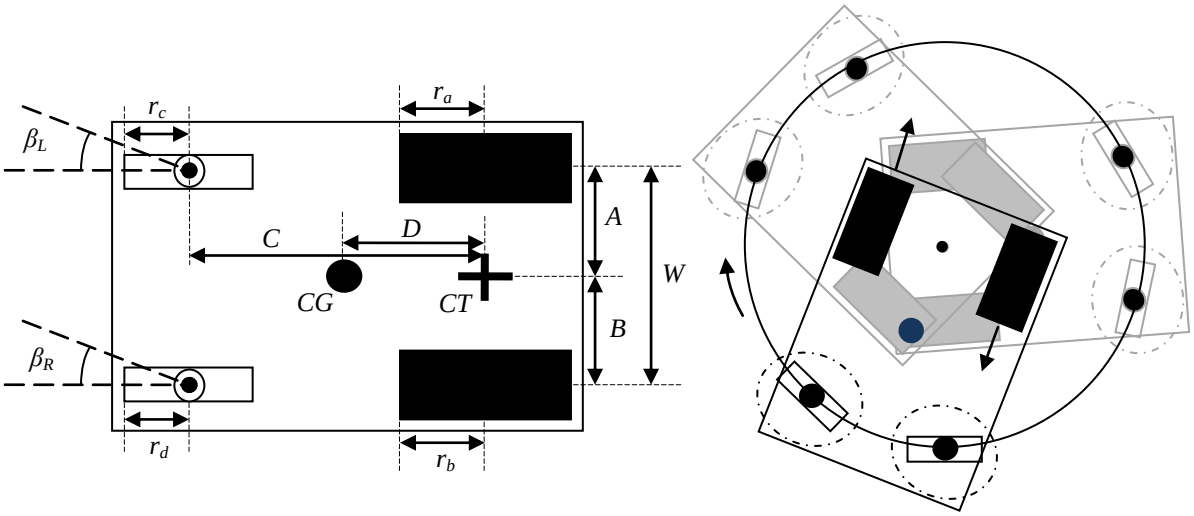

Dimensions indicator

W	= width of vehicle/distance between drive wheels
A	= width distance from left wheel to centerline
B	= width distance from right wheel to centerline
C	= axle to rear wheel pivot distance
D	= axle to center of gravity
CG	= vehicle center of gravity
CT	= vehicle center of zero radius turning
r_a	= left prime mover wheel radius (m)
r_b	= right prime mover wheel radius (m)
$r_c = r_d$	= left/right steering wheel radius (m)
β_L	= left rear wheel heading angle
β_R	= right rear wheel heading angle

Figure 3.10: (a) iAAV-1 plan view (b) zero radius steering configuration

This configuration was chosen because it offers several off-road navigation benefits when compared to some previous AAV designs of four or more wheels. The benefits from four wheel lateral stability to zero radius turn capability offers good mobility when compared with drive-steer configurations which must be translated in order to turn. The differential drive is also mechanically simpler because it does not require rotation of a driven axis. On water, proportional output velocity of both sides of the wheels allow iAAV-1 to steer on water.

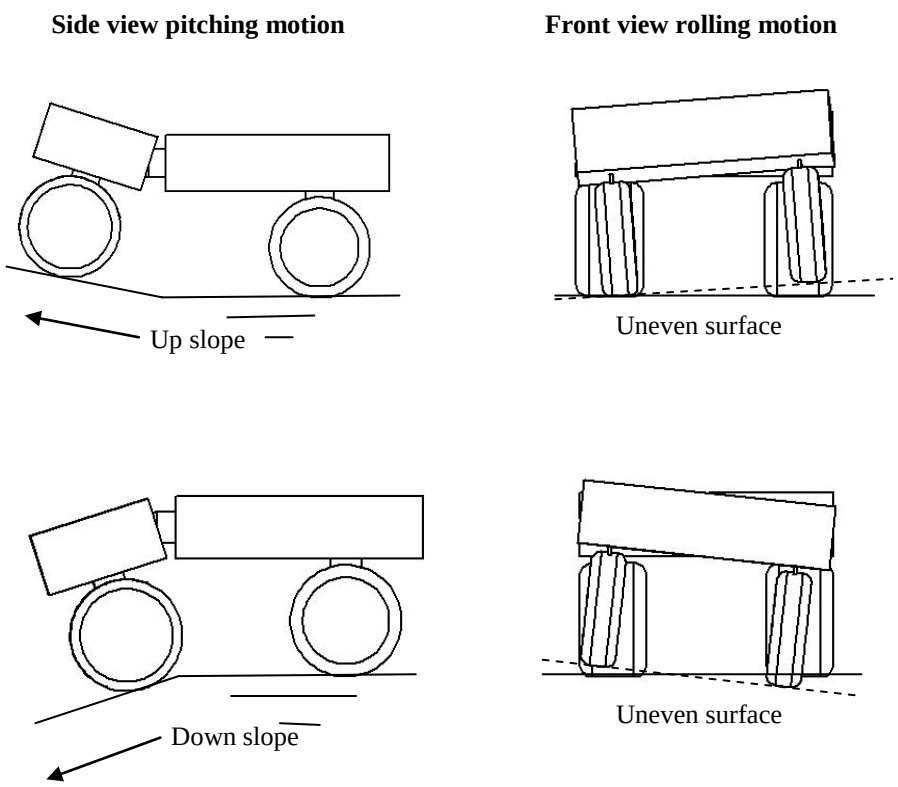

(a) Pitching motion (b) Rolling motion

Figure 3.11: Visualizing of the iAAV-1 pitching and rolling motion

Since no common rotation of driven axis is required in all the wheels, separation modules by articulation suspension can be used to improve vehicle traction on uneven surface, especially at low speed. The articulated suspension system is visualized in Figure 3.11 with the acting pitching motion and rolling motion. The main function of this system is to absorb external shock and hence protect the delicate electrical component in the chassis while moving on rough surface. This system will also help the vehicle move to a higher level surface as the front wheels are able to elevate for some level. The articulated suspension system is mounted in between the rear steering module and the main frame of the vehicle.

3.3.4 Kinematics Model

The development of the kinematic relationships for iAAV-1 defines the vehicle motion that used to develop a dynamic model of the vehicle. This modelling is used to implement in the vehicle controls development at the actuator level.

In developing algorithm for controlling iAAV-1, the relationship between the rotating wheels and movement has to be clearly defined to calculate the specific gross motion of the vehicle. The algorithm requires taking into consideration slight variations in the dimensions which may yield significant errors in the dead reckoning estimations for position errors. As shown in Figure 3.10, the iAAV-1 plan view is given a symmetric but separate vehicle dimensions to allow slight variations due to manufacture/fabrication and operation faults.

The features of iAAV-1 differential drive and the Ackermann steering moving in a horizontal plane is shown in Figure 3.12. The constraints are based on behavior of the rotating wheels when the vehicles is considered in a two dimensional Cartesian plane. The rigidity body of the vehicle moving in the planar motion consists of an imaginary point in the plane of motion known as the instant center, (x_o, y_o). The instant center is a point about which the vehicle is in pure rotation.

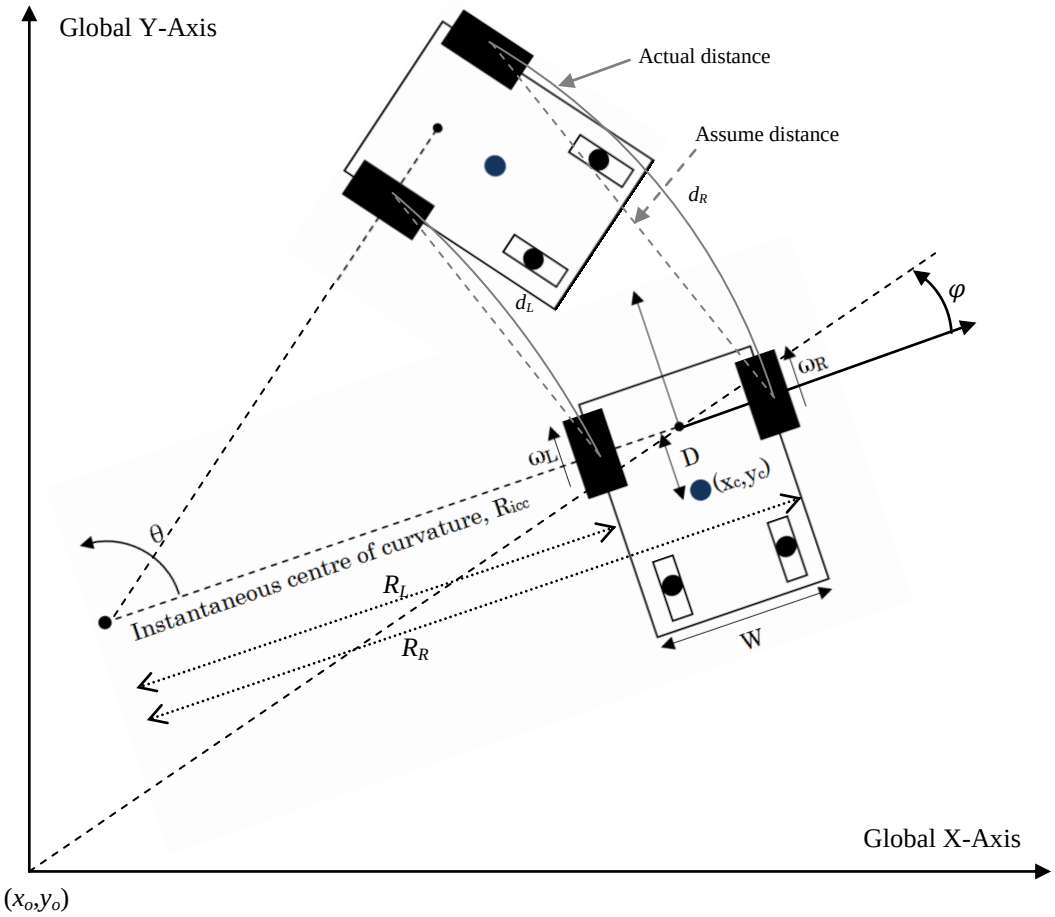

Constants indicator

(x_o, y_o) = Instant center
(x_c, y_c) = Center position of vehicle
R_{icc} = Instantaneous center of curvature radius
θ = Instantaneous center of curvature angle
φ = Heading angle
ω_L = Rotation angle of left wheel
ω_R = Rotation angle of right wheel
R_L = Instantaneous center of curvature left wheel radius
R_R = Instantaneous center of curvature right wheel radius
d_L = Distance travelled for left wheel
d_R = Distance travelled for right wheel

Figure 3.12: The iAAV-1 maneuverable classification and the depiction of distance travel of the front left and front right wheel of the vehicle in a turn

The vehicle undergoes both translation and rotation as it moves in the plane, rotating about (x_o, y_o). As the vehicle moves about the arcs, d_L and d_R, traced by the wheel path that moves around the instantaneous centre of

curvature at the same angle defined by θ. The instant center is not fixed in space, and moves as the vehicle path changes, when the rotation of wheel speed, ω_L and ω_R changes over time. They can be deduced as follows:

$$\dot{\omega}_R = \theta(R_{icc} + \frac{W}{2}) \tag{3.4}$$

$$\dot{\omega}_L = \theta(R_{icc} - \frac{W}{2}) \tag{3.5}$$

Using the velocities of Equations (3.4) and (3.5) of the rotating left and right wheels, ω_L and ω_R respectively, the instantaneous center of curvature radius, R_{icc}, and instantaneous center of angle, θ can be derived as follows:

$$R_{icc} = \frac{W(\dot{\omega}_R + \dot{\omega}_L)}{2(\dot{\omega}_R - \dot{\omega}_L)} \tag{3.6}$$

$$\theta = \frac{(\dot{\omega}_R - \dot{\omega}_L)}{W} \tag{3.7}$$

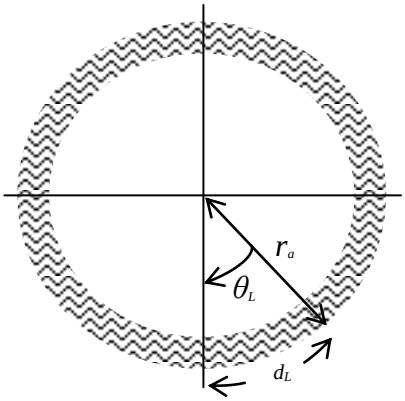

Figure 3.13: Left side drive wheel elevation view

Figure 3.13 shows the elevation view of the left wheel. As the wheel rotates through an angle, ω_L, the vehicle moves forward a distance, d_L. The vehicle is steered by driving one wheel at a greater distance than the other over the same interval of time. The shaft encoder is used to return a counter tick value; the rotation direction of the rotating wheel is given by positive or

negative value returned by the encoder, while the number of tick counts, T_i is one cycle wheel rotation. This kinematics constraints yield the following geometric relationships between wheel rotations and distance travelled:

$$d_L = r_a\theta_L = R_L\theta = \frac{2\pi r_a T_L}{T_{res}} \tag{3.8}$$

$$d_R = r_b\theta_R = (R_L + W)\theta = \frac{2\pi r_a T_R}{T_{res}} \tag{3.9}$$

Whereby, T_L and T_R are depict the number of encoder pulses counted by left and right wheel encoders, respectively, and T_{res} is the encoder resolution. By solving Equation (3.8) and (3.9), R_{icc} and θ can be found as:

$$R_L = \frac{r_a\theta_L}{\theta} \tag{3.10}$$

$$\theta = \frac{r_b\theta_R - r_a\theta_L}{W} \tag{3.11}$$

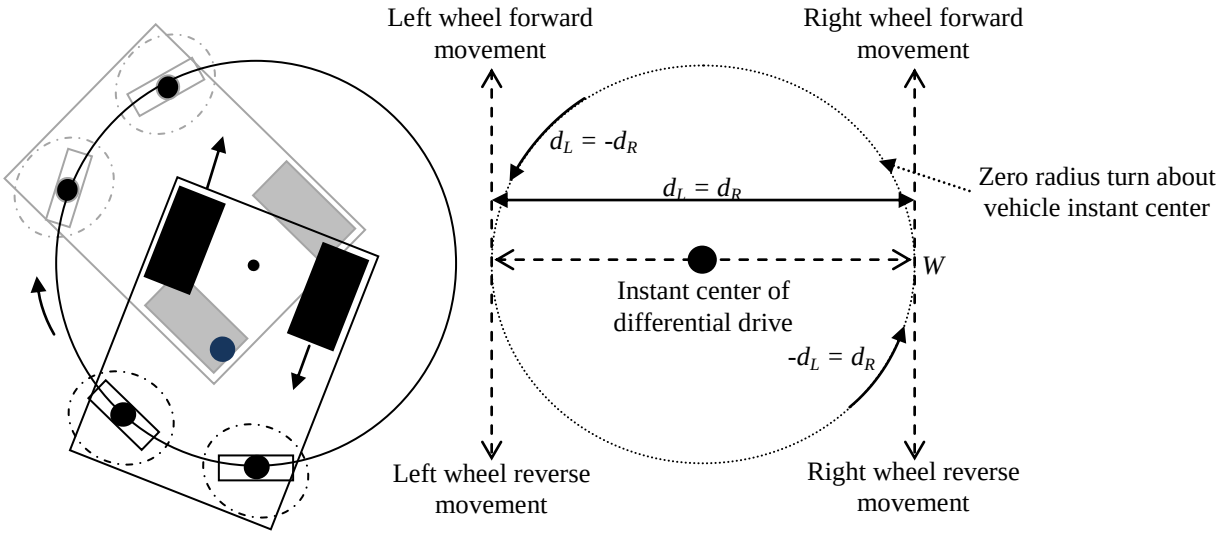

Figure 3.14: The iAAV-1 singularities about the instant center

Figure 3.14 shows the point at which the drive wheels axle and centerline intersect. The path of the vehicle will be described as the path of the

turning center traces in the plane as the vehicle rotates about the instant center. Using Equation (3.6) and (3.7), two singularities can be identified. When $\dot{\omega}_R = \dot{\omega}_L$, the radius of instantaneous centre of curvature, R_{icc} tends towards infinity and this is the condition when iAAV-1 is moving in a straight line. When $\dot{\omega}_R = -\dot{\omega}_L$, iAAV-1 will be rotating about its own center, the instantaneous center of curvature, R_{icc}, is null (Figure 3.14). By using geometry to calculate, the rate of change of heading, or turning rate can be calculated by differentiating Equation (3.11) to give us:

$$\dot{\varphi} = \dot{\theta} = \frac{r_b\dot{\theta}_R - r_a\dot{\theta}_L}{W} = \frac{\dot{\omega}_R + \dot{\omega}_L}{W} \tag{3.12}$$

The speed of the vehicle, V_v, along the path travelled by the turning center is given by the weighted average of speeds along the arcs d_L and d_R. The relationship is calculated using the following equation, whereby, for a normal case, A and B geometry (Figure 3.10) are equal:

$$V_v = \frac{r_b\dot{\theta}_R + r_a\dot{\theta}_L}{2} = \frac{\dot{\omega}_R + \dot{\omega}_L}{2} \tag{3.13}$$

Since speed encoders are used to measure the wheel angular velocities, $\dot{\omega}_R$ and $\dot{\omega}_L$, the vehicle speed and turning rate can be calculated using Equation (3.12) and (3.13). In the global coordinate system, the right-hand rule for the y-axis derived the vehicle component velocities in y-axis and x-axis as:

$$\dot{x}_c = V_x = -V_v \cdot sin\,(\varphi) \tag{3.14}$$

$$\dot{y}_c = V_y = V_v \cdot cos\,(\varphi) \tag{3.15}$$

The maneuverable iAAV-1 has three degrees of freedom, which are its position in two axes and its orientation (Equation (3.14) and (Equation 3.15)) relative to a fixed heading angle (Equation (3.12)), as shown in Figure 3.15.

Although the rate of change of the heading angle given by Equation (3.12) is a function of kinematics, without linearization of the component velocities, the absolute heading angle, φ, is not a function of the vehicle kinematics. Henceforth, given an initial heading angle, φ_o, Equation (3.12) can be numerically integrated to give an estimate of the absolute heading angle. Using this estimate for heading angle, the component velocities can be calculated using Equation (3.14) and (3.15), and numerically integrated to give an estimate of position based on dead reckoning.

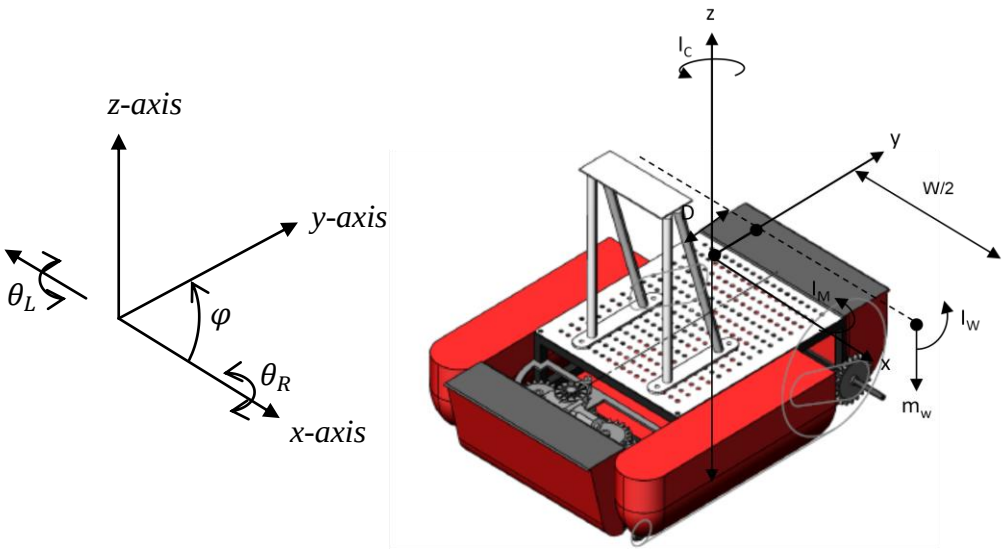

Figure 3.15: The iAAV-1 non-holonomic based on early CAD conceptual

The translation and rotation of iAAV-1 in the direction of the axis of symmetry is represented as follows:

$$V_y \cdot cos(\varphi) - V_x \cdot sin(\varphi) = D\dot{\varphi} \tag{3.16}$$

Where φ describes the heading angle of iAAV-1, which is referenced from the global x-axis. The vehicle has two controllable degrees of freedom, which control the rotational velocity of the left and right wheel affecting the changes in rotation and the heading angle of the vehicle; the relationship can be depicted as follows:

$$r_b \cdot \dot{\omega_R} = V_y \cdot sin(\varphi) + V_x \cdot cos(\varphi) + W \cdot \varphi \tag{3.17}$$

$$r_a \cdot \dot{\omega_L} = V_y \cdot sin(\varphi) + V_x \cdot cos(\varphi) - W \cdot \varphi \tag{3.18}$$

The vehicle speed and turning rate are linear with respect to the wheel angular velocities. This linearity allows for the development of a linear control based on kinematic geometry of the vehicle described above. With a desired input velocity, V_{ref}, and a desired vehicle rate of rotation, φ_{ref}, Equation (3.12) and (3.13) can be re-arranged to calculate the required wheel velocities:

$$(\dot{\omega_L})_{ref} = \frac{2V_{ref} - W\dot{\varphi}_{ref}}{2r_a} \tag{3.19}$$

$$(\dot{\omega_R})_{ref} = \frac{2V_{ref} + W\dot{\varphi}_{ref}}{2r_b} \tag{3.20}$$

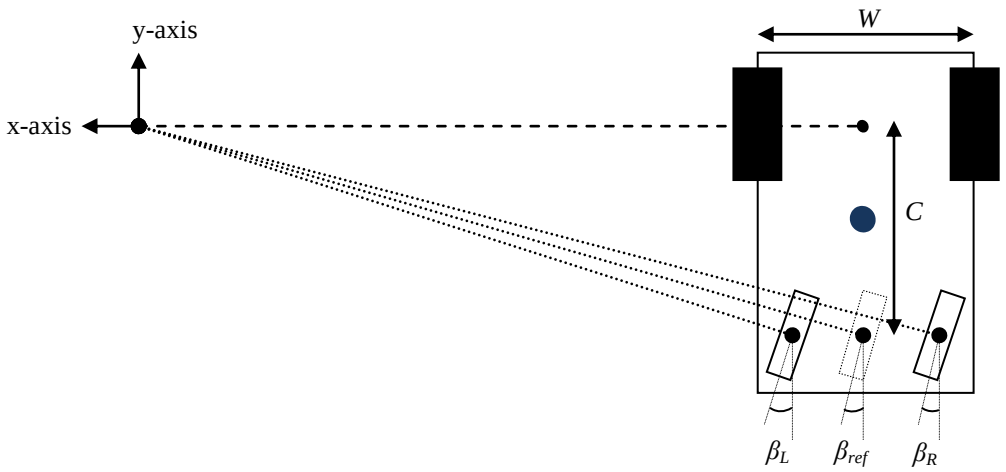

Figure 3.16: The iAAV-1 Ackermann-steered vehicle with extended axes for all wheels intersect in a common point

As seen in Figure 3.16, the extended axes for the two rear wheels intersect in a common point that lies on the extended axis of the front drive wheel axle. The locus of points traced along the ground by the center of each tire is thus a set of concentric arcs about this instant center of rotation. Such a steering geometry is said to satisfy the Ackermann equation when all the instantaneous velocity vectors will subsequently be tangential to these arcs (Byrne et. al., 1992). The relative steering angle left, β_L and right, β_R steering wheel have a relationship as follows:

$$cot(\beta_L) - cot(\beta_R) = \frac{W}{C} \tag{3.21}$$

For convenience, an imaginary center wheel steering angle, β_{ref}, can be regarded as the angle relative to the vehicle heading angle (Figure 3.16). The associated steering angle, β_{ref}, can be expressed in terms of the inside or outside steering angles, β_L or β_R, as follows:

$$cot(\beta_{ref}) = \frac{W}{2C} + cot(\beta_L) \tag{3.22}$$

$$cot(\beta_{ref}) = cot(\beta_R) - \frac{W}{2C} \tag{3.23}$$

The vehicle steering speed, V_c is calculated by:

$$V_c = r_c \cdot \dot{\beta}_{ref} \tag{3.24}$$

Since V_c lies along the vehicle centerline prependicular to V_v, the following relationship can be obtained for V_v and $\dot{\varphi}$:

$$V_v = V_c \cdot cos(\beta_{ref}) = r_c \cdot \dot{\beta}_{ref} \cdot cos\ (\beta_{ref}) \tag{3.25}$$

$$\dot{\varphi} = \frac{V_c}{C} \cdot sin(\beta_{ref}) = \frac{r_c}{C} \cdot \dot{\beta}_{ref} \cdot sin\ (\beta_{ref}) \tag{3.26}$$

Using absolute encoders to measure the β_L and β_R, these equations can be used to augment the dead reckoning obtained from the rear wheel sensors alone.

The kinematic relationship outlined is a non-holonomic constraints for iAAV-1. For simplifying assumptions, the wheel rotation of the two drive wheels is assumed to be anti-slippage when rolling. Also, because the equation of the vehicle speed and turning heading angle rate are functions of the derivatives of the generalized position coordinates, this leads to a non-integral expression for the absolute vehicle position, and adds complication beyond the research scope. The main concern for control development is that the steering and velocity control are stable. A high-level function, such as navigation and mapping in autonomous control are ones that concerned with the absolute position. However, the low-level motor controls are not concerned with the vehicle position. Therefore, the absolute position can be neglected. The wheel rotations are the only needed entity for the system to become a holonomic system with only two generalized coordinates for both drive wheels, θ_L and θ_R. To put forth these control relationships, the vehicle architecture used for the vehicle controls, as well as the details of the motor control algorithm can be developed.

3.4 Control and Components Architecture

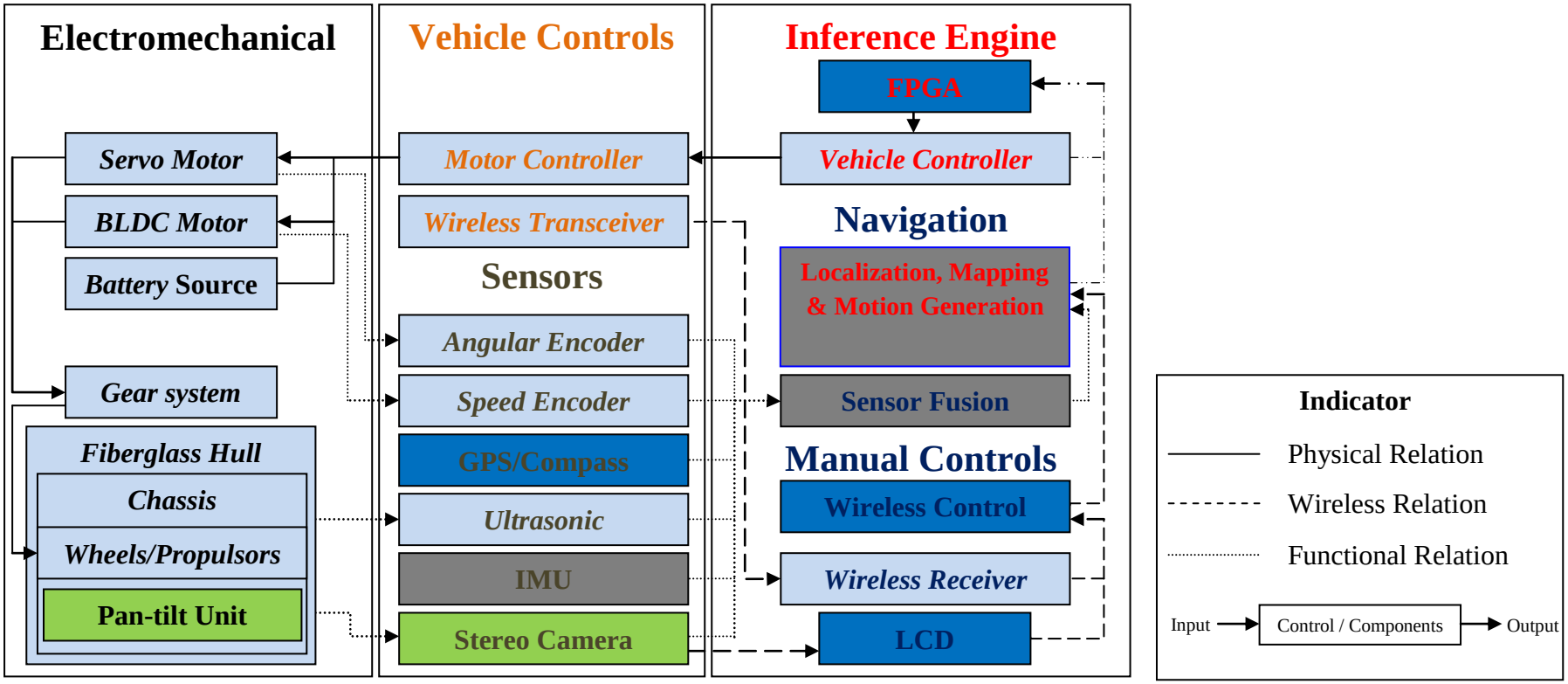

Figure 3.17: The iAAV-1 physical & functional decomposition

This section gives a description of the three architectures that are proposed for iAAV-1 use together with the organization of the controls, components, and software architectures. The vehicle controls obtained a modular, scalable design which reduces the overall complexity of the design such that the subordinate modules receiving commands from main-ordinate modules. Figure 3.17 shows the physical of iAAV-1 which decomposes of the following three functional levels:

1. **Vehicle electromechanical level** - hardware and mechanical design of iAAV-1. They were made up of two brushless DC (BLDC) motors, two servo motors, batteries to supply energy, gear system on each drive wheels, the fiberglass body hull encloses a waterproof compartment for electronics components, the structural chassis, wheel propulsors, and the camera pan-tilt unit.

2. **Vehicle control level** - comprises of motor controller, wireless devices, and various sensors such as angular encoders, speed encoders, global positioning (GPS) unit, digital compass, ultrasonic range finder, inertial measurement unit (IMU), and stereo camera. The motor controller using specific pulse-width modulation (PWM) generator is responsible for the vehicle motion control using microprocessor in each DC motor controllers to handle the two-wheel drive configuration which incorporates the rotatable rear wheels at a low level function.

3. **Vehicle inference engine level** - comprises of the Field Programmable Gate Array (FPGA), allowing the program generator and process analyzer to execute the vehicle command through the vehicle control module. It is

demonstrated by combining the image processing, obstacle avoidance and sensor fusions task simultaneously. Information provided will be processed by the real-time control system to allow path planning, navigation and mapping. A manual remote control will handle the serial communication between the computer and the iAAV-1 platform with the low level controller that controls the BLDC and servo motor controllers for driving tasks.

The initial tier of operation involved the hardware acquisition, set up, and calibration of the sensors of the said platform. They are indicated (Figure 3.17) in ▭ colour and italic wordings. The second tier will be to integrate the data from sensors into useable navigation data. Teoh et. al (2010) launched the research with the aim to provide solution for a near-range visual guidance in the rainforest terrain. The scheme and hardware which Teoh et. al. developed was based on stereo camera as indicated in Figure 3.17 is shown in ▭ colour how it is acquired into iAAV-1. The visual guidance using stereo camera will handle the movement of iAAV-1 by guiding the vehicle to move around and subsequently handles obstacle avoidance. The other visual guidance as part of the real-time controller is the ultrasonic range sensors, GPS, digital compass, and IMU sensor data fusion. Chan et. al. (2010) works was responsible for most of the third and final tier which involved integrating FPGA and sensors. Implementing FPGA technology for parallelization across multiple modules is reported to be sufficient to provide the necessary basis for the high-level function system design. The highlighted functions in ▭ colour will be the future focus before placing the end-product in the field.

3.4.1 Vehicle Architecture

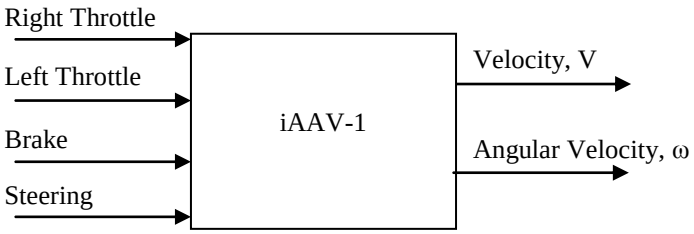

Figure 3.18: Work principles input-output

Figure 3.18 shows the incorporated drive control system receiving input from the varying speed of each individual's transmission on the left and right. Accordingly, the adjustable actuators will output the direction and speed of the vehicle to be driven or steered. The brake actuator signals the brake system located on each transmission on the left and right as an integrated device with the prime mover. The steering wheel is a separate device which co-operate with the differential drive and facilitates the steering for a zero radius turn. Figure 3.19 is a block diagram of the vehicle in accordance with the principles presented above.

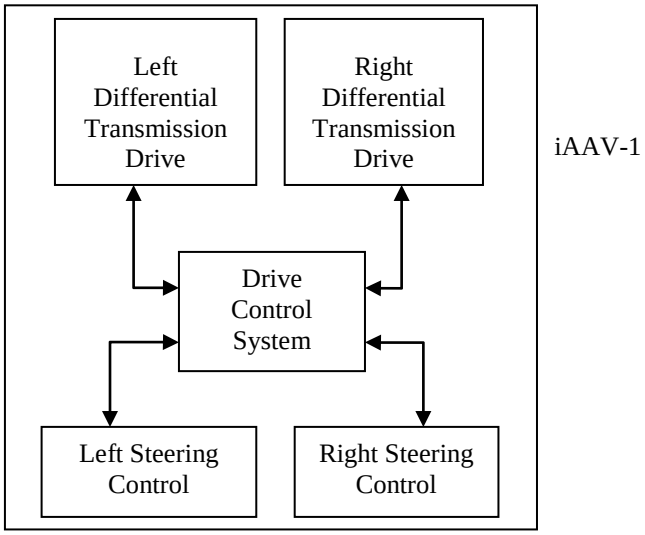

Figure 3.19: Block diagram

Components in this control system can obtain a modular, scalable design, which reduces the overall complexity of the design. Each module receives a command from the drive control system module. Each module here (Figure 3.20) is generally responsible for handling a symmetric task, with the resultant output provided as an input to a sub-module. Typically, these modules are decomposed based on the functional requirements developed earlier. These functional modules must be complete before iAAV-1 can be operated. On the other hand, modularity is the strength of this system. Necessary changes or problem debugging of the entire system can come down to a singular modular. Provided the interfaces do not change in the control system, changes to one hardware module can be isolated from the other modules.

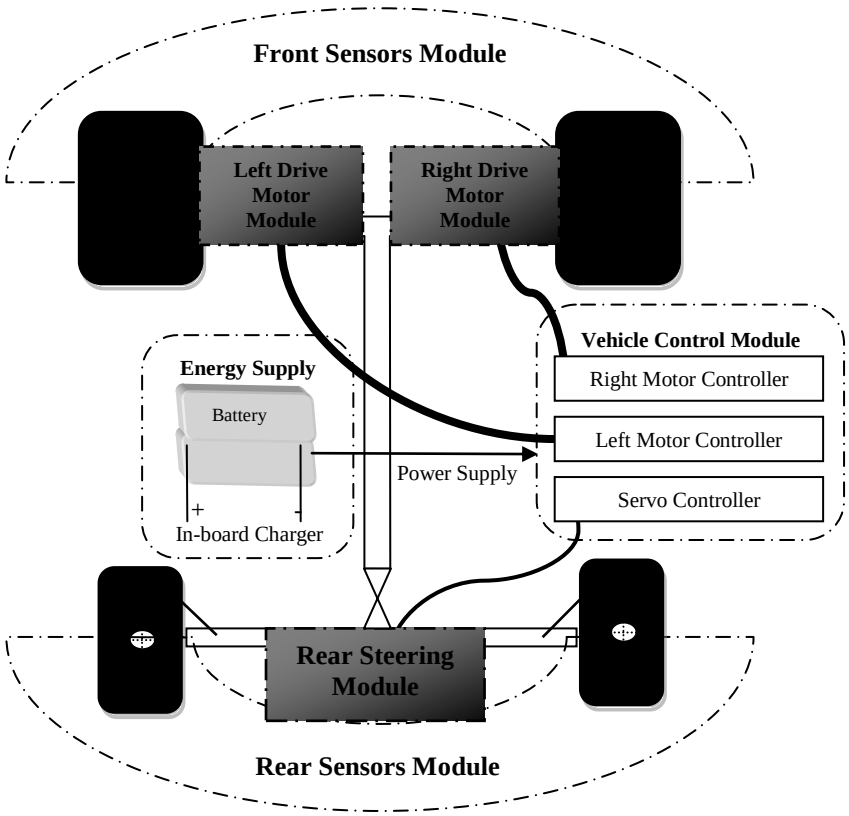

Figure 3.20: Mechanical schematic

One aspect of iAAV-1 design is the vehicle which comprises of five separate modules as indicated in Figure 3.20:

- Front prime mover module
- Rear steering module
- Vehicle control module
- Sensors module
- Energy supply module

The basic details of each individual hardware components are researched and selected before being built up to a more sophisticated level of operation. From a high-level viewpoint, the vehicle was envisioned to be an end-product capable of being remotely control and communicated with the operator to provide new command containing a map of predefined locations where the vehicle needs to go. Autonomously, the vehicle will decide appropriate actions to move to the desired location. Simultaneously, the vehicle will send the vehicle status to the user so that the operator would know if the vehicle becomes lost, encounters an error, or reaches its destination. Once a command is given to the vehicle, the low-level function takes over by ascertaining its position using internal GPS and a digital compass. The vehicle may not be facing the correct direction initially, and it requires orientating itself using zero radius turn in the proper direction. By utilizing the stereo camera to make sure the starting location is on the path, the vehicle will start moving forward, turning where needed, and speeding up or slowing down to improve the accuracy of the data being taken in by other sensor sampling vehicle condition data such as IMU, ultrasonic, and encoders.

This operation will be executed in the form of several feedback loops between sensors and algorithm to maintain the vehicle on paths. Differential electromechanical DC drive motors and zero radius turn module are two motion control hardware to execute commands from the path planning. This is accomplished by dynamically changing the prime mover motor speed and rear wheels steering angles. Figure 3.21 below is the whole vehicle architecture.

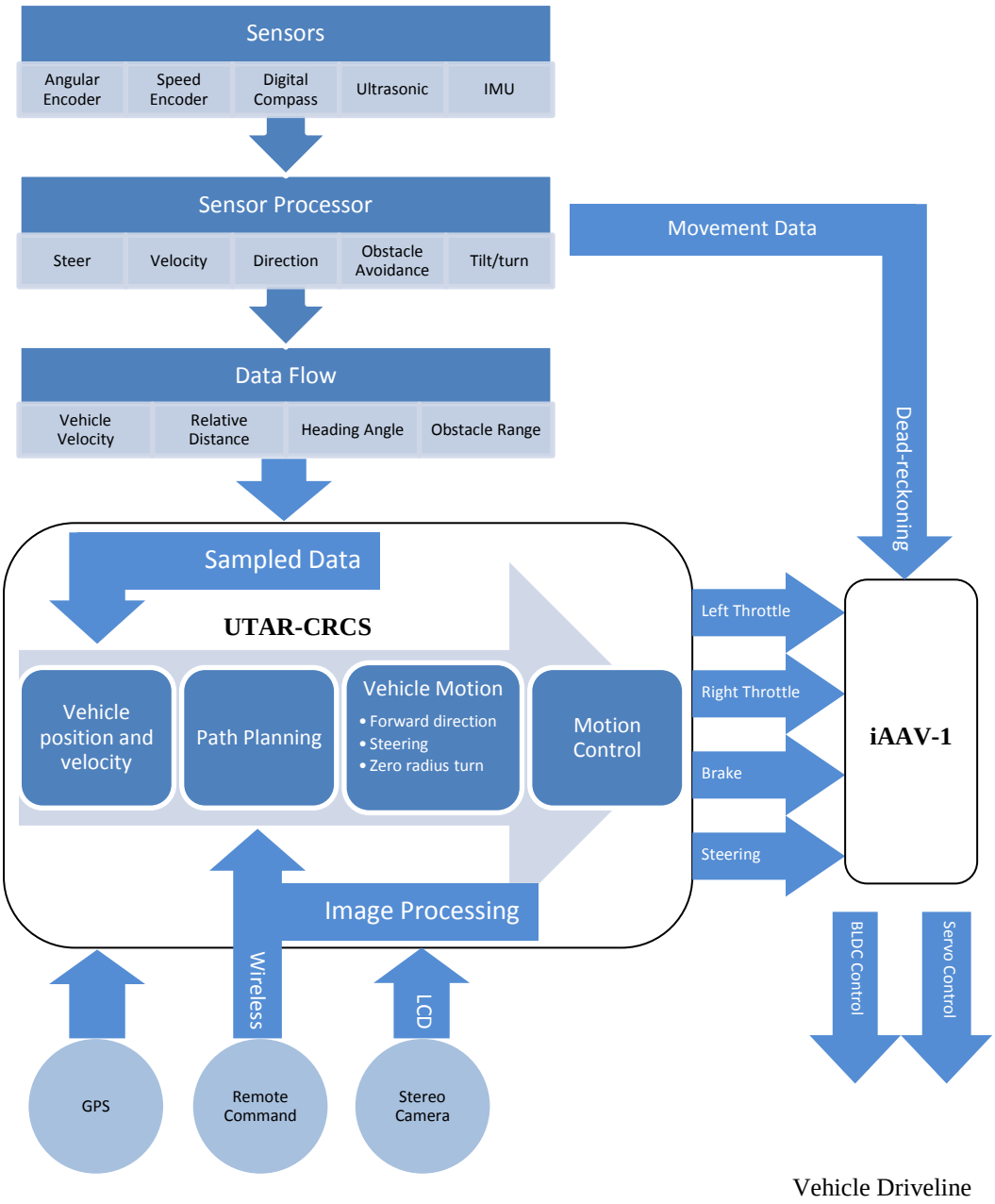

Figure 3.21: The iAAV-1 architecture system

3.4.2 Vehicle Control

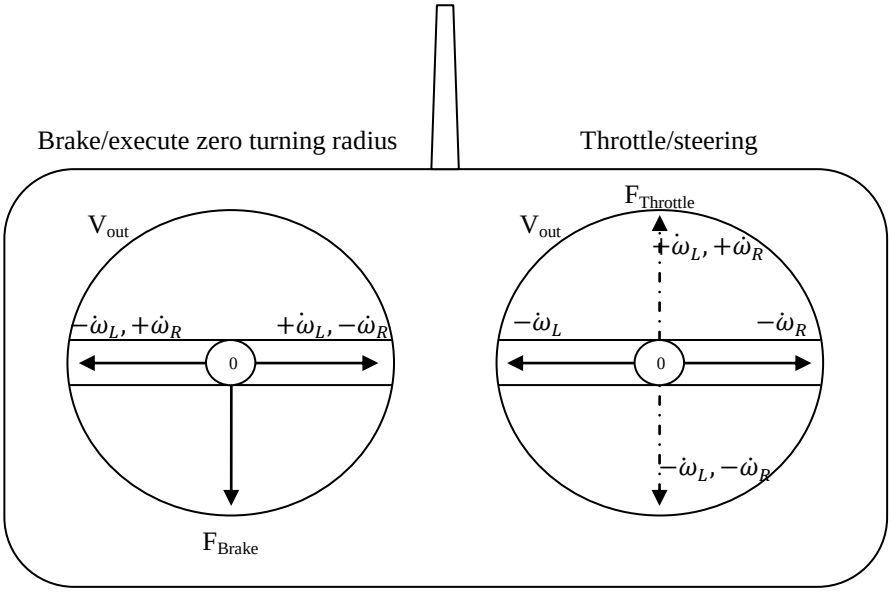

Figure 3.22: Illustration of remote control configuration

The iAAV-1 can be operated in manual mode by specifying the vehicle speed, V_{ref} and rate of change of heading angle, $\dot{\varphi}_{ref,}$ directly through a remote control. Given the desired V_{ref} and $\dot{\varphi}_{ref}$ in Equation (3.19) and (3.20), the desired wheel velocities, $\dot{\omega}_L, and\ \dot{\omega}_R$ can be calculated. Figure 3.22 illustrates how to facilitate the remote control configuration in manual mode. The right-hand-side joystick (RHS) operates the drive wheels while the vehicle is in motion. On the other hand, the left-hand-side (LHS) joystick operates the vehicle while the vehicle is in static position; stop-and-steer-mechanism allow to perform the zero radius turn. Besides, the brake is placed with the LHS joystick as a separate trigger when there is an emergency. When both LHS and RHS joystick are pushed to the left/right, the output voltage source is reduced in the direction to reduce the drive wheel velocity, simultaneously. The regenerative braking is activated to slow down the wheel velocities for steering.

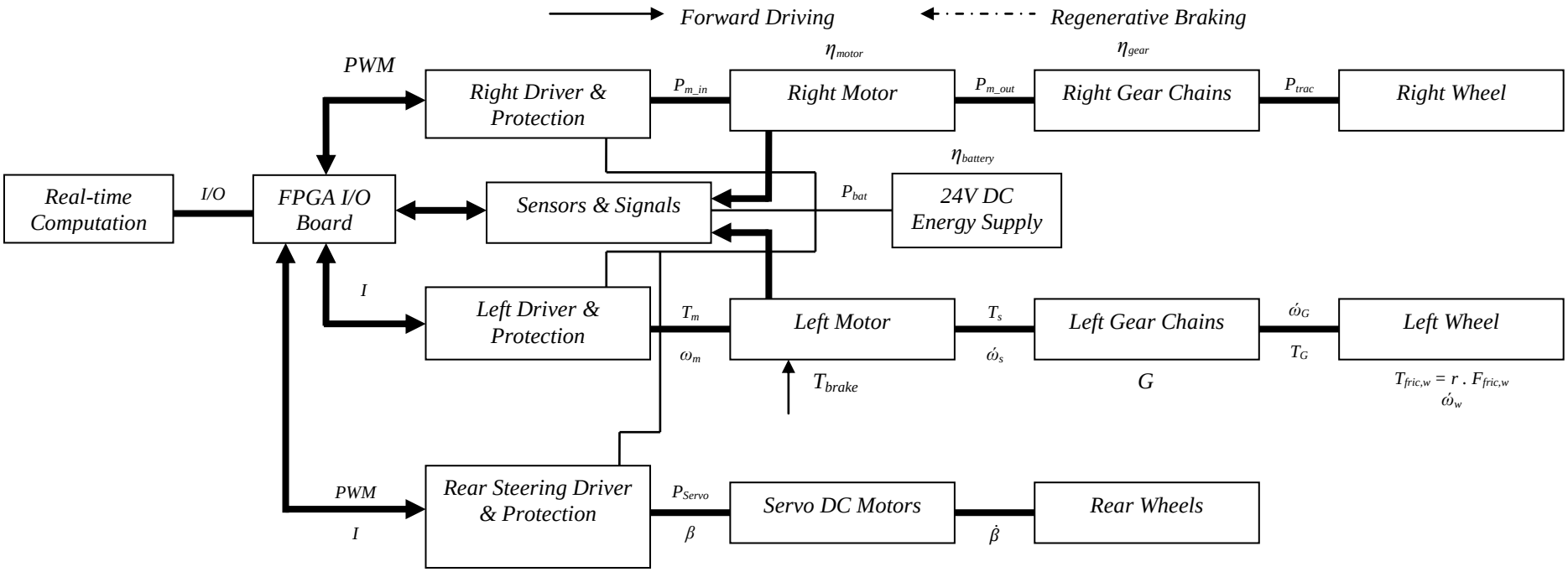

Figure 3.23: Driveline modelling (top flow), energy flow (centre flow), and zero radius turn modelling (bottom flow)

The vehicle driveline consists of the structure of differential and zero radius turn as shown in Figure 3.23 along with their distributed torques, speeds, and energy. The driveline of iAAV-1 is equipped with speed sensors on the respective motors for measurements of the motor speed and IMU is to provide the iAAV-1 attitude, orientation and rotational speed for signal processing. The differential drive and the brake system will decide the movement and turning of the vehicle. The differential distributes the torques separately from motor to each gear chain to run the wheel. The additional rear steering module is engaged in assisting the vehicle on the stop-and-turn zero radius turning which is controlled separately by the servo DC motor on two rotatable wheels. An external I/O board was specifically built to interface between FPGA and DC motor controllers. The real-time computation system (RCS) continuously send digital data stream through the FPGA Serial Peripheral Interface (SPI) through the digital-to-analogue convertor (DAC) to control all the DC motors. All the hardware, including the sensors are connected to a DC voltage source. In this case a battery, before channelling through the I/O board and uses pulse-width-modulation (PWM) to generate output voltage to the motor drivers. The motor control signals in the range of 0 to 5 VDC, and can generally be regulated to draw current based on the difference between supplied voltage and the counter-electromotive-force (EMF); the transfer of energy to the load provides the braking effect. For a given supply of voltage, the motor will accelerate until the counter-EMF balances the supply voltage such that the torque produced by the current matches the wheel load torque.

3.4.3 Differential DC Motor Drive

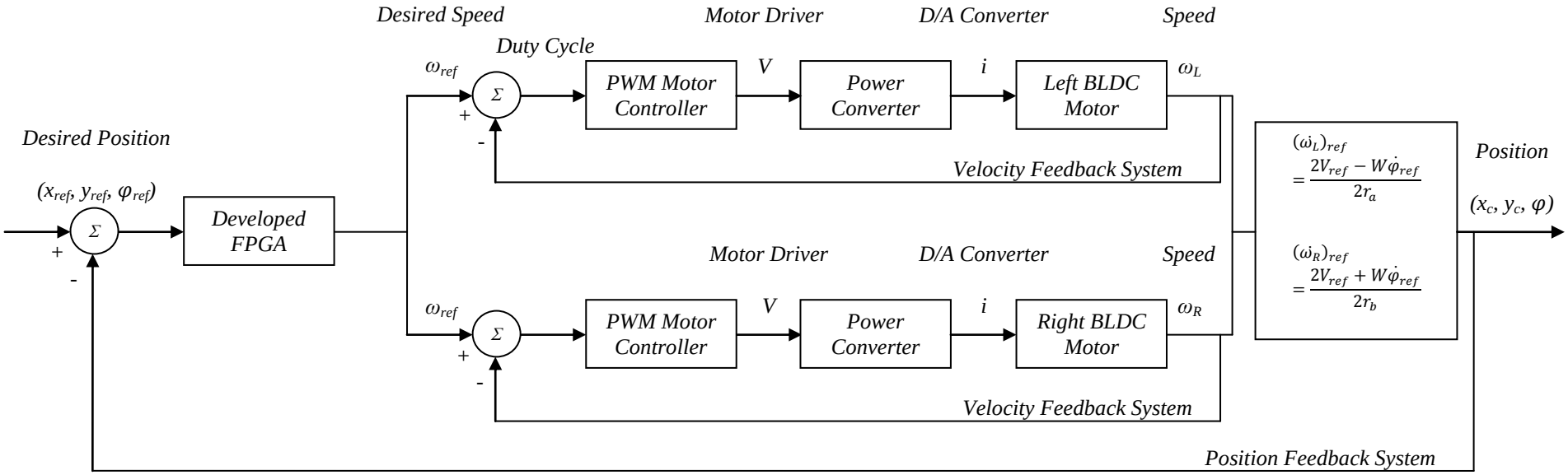

Figure 3.24: The control feedback system of the differential DC motor system

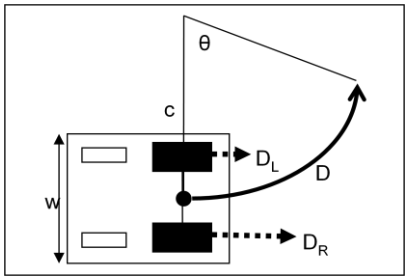

Figure 3.25: Differential drive

Figure 3.25 shows a simple approach of the differential drive vehicle driving forward, tackling a corner by increasing the speed of an outer wheel while slowing the inner one, and performing a zero-radius steer. Unlike an ordinary car steering, the differential drive eliminates the need for a complex mechanical design of vehicle steering. It directly transfers the power from the motor through a transmission gearbox used to increase the torque at wheels, while reducing the operation speed of the motor. Besides the dynamic angular velocity or direction of the drive wheel determines the directional motion on ground, different drive favours the travel in water with proportional outputs.

The controller block diagram shown in Figure 3.24 consists of two control loops: the velocity loop and the position loop. The position loop includes a Global Positioning System (GPS) signals with gains calculated to give the vehicle's real-time positioning. The motor speed controller has an encoder which signals the rotating speed of the motor to achieve a certain phase margin and bandwidth. The desired speed processed by the developed FPGA will simultaneously generate the PWM signals to both side of the motor through each motor controller and power converter before delivering variable torque load to the BLDC motor.

Figure 3.24 is compiled and transferred to the iAAV-1 and used for control of the actual vehicle using the developed FPGA board. Using this algorithm, the motor equation is transformed in a coordinate system that rotates with the rotor flux vector. The PWM motor controllers function for controlling the power converter so that the desired currents are supplied to the motor. The PWM motor controllers use Hall-effect sensors which feed the FPGA board with three phase reference currents, which is later converted to three phase reference control voltages. The three phase reference control voltages are given as follows, whereby, f = Frequency, and $\hat{u}_x$ = Amplitude:

$$V_A(t) = \hat{u}_x \sin(ft) \tag{3.27}$$

$$V_B(t) = \hat{u}_x \sin(ft - 2\pi/3) \tag{3.28}$$

$$V_C(t) = \hat{u}_x \sin(ft + 2\pi/3) \tag{3.29}$$

Assuming $\hat{u}_{tri}$ = amplitude of triangular voltage = 1, the duty cycles for the three phases are generated according to the following:

$$D_A(t) = \tfrac{1}{2} + \tfrac{1}{2}[\hat{u}_x/\hat{u}_{tri} \sin(ft)] \tag{3.30}$$

$$D_B(t) = \tfrac{1}{2} + \tfrac{1}{2}[\hat{u}_x/\hat{u}_{tri} \sin(ft - 2\pi/3)] \tag{3.31}$$

$$D_C(t) = \tfrac{1}{2} + \tfrac{1}{2}[\hat{u}_x/\hat{u}_{tri} \sin(ft + 2\pi/3)] \tag{3.32}$$

The duty cycles are fed into the PWM controller through the MOSFET to generate three phase voltages average values as follows, whereby, assuming V_{DC} = DC voltage source = 24 V:

$$\hat{u}_{A(ave)}(t) = V_{DC}/2 + V_{DC}/2\ [\hat{u}_x/\hat{u}_{tri} \sin(ft)] \tag{3.33}$$

$$\hat{u}_{B(ave)}(t) = V_{DC}/2 + V_{DC}/2\ [\hat{u}_x/\hat{u}_{tri} \sin(ft - 2\pi/3)] \tag{3.34}$$

$$\hat{u}_{C(ave)}(t) = V_{DC}/2 + V_{DC}/2\ [\hat{u}_x/\hat{u}_{tri} \sin(ft + 2\pi/3)] \tag{3.35}$$

3.4.4 Zero Radius Turn Module

A zero-radius steering for autonomous amphibious vehicle is achievable to improve the efficiency of the vehicle's autonomy driving ability which will take advantage of the two-wheeler design while adapting the track vehicle turning ability by using skid steering/differential drive system. As shown in Figure 3.27 (a), the iAAV-1 adopts the zero-radius steer (Figure 3.27 (b): zero radius turn) for navigation and performs obstacle avoidance in narrow areas. The vehicle uses a single drive system to maneuver on both land and water. An improved motion generation will regain the speed and potential of the autonomous vehicular without the stop-and-steer mechanisms, hence, enables the vehicle to perform an ordinary steering mechanism (Figure 3.27 (b): Ackermann steering) like conventional vehicular on road with less obstacles.

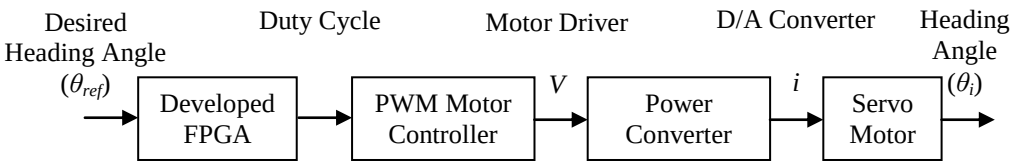

Figure 3.26: The control system of the zero radius turn steering system

The zero radius turn steering module is a separate independent open-loop function for wheel positioning. The module comprises a control system as shown in Figure 3.26. The DC motor driven vehicle requires the capability to negotiating a sharp turn such as a narrow route that is impassable for iAAV-1. In such a vehicle design, normally a pair of wheels with complicated assemblage of cams, levers and linkages is powered by small horsepower

motor to provide steerage for the vehicle. In addition, a separate forward-reverse direction control is required to change the direction of the motion of the vehicle. An electromechanical control is implemented on iAAV-1 with an open-loop block diagram that delivers any positioning the vehicle needs the wheel to be. The pair of steering wheels is independent of each other, thereby controlling the actual speed and actual steerage is included in the control. This control kept the excessive weight, error and even instability in check particularly because of the unknown load when excessive mechanical parts are used.

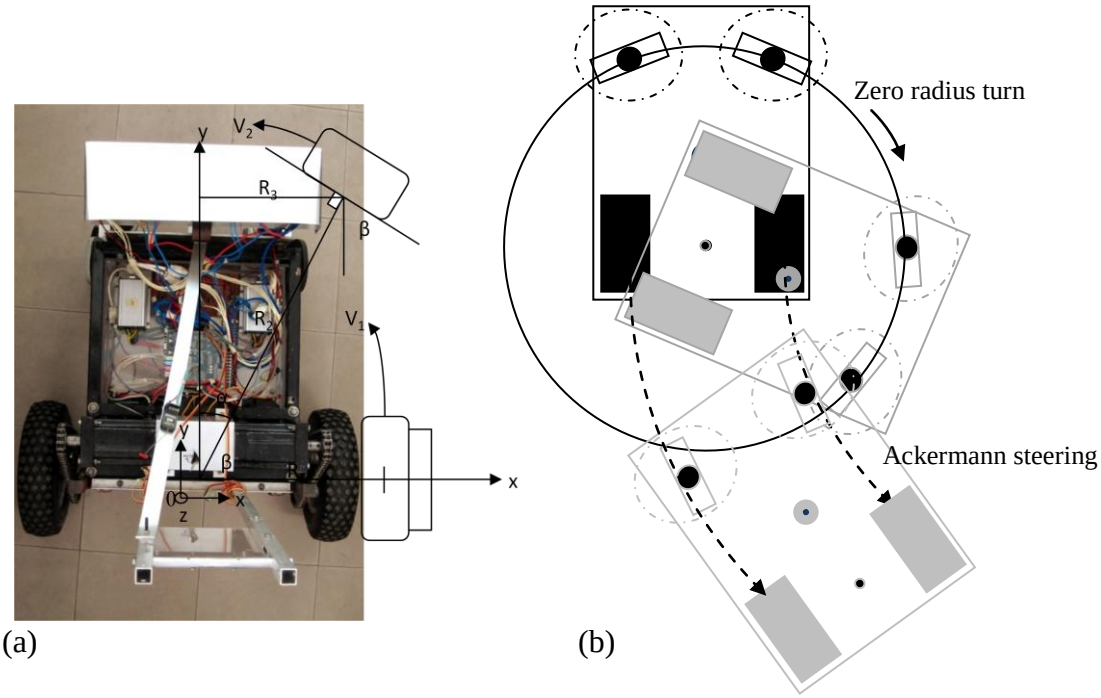

(a) (b)

Figure 3.27: Zero radius turn setup and steering configuration on the iAAV-1

Figure 3.27 shows the structure of the iAAV-1 where the zero-radius steering configurations were implemented. From the figure, the pivotal rear steering wheels are underneath the aluminium plating, while the two prime mover can be seen attached using the chain gear system at both sides of the vehicle.

3.4.5 Autonomous Planning

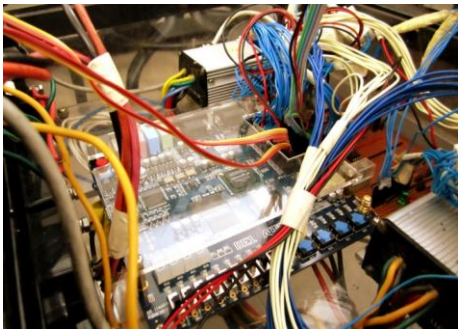

Figure 3.28: The Altera DE1 development board using Quartus II software

Field Programmable Gate Array (FPGA) (Figure 3.28) works as a processing units, microcontrollers and digital signal processors for iAAV-1. FPGA is a programmable semiconductor device which consists of configurable embedded SRAM & logic blocks, high sped transceivers and high speed I/Os and routing. Motivated by the need of the compact autonomous system in confined environment, the construction of FPGA based compact real-time control system have been rigorously tested by Chan et. al. (2010) before integration into UTAR's Compact Real-Time Control System (UTAR-CRCS) to perform specific operations such as data acquisition and communication.

UTAR-CRCS is the inference engine and navigation system of iAAV-1 platform. Components such as sensor, controller, driver, and remote control receiver were connected to the pins of Cyclone II 2C20 FPGA. The LCD monitor was connected to the VGA port on the board for real-time image display. Besides, GPS receiver module has also been developed to

communicates with DE1 board through RS-232 port. Each functional modules was constructed individually and separated from each other. They were integrated using Quartus II software together with custom build blocks and intellectual property (IP) blocks. An example of low-level vehicle control module is shown in Figure 3.29. In Quartus II, the logic structures of FPGA is written in VHDL or Verilog code, and all design blocks communicate in parallel link during real-time operation to exchange data and control signals. After compilation, UTAR-CRCS performance was analyzed from various aspects such as functionalities, timing requirements and stability; improvement can be made on individual block and then on the integrated system.

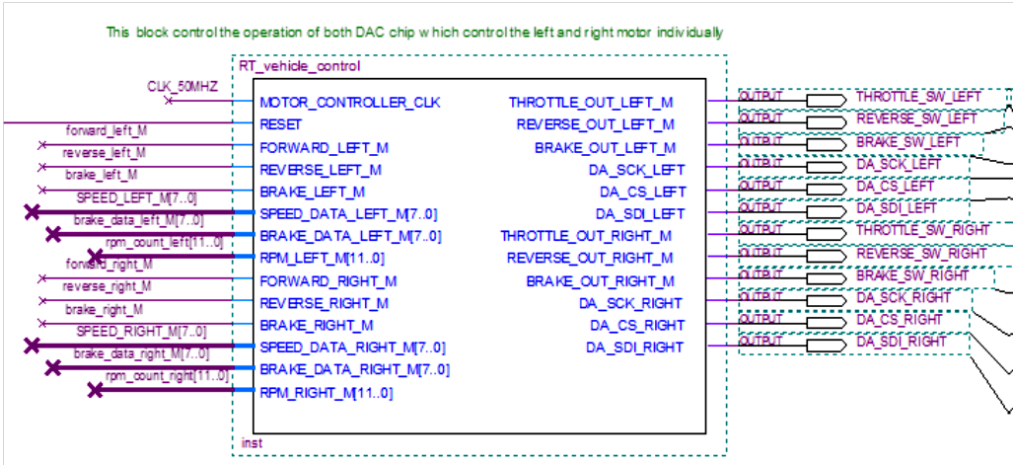

Figure 3.29: Low-level vehicle control module

The advantages of using UTAR-CRCS FPGA against other control systems of various autonomous vehicles:

- Ease of re-configuration. Some real-time control system was built using multiple PCs, micro-controllers and signal processor which can be challenging to carry out modification.

- The compact size of DE1 board weighs at only 0.28kg and needed a maximum 2.5W power consumption (USB power rating) to operate.

Autonomous planning for off-road and confined narrow environment navigation required the sensors system to complement each other for obstacle detection. Stereo range measurements rely on a colour-based camera for ground classification. The positioning of the camera has to be high so that projection on the ground will be finer. A stereo camera will not be effective with close obstacle detection, as ultrasonic range sensor detects anything within its radii and 3 meters close-up obstacles and prevent vehicle from collision. The GPS will be placed on top of the vehicle and is used for validation. However, the GPS may be able to acquire good position data in bad weather or confined area condition. In order to allow the real-time control system to track the vehicle's position, IMU is used to measures the orientation of vehicles on rough terrain, true vehicle velocity and gravitational forces using dead reckoning. Although IMU has the disadvantage of accumulated errors, IMU is compensated by other visual guidance sensors. Figure 3.30 illustrate a concept art of iAAV-1 with all the sensors equipped.

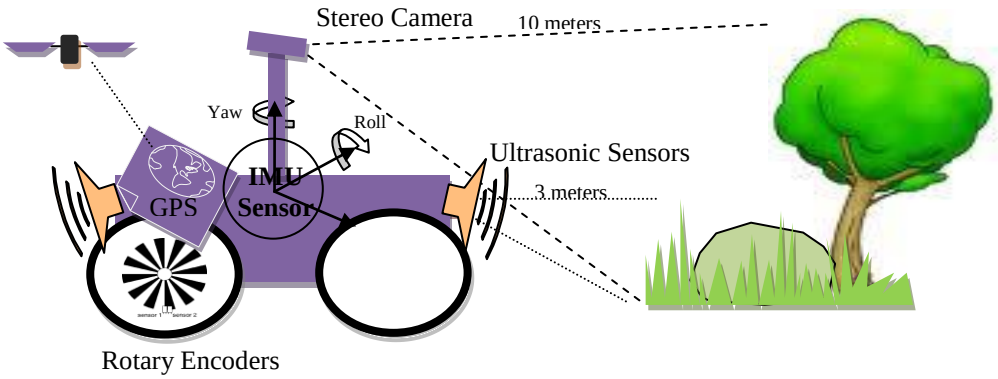

Figure 3.30: Concept art illustrating all sensors equipped on the iAAV-1

3.5 Prototype Platform

3.5.1 Mechanical Design

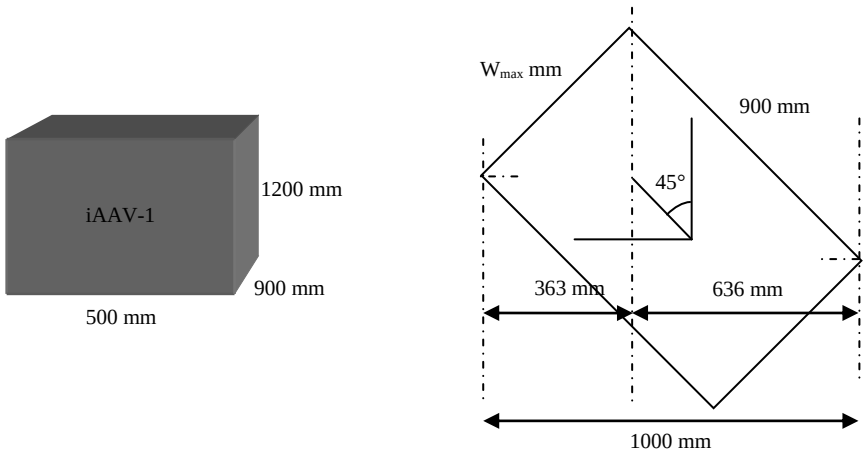

Figure 3.31: Black box considering maximum dimensions and computing maximum width length

General Dimensions - The vehicle was represented as a black box as the embodiment of the vehicle is unknown. Step by step the vehicle design was refined and each different module in the black box (Figure 3.31) will be given a particular embodiment to form the developed mechanical platform. In order for the iAAV-1 to access its way through the sewerage tunnel and a narrow space, the maximum dimensions of the black box are stated as: $L_{max} \times W_{max} \times H_{max} = (900 \times 500 \times 1200)\text{mm}^3$. The maximum length of the vehicle is kept within the minimal conduits size of 800 mm. As shown in Figure 3.31, the iAAV-1 is at its longest length at the sideways at 45° heading angle. Therefore, the maximum width of the vehicle is kept within 500 mm size. The height is a non-factor, but it is a good reference to place a stereo camera for visual guidance up high.

Chassis frame - With emphasis on the compact design, RCS was placed within an enclosed transparent waterproof casing, to prevent contact with water. The RCS compartment was held and located within the aluminium-metal chassis of the vehicle. The design of the chassis allows for buoyancy attachment made from fiber-glass material to be fitted. The electro-mechanical parts were elevated while the electronic components were sealed for protection.

Gear system - The transmission in the electric vehicles (EV) is inherently simpler than that of IC engine vehicles. The conventional gear box is not required, as a single ratio gear was all that is needed. A gear system connecting each motor to each wheel via a single ratio chain drive was used in the iAAV-1 prototype. This transmission system has the advantage of better weight distribution within the vehicle and prevents the electro-mechanical drives from continual exposure to wet conditions.

Fiber-glass reinforced hull - The fabrication of the fiber-glass hull was a tedious process. The process involved construction of the mold before applying fiber mats, glue, and concentrated liquid hardener (resin) to form the hull shape. After machining away the excesses, the fiber-glass reinforced body was touched-up before painting to improve the vehicle aesthetics. The chassis frame and fiber-glass hull were assembled to serve as support for one another on land and water maneuvering.

Wheel-based maneuvering system - With some modifications on the driven wheels, the same mechanisms for both land and water was used in the vehicle. In application, the amphibious vehicle will be propelled across the water by paddling or spinning the wheels. The total volume of water displaced increases linearly with the vehicle speed. On road, the amphibian travels using the conventional wheel-based driving system. In addition to the modified guided propulsion, the wheel spin is the most common form of engineered water propulsion. The vehicle will steer by varying the velocity of both sides of the wheels. When stopping, both wheels will reverse their directional velocity to counter-momentum and interrupt the flow. The design details of wheel-based guided propulsion system will be discussed in Chapter 4.

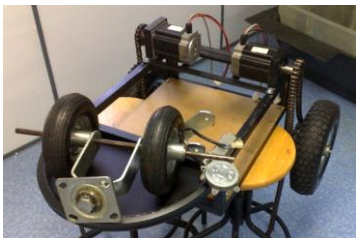

(a) Vehicle chassis base

(b) Motor and drive assembly

(c) Fiberglass hull mold with naked iAAV-1 placing along side

(d) Assembled iAAV-1 with completed body hull

(e) iAAV-1 after machining, touched-up and painting

(f) iAAV-1 preparation for water field test

Figure 3.32: Construction of the iAAV-1 platform

Figure 3.32 shows the construction of the overall physical iAAV-1 system. Figure 3.33 shows a CAD drawing showing the conceptual design of iAAV-1.

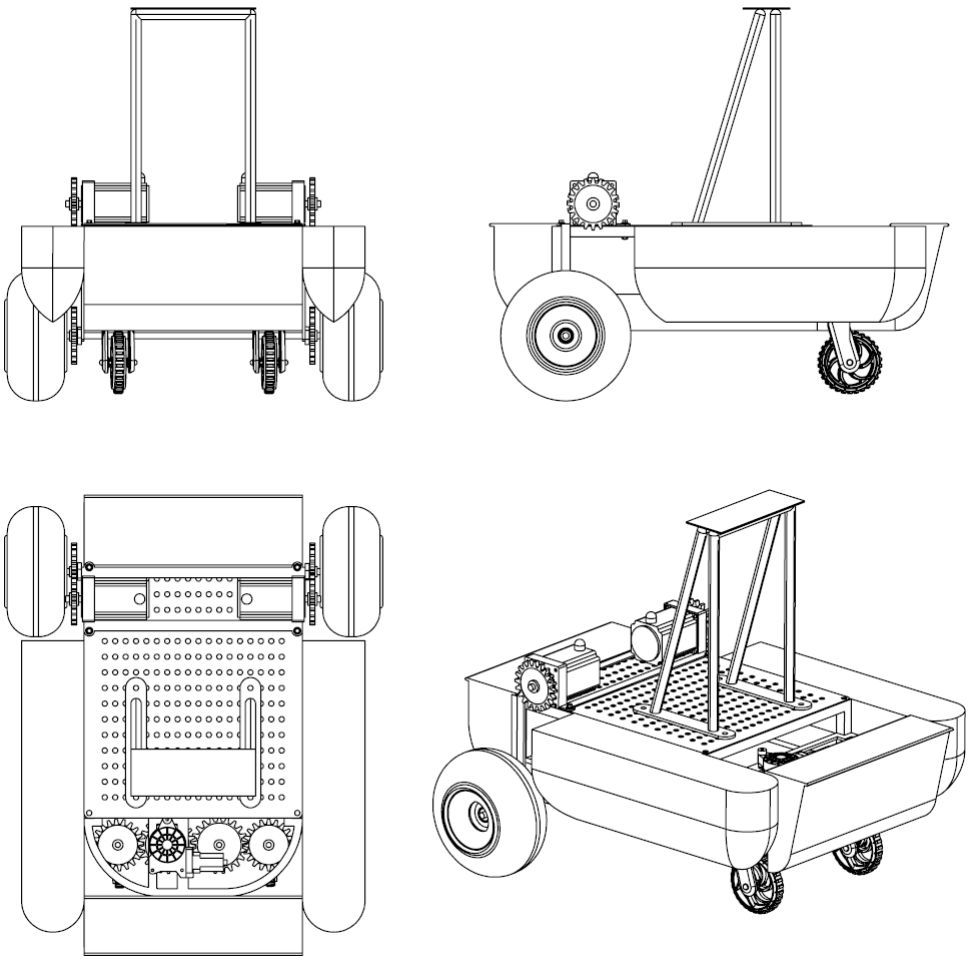

Figure 3.33: The iAAV-1 CAD

3.5.2 Electrical and Electronic Design

Energy Supply - A full electric propulsion in the design of iAAV-1 was employed. Operating a battery electric vehicle (EV) in autonomous mode is mechanically simple compared to the internal combustion engine. EV eliminates the complicated actuator design to start and control the engine. Although EV has more motors to control compared to a gasoline engine, the more control one has over a vehicle, the easier it is to have a computer takes over for more efficient maneuverability. The choice of electric energy also made the design feasible and eased arrangement difficulty. This is because the vehicle was powered by a single generator set located on both sides of the vehicle to provide direct drive for both amphibious modes. Besides, in amphibious search and rescue operation, optimizing the weight and power requirements is vital. The EV offers a much lighter with lesser mechanical parts. This means no lubricant system, coolant system, timing control between electric and gas responses, or transmission problems. EV platform only needs to derive electrical energy from batteries.

The iAAV-1 will be taking 24V as an appeasement voltage instead of 12V because of additional electronics components. Besides, rechargeable SLA batteries will be the energy source for iAAV-1 to perform tasks. SLA battery was selected because they were found to be the lowest cost and easily available in the market. Table 1 in Appendix B displayed the common rechargeable batteries used in autonomy. The table also highlight other

advantages that SLA battery has over other more expensive batteries in the market.

Despite having a very low energy-to-weight ratio and low energy-to-volume ratio, SLA batteries are able to supply high power-to-weight ratio required by automobile motors. Although other types of rechargeable batteries have higher specific energy and higher energy density than SLA batteries, but they are very expensive and hard to charge and a control unit is desirable. In spite of the limitation of research cost, SLA provides a good lifespan of 5 – 8 years. Two unit GPP12170 SLA batteries were used in this research with the following specifications:

- Sealed Lead Acid Battery 12V. 17Ah
- Weight: 11.4kg; Size: 181mm, width 77mm, height 167mm
- Specific energy: V × It/ W = 35.8Wh/kg
- Energy density: V × It / A = 8807.8 Wh/m^3

(a) 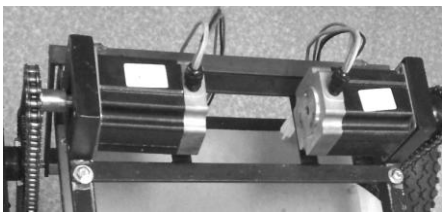 (b) 

Figure 3.34: (a) Twin 800W BLDC motors, (b) KBS motor controller

Brushless DC (BLDC) Motor and Controller - Two sets of 48 VDC, 2860 rpm, 800 W brushless DC (BLDC) motor (Figure 3.34) were used in the iAAV-1 prototype. The motor controller parameters were selected using the motor's manufacturer data shown in Table 2 (Appendix B). The primary

advantage of using brushless DC motors does away with the disadvantages of the split rings and brushes for commutation in vehicular application; BLDC motors have high efficiency, low mass for a specified torque rating, required little maintenance, longer life, improved safety, and operates silently.

The Kelly's programmable motor controllers (Figure 3.34 (b)) were used to control the operations of BLDC motors. The controller used high power MOSFET, PWM and powerful microprocessor to give comprehensive and precise control to equalize the torque required in each wheels. It was easily configurable and programmable with throttle input and enhanced regenerative brake function with novel ABS technique. Each controller has an independent three-phase PWM inverters within for complete simultaneous control for each motor at the same time. Figure 1 (Appendix B) shows the connecting wiring schematic between the PWM motor controllers to the BLDC motor in accordance with the manufacturer's manual. The DC motor can be modelled from the generating torque:

$$T_{peak} = (T_{load} + T_{inertia} + T_{friction}) \times 20\%\ safety\ margin \quad (3.36)$$

$$T_{inertia} = (J_L + M) \times \alpha \quad (3.37)$$

Whereby, $J_L + M$ = sum of load and rotor inertia; α = required acceleration

$$T_{load} = (W_{vehicle} / N_{wheel}) \times r \times G \quad (3.38)$$

Whereby, $W_{vehicle}$ = maximum sum of vehicle weight; N_{wheel} = number wheels on vehicle configuration; r = radius of wheel; G = gear ratio = 2.4

$$T_{fric} = \mu \times (W_{vehicle} / N_{wheel}) \times R \quad (3.39)$$

Whereby, μ = coefficient of friction between tire and rough terrain = 0.9

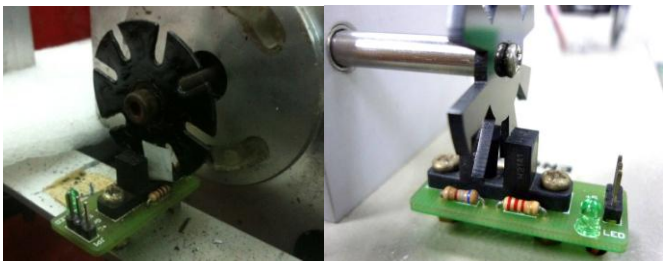

Figure 3.35: RE08A rotary encoder with self-fabricated 8 slots metal disc

Rotary Encoder - Encoders were used to enable the vehicle to measure the angular rotation of its wheels. Due to the non-holonomic manner, the position of the vehicle is related to the wheel rotation. The wheel velocities are needed to calculate the component velocities and rate of rotation of the vehicle. The angular velocity of the front drive wheels can be calculated if the rotary encoder is used to obtain the rotation data. As shown in Figure 3.35, the RE08A rotary encoder is attached to the back of the BLDC motor along the rotating shaft to measure the rotating wheel speed. It comes with a 8 slots plastic disc, but was replaced with a metal plate. The encoder sensor has a 8 pulse/rev resolution data before converting into a series of electrical pulses. With this digital counter, the wheel speed can be calculated:

$$\omega = 2\pi(T_c/T_{rev}) /G_R \tag{3.39}$$

Whereby, *Trev* = 8 pulse/rev;

T_c = Encoder signal output pulse/sec;

Gear Ratio, G_R = 2.4

Unfortunately, the calculated vehicle velocities, and position estimation are subjected to accumulating error in a local map, mainly due to inaccuracies in measuring the kinematic properties of the vehicle. Other source of localization error include wheel slippage and ground unevenness can also occur. Fortunately, a map is continuously being updated, which enables to use the relative displacements of instantaneous velocity, which is based on the updated local map.

(a)  (b) 

Figure 3.36: (a) MD10B 10A motor driver, (b) 12VDC motor

DC Motor and Driver - Rear servo motors were replaced with an absolute contacting encoder (ACE) attached to a 12V DC motor, as shown in Figure 3.36. This configuration setup acts in the same way as when a servo motor was used. Along with the MD10B 10A motor driver, the rear wheels can be oriented in any angle under different operating terrain for steering and zero radius turn. The PWM generated from FPGA was used to control the current input to the DC motor.

(a)  (b) 

Figure 3.37: (a) absolute contacting encoder, (b) ACE attached to DC motor

Absolute Encoder - A low-cost alternative to replace the more expensive servo DC motor is to include an absolute contacting encoder (ACE) (Figure 3.37 (a)). An attached ACE can sense the orientation of the rear wheels under different operations, especially useful when positioning the rear wheels for zero radius turn. As shown in Figure 3.37 (b) is the assembled ACE sensor on a DC motor. Through the use of a combination of 8-bit code with 128 absolute states, and gray-code pattern, ACE was able to provide an absolute digital output position that is useful to pre-program every rear wheel orientation in accordance with the front drive wheel speed.

Figure 3.38: LV-MaxSonar-EZ1 ultrasonic range sensor

Sonar Range Finder - These low-cost ultrasonic range finders shown in Figure 3.38 were used in the iAAV-1 as an accurate device, capable of generating repeatable measurements in confined area when obstacle are in close range within 3 meters radii. These sonar range finders were installed around the body hull of iAAV-1, pointing outwards in the direction of the vehicle motion. This device measures the distance from the sensor to the object from 0 inch to 254 inches with a 1 inch resolution. The computations of these devices were implemented on FPGA by using pulse width input to decode the distance value.

Remote Control Module - Operators often communicate with an autonomous through real-time control system. A search and rescue mission in a disaster area requires numerous application scenarios with local intelligence in the vehicle. It is said that the vehicle could be remote controlled and transmit video images and sensor data. However, it might automatically adapt the speed according to its on-board orientation sensors, or even to refuse driving command when its local sensors detect a potentially dangerous situation like a steep decline which can likely lead to the loss of the vehicle. In other cases, the vehicle might go under a tunnel or human-made structure and looses its communication link. This requires the local intelligence in the vehicle to traverse itself to its destination until wireless communication link is restored. In this work, a remote control or manual mode comes in when the iAAV-1 is in an indecisive state or during emergency, all control signals from autonomous navigation systems will be turned off. By moving the joysticks of the remote control as shown in Figure 3.39, it can be operated the same way it was illustrated in Figure 3.22. The details of the remote control functionality were explained earlier in Section 3.4.2.

Figure 3.39: 4-channel, 2.4GHz remote control

To prevent damage to the electrical components, the vehicle operates using the flow process as indicated in Figure 3.40. The user will use the necessary power and control switches, along with LED indicators for vehicle status.

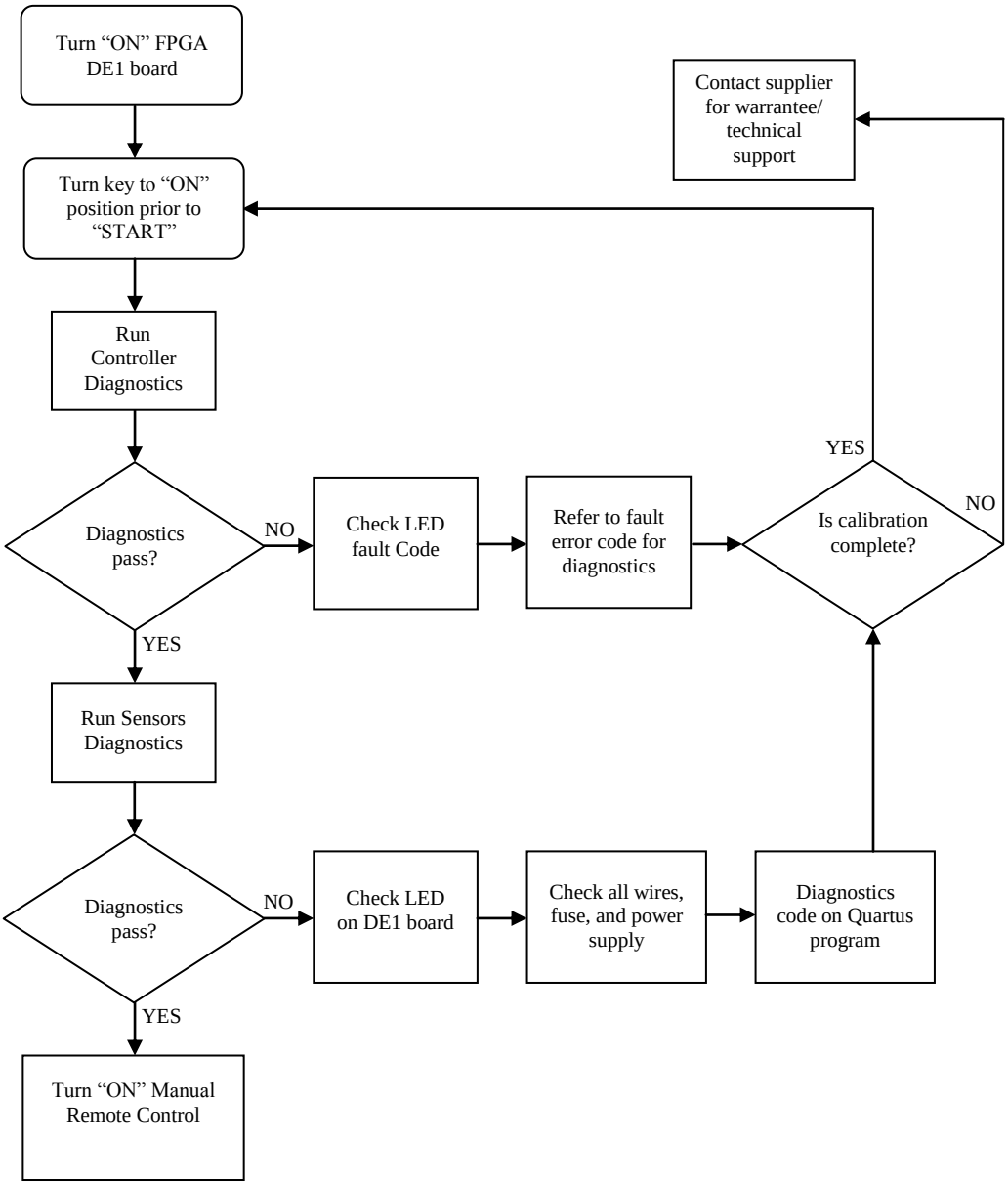

Figure 3.40: Process diagnostics performed prior to allow vehicle to be started

3.6 Summary

The goal of the iAAV-1 platform development was to stimulate research in the actual vehicle systems. The development of iAAV-1 was a major undertaking with variety of tests in the field. Unfortunately, these tests were time consuming and can only come at the end of the design cycle. The modular design approach used on the iAAV-1 platform proved to be easy to assemble and maintain. The selected locomotion mechanism for iAAV-1 has pointed out a new approach for an amphibian using single drive wheel-based maneuvering system. Besides, the iAAV-1 incorporates fiber-glass reinforced as watertight body when the vehicle meets the water surface.

One common goal in all autonomous vehicles is the incorporation of a navigation scheme to enable maneuvering as commanded. With this in mind, the iAAV-1 was tested most of the time using the remote control to set out suitable test platform for navigation strategies. The simplicity of design and mobility of the vehicle were major contributions in this research. The decision to use electric motor further simplified the control. Using commercially available 800W twin brushless DC motors, rated at about 2HP and 20A of current, the vehicle is able to perform close to the desired speed of 30km/hr on ground surface. Both the low-level function controls and high-level navigation functions require FPGA computational resources, which is also used by the system for debugging errors in Quartus II software. The implementation of the motor control is based on the formulation of the kinematic model with the desired wheel speed as calculated in Equation (3.19) and (3.20).

CHAPTER 4

DEVELOPMENT OF THE CENTRIPELLOR FOR WATER PROPULSION

4.1 Overview: Centripellor

A commercial centrifugal pump could not be installed on to the iAAV-1 due to it being too heavy and impractical to use for water propulsion. This Chapter presents a new centrifugal pump design having a single impeller attachment to the drive wheels of a wheel-based propulsion system for an amphibious vehicle. The goal is intended to prove its feasibility through calculation, simulation, and practical results in propelling the iAAV-1. Figure 4.1 shows the Centripellor model attached to the iAAV-1. Centripellor is a name given to the invention to indicate a centrifugal pump built on an amphibious vehicle wheel. Simply by spinning the wheels, the Centripellor will achieve the water propulsion of the vehicle in water.

Figure 4.1: The Centripellor prototype

The objectives of the Centripellor design and analysis are to:

1. cut down the extra payload for a separate water thrusters.
2. increase the thrust of the standard wheel using pump extension.
3. provide better flow by means of a guided propulsive force.

4.2 AAV Mobility: Water Propulsion

The progress made on amphibious vehicles over the years can be grouped into several categories by their propulsion device which was an important consideration in the development of amphibious vehicle to possess the inherent capability of cross terrain between land and water (Ehrlich et. al., 1970):

1. Screw Propeller
2. Kort Nozzle
3. Water Jets
4. Wheel Propulsion
5. Archimedes Screw
6. Paddle Wheels
7. Track Propulsion
8. Rowing

Apart from the naval architect in dealing with propulsion devices, the mechanical devices need self-propulsion with the propelling force derived from a pulling or a pushing on some external matter. In practice, the accelerating device was usually categorized as: Propeller, Pump, and Paddle.

In Chapter 2, separately integrated water jets and pump jets were mentioned. Two propulsion systems commonly used, but were found to present serious design complications for autonomous application. Considered part of the research process, all of the benefits and detriments in using each water propulsion device for amphibious applications were explored.

4.2.1 Screw Propeller

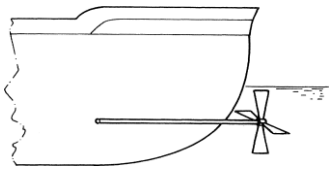

Figure 4.2: Illustration of a screw propeller design (Carlton, 2007)

The screw propeller (Figure 4.2) is the primary method for ship propulsion. It comprises a number of blades driven by a horizontal shaft which penetrated into the hull below the waterline. Screw propeller treats the open blades section as foils to computes the lift and drag forces to resolves for thrust and torque. The design of the propeller blade is critical in determining the amphibious vehicle performance. It required a priori knowledge in propeller designs and the consideration in the number of blades, optimum diameter, and cavitations. For amphibious application, the propeller will ideally need to be retractable when operating on-land and in-water surface for ground clearance. Cavitations will often be associated in this operation environment when formation of water-vapour bubbles can cause wear upon the fan blades. Besides, the added weight, cost and size of the propeller can limit the form of autonomy.

4.2.2 Kort Nozzle

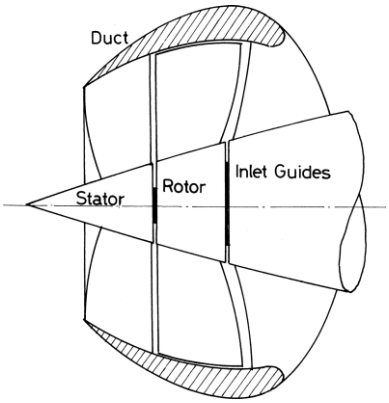

Figure 4.3: Illustration of a ducted propellers (Kort nozzle) (Carlton, 2007)

Kort nozzles are ducted propellers (Figure 4.3) placed outside of the amphibious vehicle in an enclosed shroud. It was designed to increase thrust capability while obtaining better cavitations performance (Carlton, 2007). Kort nozzles are often found in applications where high thrust was required at low speed operation. Therefore, these ducted propeller designs are especially attractive to use as a secondary propeller to improve the water speed of a wheel/tracked amphibious vehicle; wide variation of water speed is difficult to attain because large Kort nozzle is not suitable for an amphibious vehicle. The propeller size is required to be reduced and installed at the bottom of the hull to overcome the larger hydrodynamic resistance of the amphibious vehicle possesses. To control the Kort nozzle, two or more additional actuators are required for the directional control and rotation speed of the rotor. The shrouded condition provides measure of protection for the propeller blades. However, Kort nozzle is not a simple system that covers the significant effectiveness at high speed for an AAV without adding more actuators and controllers.

4.2.3 Water-Jets

The water-jet as shown in Figure 4.4 was a separate centrifugal pump attached to the end of the amphibious vehicle to draw in water, and raises pressure to eject water at a higher velocity than it had when it entered. This accelerating device requires internal ducting to be formed in the hull design. The water-jet requires a comparatively large volume inside the hull to fill with water for projection. Since water flow and large velocity changes were large in water, this often detriment the buoyancy effect and propulsion efficiency when compared with screw propellers or paddle wheels (Ehrlich et. al., 1970).

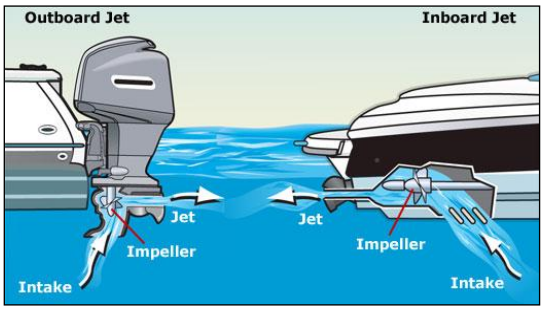

Figure 4.4: Illustration of a water jets system

4.2.4 Archimedes Screw

The Archimedes screw amphibians shown in Figure 4.5 demonstrated the ability to propel in semi-fluid conditions, especially in the transition zone between land and water. This device comprised of two large heavy-weight helix screw blade at both sides of the amphibian. The drawbacks of this design involved trade-offs in weight, cost and size. Besides, this design presents serious problems on hard surface maneuvering.

Figure 4.5: An Archimedes screw amphibians (Ehrlich et. al., 1970)

4.2.5 Paddle Wheels

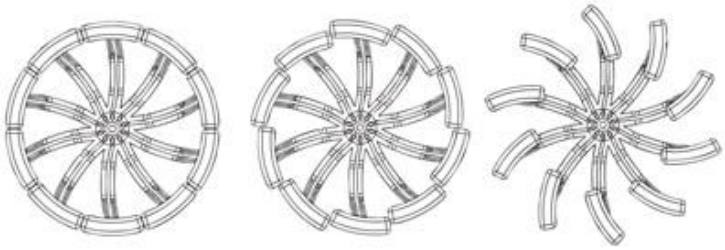

Figure 4.6: Illustration of CAD concept of an amphibious paddle wheel (Tuvie, 2012)

For shallow water application, the paddle wheel (Figure 4.6) was a practical device for amphibious operations that required single drive with pre-determined loading. They were found to be exceptionally maneuverable with good directional controllability using both side of the paddle wheels. The water propulsion machinery already exists as part of the land-operation drive train; the vehicle can be reduced in weight, cost, and control complexity with the wheels acting as the only auxiliary propulsion device. However, there were reports (Ehrlich et. al., 1970) on the disadvantages of using paddle wheels at variable immersion. Varying loading can cause amphibious vehicle to take

irregular course and affect the vehicle's dynamic in autonomous navigation. These amphibious vehicles also come in an increased vehicle width with the bulky wheels of a larger diameter. Figure 4.6 illustrates how a paddle wheel concept changes shape to propel on water and traverse on land.

4.2.6 Track Propulsion

Similar with the paddle wheels propulsion, tracks were used as paddles as the only auxiliary propulsion device for on-land and in-water operation. The complexity of the track system (Figure 4.7) was a huge drawback that degraded water performance due to the hydrodynamic resistance. Track propulsion had shown great promise as a propulsion device especially where it was commonly used for military operation (Gonzales et. al., 2007) (Flom, 2009). However, the integration of tracks required more extensive and complicated open-water tests; no test can be carried out without a considerable large budget.

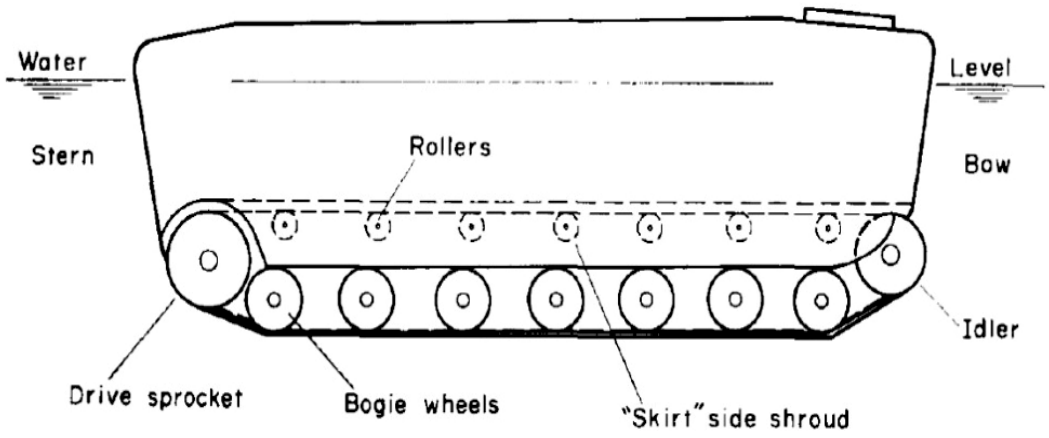

Figure 4.7: Sketch of a track configuration (Ehrlich et. al., 1970)

4.2.7 Wheel Propulsion

Based on literature review, extensive effort have been placed into improving the wheel propulsion since World War II because it was the quickest and most effective method to convert a tactical vehicle that already have sufficient buoyancy, propulsion, and control to cross relatively shallow water in an effective manner. The use of screw propeller on DUKW series (Gonzales et. al., 2007) or water-jet on amphibious Sealegs (The Star, 2009) have achieved reasonable water speeds. Unfortunately, these secondary marine propeller systems add weight, complexity, and cost to a vehicle and usually degrade its cross-country mobility. Some investigations on these amphibious wheel vehicles using wheel-shroud design had improved the water speed up to 70% (Rymiszewski, 1964). While using the disc portion of the wheel hub as an axial or centrifugal flow pump had demonstrated an effective water control and ability to complete a 360 degree turn in a much improved turning radius (Ehrlich et. al., 1972). However, no significant effort was seen to market and/or improve the fitting of the wheel pump onto an amphibious vehicle. Instead, the wearable all-terrain tires (Figure 4.8) were acting as a primary propulsion force with moderate water speed in the likes of these ARGO AAV (Ha et. al., 2005) (Tran et. al, 2007).

Figure 4.8: All-terrain vehicle (ATV) tires

4.3 Centrifugal Wheel Pump Propulsor (Centripellor)

The wheel propulsion had shown promise as a low-penalty water propulsion system that gives the advantage of having a single drive system for an amphibious vehicle to travel on both land and water surface.

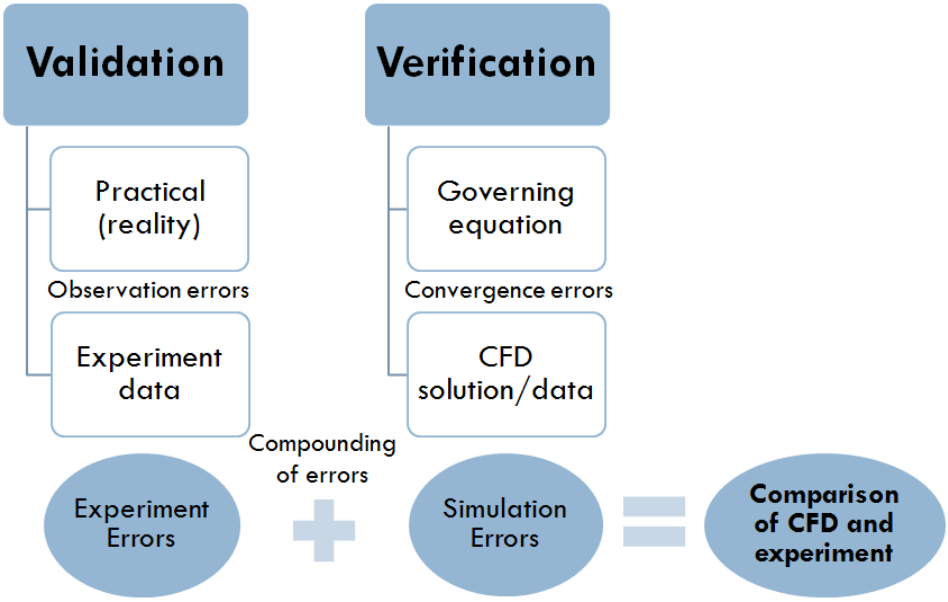

Figure 4.9: Methodology for the Centripellor design

The invention used the methodology shown in Figure 4.9. Computational Fluid Dynamics (CFD) was used as a verification tool to predict the propeller performance and to analyze the design. Specific attention will be paid to the design and geometry of the propeller based on iAAV-1 geometrical constraints. Essentially the Centripellor design was slowly refined and optimized by improving the control variables: mass flow rate, wheel speed, thrust, and power generated. Experimental validation was then made possible using similar model scale to setup on the iAAV-1 for field tests. Sets of experiments were carried out to measure the variables intended to compare

with simulation results. Thus, to improve the iAAV-1 thrust gain by improving mass flow rate and the outlet velocity of the Centripellor.

4.3.1 Mechanics of the Centripellor

The Centrifugal pump is a piece of equipment used to increase the pressure energy to accelerate the fluid further. The centrifugal pump converted energy from the prime mover (electric motor) into the velocity or kinetic energy and then into pressure energy of a fluid that was being pumped. The energy change involved two parts, the impeller and the volute/diffuser. The impeller is the rotating part that converts driver energy into kinetic energy. The volute is the stationary part that converts kinetic energy into pressure energy. This thesis proposed the use of the Centripellor on the iAAV-1 to navigate through water plains. The centrifugal pump was installed on the drive wheels to improve the efficiency of wheel-based propulsion.

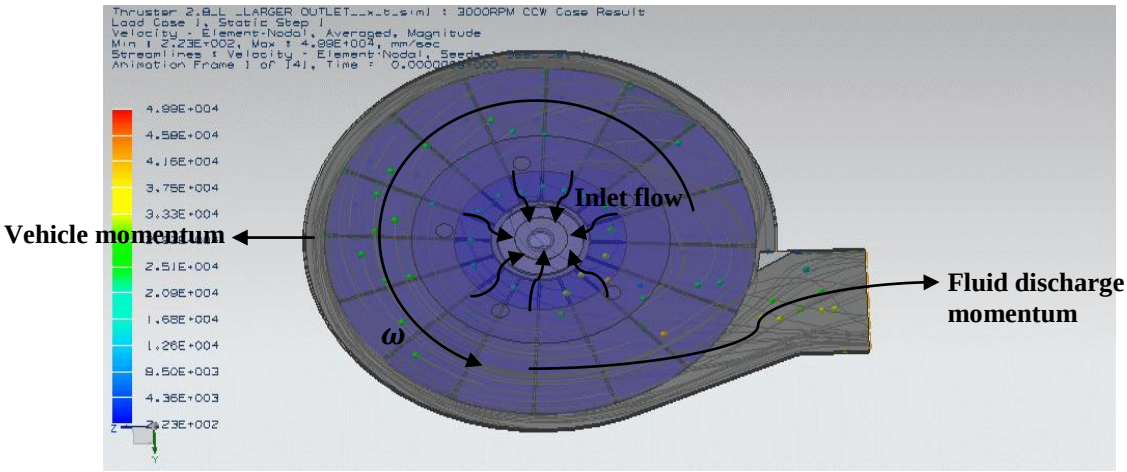

Figure 4.10: Guided flow visualization of a fully submerged rotating disc in an enclosed housing (side view)

The present invention shown in Figure 4.10 is an enclosed impeller rotating in a fluid in which the wheel was fully submerged. The internal impeller is attached to the rotating drive wheel and is controlled by the drag difference on both sides of the vehicle. The drive wheel will act as centrifugal pumps and cause circulatory flows parallel to the wheel axle on either side of the wheel. The fluid swirl around in the direction of wheel rotation will be pumped outward and in a guided propulsive resultant force. On the other hand, conventional wheel propulsion will be pumped outward around the direction of wheel rotation with no resultant force. The flow system in a conventional wheel cannot produce directed propulsive force on its wheel, only a torque, because of its symmetry. The energy transferred from the wheel to the fluid was dissipated as heat by means of viscous forces.

The additional impeller vanes and guided flow will increase the flow and the torque in the system. It then follows to obtain thrust in a particular radial direction, where the fluid gained momentum in the opposite direction of the opening exit. The horizontal thrust was achieved by suppressing and pumping the fluid around the region of the wheel hub towards the opposite direction of the vehicle motion. This is, of course, a conversion of a useful thrust as it increased the conservation of a mass of fluid momentum and slightly reduces the resistance in the direction motion of iAAV-1.

To simplify the performance characteristics of the propeller, it is convenient to make these theoretical assumptions of the momentum theory, and parenthetically, the major corresponding consequences:

1. Ideal flow conditions.
2. Open water characteristics with uniform fluid stream (average one dimensional laminar flow as it passes between the inlet and the outlet).
3. Fluid density is constant, ρ = 1000 kg/m^3 (incompressible flow).
4. Fluid is inviscid/non-vicious (μ = 0)
5. No formation of water-vapour bubbles (no cavitations).
6. Water enters the impeller radially in centrifuge (without whirl).
7. Tangential velocity components of water entering the blade is zero (v_θ = 0).
8. No solid handling in amphibious terrain with no slit, sand, or debris (no exposure to abrasion elements).

The global terms in relation to the continuity equation of fluid mechanics for incompressible flow in a guided closed conduit between two points was given by:

$$\rho_a A_a v_a = \rho_b A_b v_b \tag{4.1}$$

Whereby, ρ = fluid density

A = cross-section area

$v = r\omega$ = fluid velocity at cross-section area.

r = radial distance from the axis to blade edge

ω = rotational speed

$P^2 \propto T^3$ proportionality constant can be solved for a uniform flow as the power actually delivered to a single propeller to propel an amphibious vehicle was given by:

$$P^2 = \frac{T^3}{4\rho A} \tag{4.2}$$

Whereby, P = delivered power to propel the amphibious vehicle

T = thrust generated

The thrust produced by the impeller is the product of the mass flow rate through the Centripellor and the change in velocity of that mass can be written as:

$$T = \frac{dm}{dt} \cdot v = \rho A v^2 \tag{4.3}$$

Whereby, $\frac{dm}{dt}$ = mass flow rate at outlet point = $\rho A v$

Impeller blades considered as part of Centripellor rotor design were classified as:

1. Axial impeller (Figure 4.11 (a))
2. Radial impeller (Figure 4.11 (b))

(a) 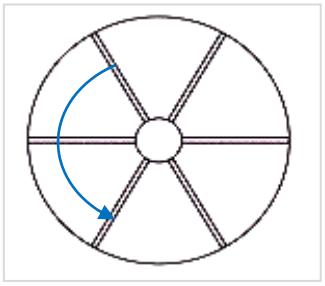 (b) 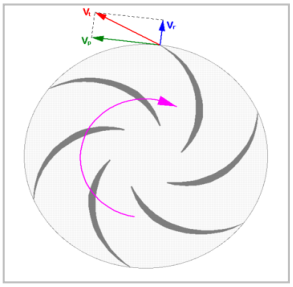

Figure 4.11: (a) axial impeller, (b) radial impeller

Most of the common centrifugal pumps use radial impeller that operate most efficiently for applications requiring high heads at relatively low flow rates. Radial impeller imposed shear stress to the fluid, and were used, e.g.,

mixing of very viscous fluid. The application associates with high flow rates at low heads require axial-flow impeller, often called propeller pumps (Munson et. al., 2006). The head developed from the axial impeller was primarily from the tangential force exerted by the impeller blades on the fluid. As it rotates, the fluid sucked in through the inlet was discharged through guided impeller base plate leaving the rotor. Under the circumstances not knowing which impeller design fits into the Centripellor, both axial and radial impeller will be taken into consideration. The power required to develop thrust will be estimated by the momentum theory, it is necessary to analyze the flow of water relative to the impeller blade. Considering the rotor was driven at constant angular wheel velocity, ω, by the BLDC motor, the blade speed was denoted as:

$$U = \omega r \tag{4.4}$$

The absolute velocity, V and relative velocity, W as shown in Figure 4.12 were denoted in the velocity triangles relationship given by:

$$V = W + U \tag{4.5}$$

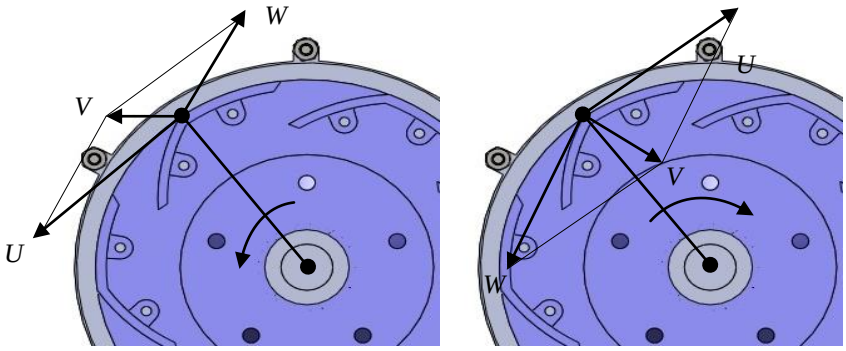

Figure 4.12: Idealized through bi-directional radial impeller for (left) backward radial impeller, (right) forward radial impeller

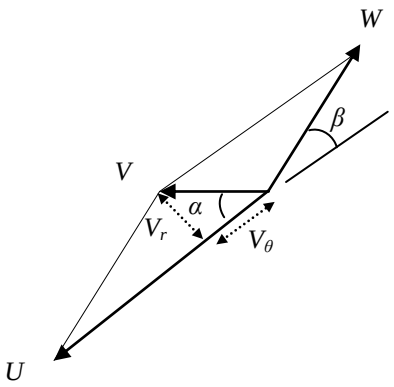

V_r = Relative absolute velocity
V_θ = Tangential absolute velocity

Figure 4.13: Velocity diagrams at the exit of a radial impeller

As shown in Figure 4.13, within a blade of Figure 4.12, considering $V_1 = W_1 + U_1$ is the passage, while $V_2 = W_2 + U_2$ is the exit, the momentum-of-momentum equation indicates the torque required to rotate the Centripellor impeller is given by:

$$T_i = \dot{m}(r_2V_{\theta 2} - r_1V_{\theta 1}) = \rho Q(r_2V_{\theta 2} - r_1V_{\theta 1}) \quad (4.6)$$

Hence, the power transferred to the impeller, P_i, was given by:

$$P_i = T_i\omega = \rho Q(U_2V_{\theta 2} - U_1V_{\theta 1}) \quad (4.7)$$

The power transferred to the flowing fluid, P_w, was given by:

$$P_W = \frac{P_i}{\rho Q} = U_2V_{\theta 2} - U_1V_{\theta 1} \quad (4.8)$$

The ideal/maximum head rise, h_i was found from:

$$P_i = \rho g Q h_i \quad (4.9)$$

From equation (4.7) and (4.9), we obtained:

$$h_i = \frac{1}{g}(U_2V_{\theta 2} - U_1V_{\theta 1}) \quad (4.10)$$

Alternatively,

$$h_i = \frac{1}{2g}[(V_2^2 - V_1^2) + (U_2^2 - U_1^2) + (W_1^2 - W_2^2)] \quad (4.11)$$

Whereby, $(V_2^2 - V_1^2)$ = increase in the kinetic energy of the fluid

$(U_2^2 - U_1^2)$ = pressure head rise across impeller blade

$(W_1^2 - W_2^2)$ = diffusion of relative flow in the passages

Based on assumptions, $V_{\theta 1} = 0$ and α = 90°, h_i was reduced to:

$$h_i = \frac{U_2 V_{\theta 2}}{g} \tag{4.12}$$

From Figure 4.13, β can be solved by:

$$cot(\beta) = \frac{U_2 - V_{\theta 2}}{V_{r2}} \tag{4.13}$$

The water mass flow rate, Q_i related to the radial component of the absolute velocity of the impeller blade is given by

$$Q_i = 2\pi r b V_{r2} \tag{4.14}$$

Whereby, r = impeller radius

b = impeller blade height

4.3.2 Design Geometry and Variables

Turning radius of iAAV-1 in water propulsion was a very complex calculation. However, in practice, the turning circle of an amphibious vehicle can be affected by the design consideration as follows:

1. Impeller blade design.
2. Number and type of propelling devices and location.
3. The shape of underwater part of the hull and its dimensions.
4. Impeller casing for tunnelling flow.
5. The rate of vehicle travel.

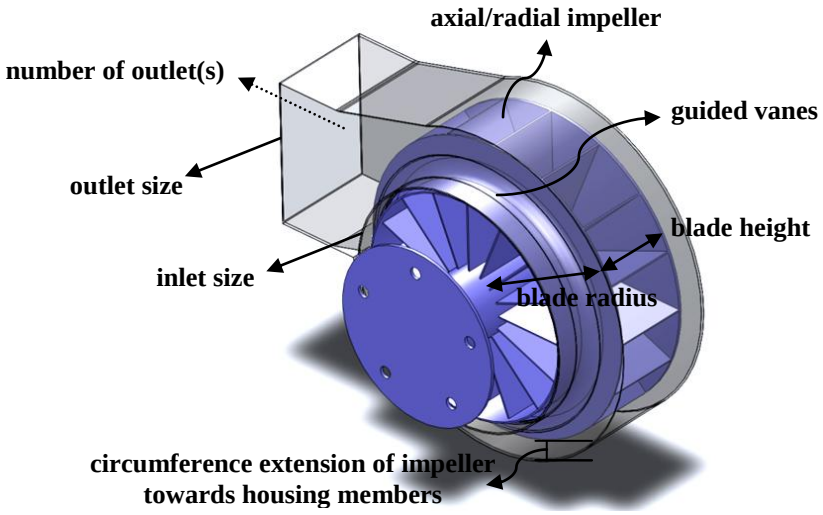

Figure 4.14: Rendered CAD concept of the Centripellor

Consequently, as shown in Figure 4.14, the Centripellor will take account of the following design variables with each representing different impeller geometry:

1. Impeller radius.
2. Impeller blade height.
3. Impeller types: axial and radial blade.
4. Circumference extension of impeller towards housing members.
5. Guided vanes.

On the other hand, the Centripellor will take account of the following design variables with each representing different concept and geometry for the housing members for guided propulsive force:

1. Inlet size
2. Outlet size
3. Number of outlets: duo outlets (bi-directional) and single outlet

4.4 Verification: CFD Modelling

Computational Fluid Dynamics (CFD) is a tool used for studying the Centripellor components by analyzing and understanding the behaviour, and hence, to improve the propeller performance by varying the design parameters. This was the method used to optimized the Centripellor design by increasing the thrust gained by improving the mass flow rate and the outlet velocity. Since it was not profitable to obtain various experimental data, various computations will be carried out until the results suggest it was experimentally and computationally feasible to carry out a field test. Using the simulation results obtained from commercially available NX Unigraphics (U-G) software, a comparison was made between the simulation results and the experimental data for different impeller designs, housing members, and conventional wheel-based propulsion. NX is a software packaged with CAD/CAM/CAE (Computer-aided Design/Computer-aided Manufacturing/Computer-aided Engineering) developed by Siemens PLM (Product Lifecycle Management) Software.

4.4.1 NX: Advanced Flow

The NX software allows for the omission of costly physical prototypes that was needed to perform preliminaries experiments and help gain further insight of multi-physics analysis involving fluid flow within the Centripellor. The NX advanced flow allow for the extending of the flow solution by visualizing real-life simulation through a finite volume element-based scheme

used to compute the 3D fluid velocity, temperature and pressure by solving the Navier-Stokes equations. The methodology used in NX advanced flow was based on the rotational frame of reference capability.

4.4.2 CAD Modeling

The CAD model shown in Figure 4.14 was designed and imported into the NX advanced flow. The fluid domains were constructed via wave geometry link tool. The fluid domains were water body when the Centripellor was fully submerged. Using synchronous modelling, model radial impeller (Figure 4.15) was constructed as the internal fluid domain shown in Figure 4.16.

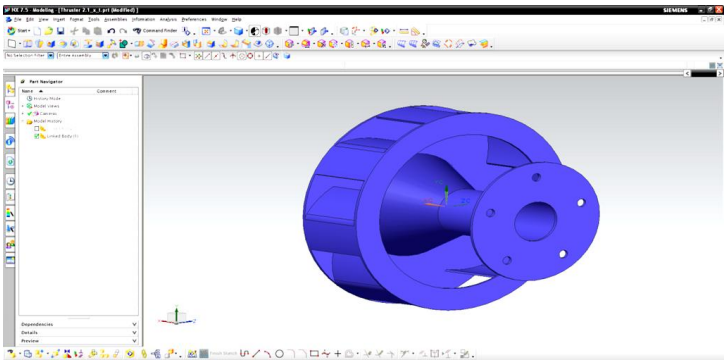

Figure 4.15: Radial-flow impeller model

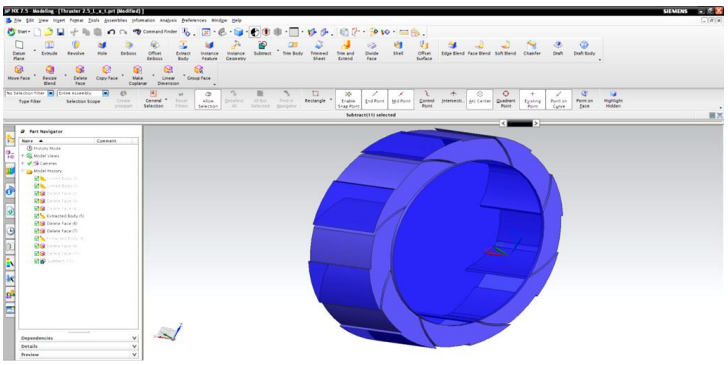

Figure 4.16: Internal fluid domain of radial-flow

Similarly, a constructed axial impeller internal fluid domain was shown in Figure 4.17.

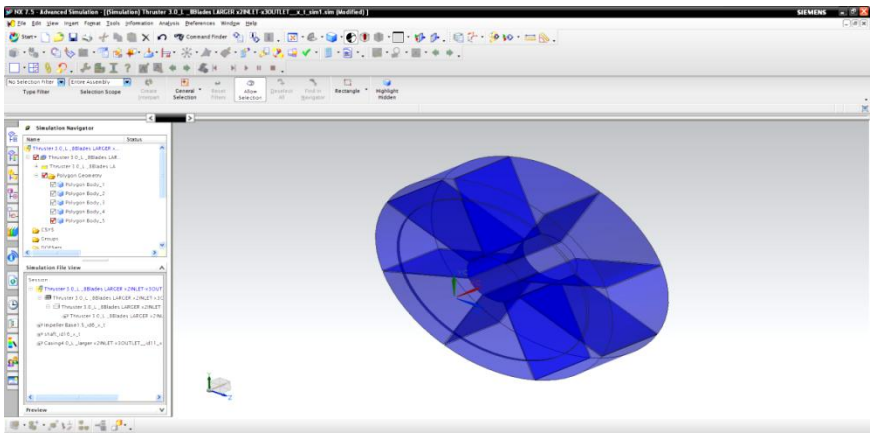

Figure 4.17: Internal fluid domain of axial-flow

On the other hand, the water body within the casing was constructed as the external fluid domain using similar method shown in Figure 4.18.

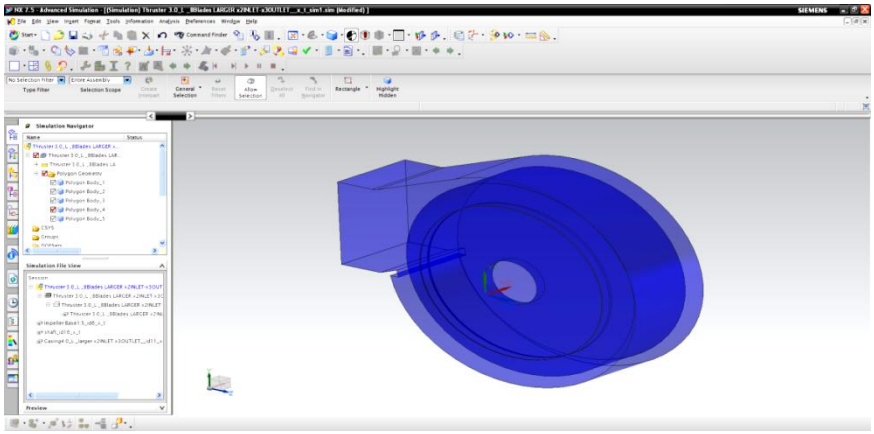

Figure 4.18: External fluid domain within the case

Next, the external fluid domain was subtracted with the impeller body and internal fluid domain to give the final constructed model before simulation. The final product was shown in Figure 4.19.

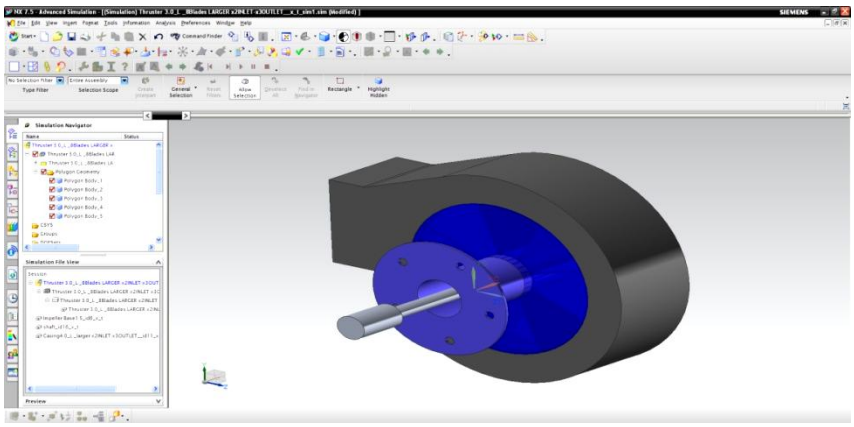

Figure 4.19: Final constructed model with fluid domain with extracted internal domain and the impeller body

4.4.3 Solution Setup and Boundary Conditions

With the developed fluid domains, the following task was to set up the solution and boundary conditions. Under the solution details, a steady-state was selected using K-Epsilon turbulence model as a solution solver. The 3D flow solution and high speed flow was checked because the simulation will be running at high rotation speed in excess of 2000 RPM. As shown in Figure 4.20, the boundary conditions was set up for both inlet and outlet as the opening flow with the enclosed fluid bodies characterized as water element.

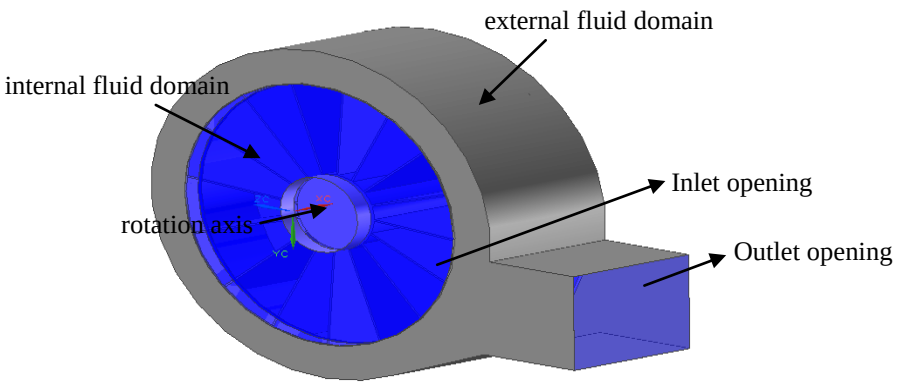

Figure 4.20: Boundary region and moving frame reference

Next, the internal fluid domain constructed was selected as a rotating body of the moving frame of reference. The center of the impeller was the rotation axis where the rotation direction was pin-pointed by the direction of the arrow. The arrow pointing downward indicating that the impeller was rotating at clock-wise direction, and vice versa.

A runtime report as per region was generated for the outlet and inlet opening face. This allowed the generating of the result for mass/volume flow rate, velocity and pressure data at the cross-section area.

4.4.4 Mesh Element

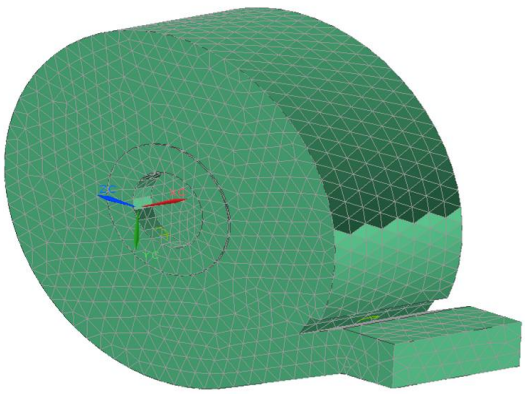

Figure 4.21: 3D tetrahedral mesh on multiple bodies

In order to analyze the fluid flows, flow domains were split into smaller sub-domains made up of 3D tetrahedral elements. As shown in Figure 4.21, the 3D boundary mesh contained only triangular faces. They were automatically meshed on the surfaces and the volume of multiple bodies. This was a smooth transition from a hex mesh to a tetrahedral mesh for complex

geometries with no topology restriction. Although most of the complex 3D flow phenomena occurring in the impeller blade can be captured with relatively coarse meshes, many detailed flow features are dependent on the mesh size, on the turbulence and transition models. The mesh size influences the solution accuracy and for getting a good convergence. In this simulation, the minimum allowable distortion for tetrahedral mesh size was 9 mm.

4.4.5 CFD Solution

In NX flow, the flow solver computes a solution to the non-linear, partial differential equations for the conservation of mass, momentum, energy, and general scalars in general complex 3D geometries. The computational method used an element-based finite volume method and a coupled algebraic multi-grid method to discretize and solving the governing equations. Details of the mathematical model, the discretization of the equations, and the solution method used in the NX flow solver are presented in Appendix A.

The simulation was started and the equations were solved iteratively as a steady-state and/or transient in a minimal 0.9 s time step. Once the convergence was completed, the result can be retrieved for analysis and visualization of the resulting solution. The whole CFD process was repeated by varying different design parameters.

4.5 Validation: Field Tests

Based on the conventional fluid mechanics, using energy and momentum relation and a number of simplifying assumptions, the design analysis has shown that the Centripellor was a feasible water propulsion system with three times of improvement from the conventional wheel-based propulsion system.

4.5.1 Prototype Setup

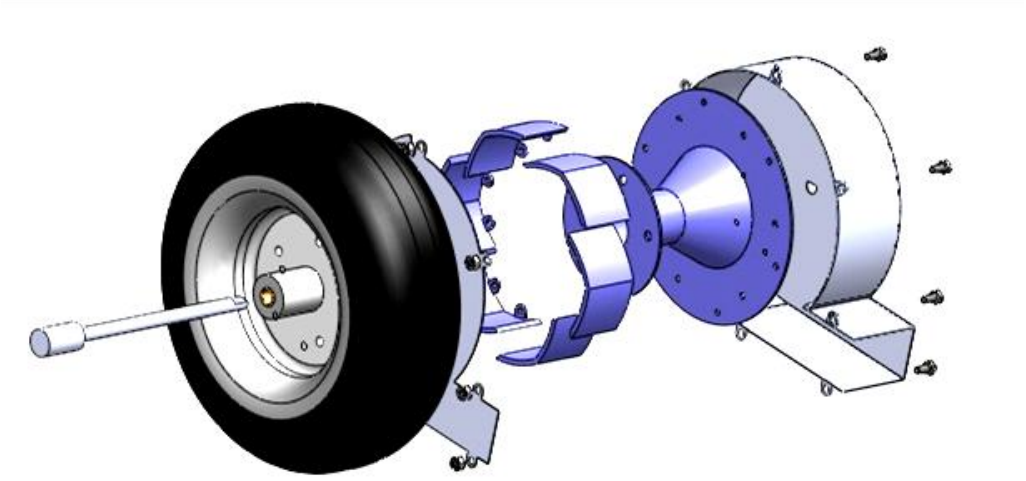

Figure 4.22: An assembly form the Centripellor on the drive wheel

The design, as shown in Figure 4.22, consisted of a flow collector, impeller blades, impeller attachment base plate, and a discharge housing member mounted on the wheel of each drive wheel. The design was laid out under mechanical restrictions in the wheel hub and geometrical constraints imposed by the vehicle width. For the test bed, the Centripellor structure will be laid outside the wheel centerline by 10 cm. For ease of fabrication, the experimental Centripellor aerodynamics was not considered and the

Centripellor was fabricated using steel and plastic materials. The completed system added an approximately 3 kg to the weight at each wheel.

Two scale models were fabricated including the radial impeller (Figure 4.23), an axial impeller (Figure 4.24), and two different geometry and structure of discharge housing member to validate the simulation data accuracy. These Centripellors were deployed on iAAV-1 for a series of tests to find out the characterization and performance.

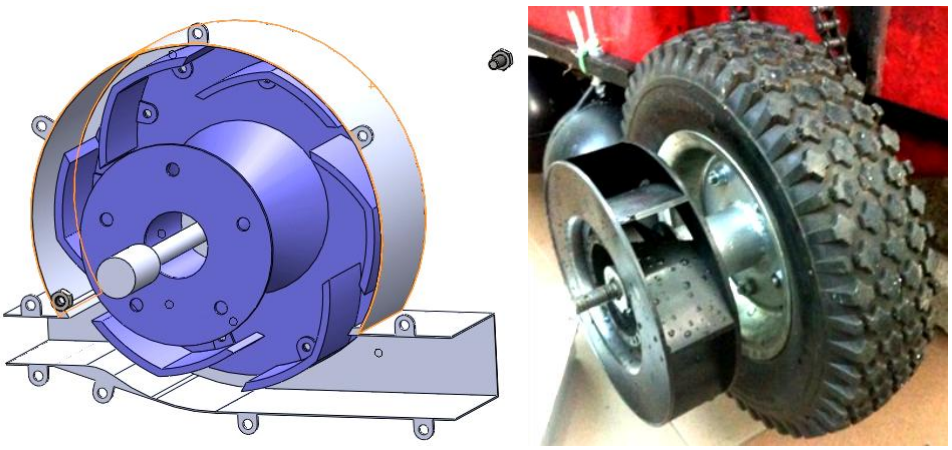

Figure 4.23: Radial-flow impeller with bi-directional housing diffuser

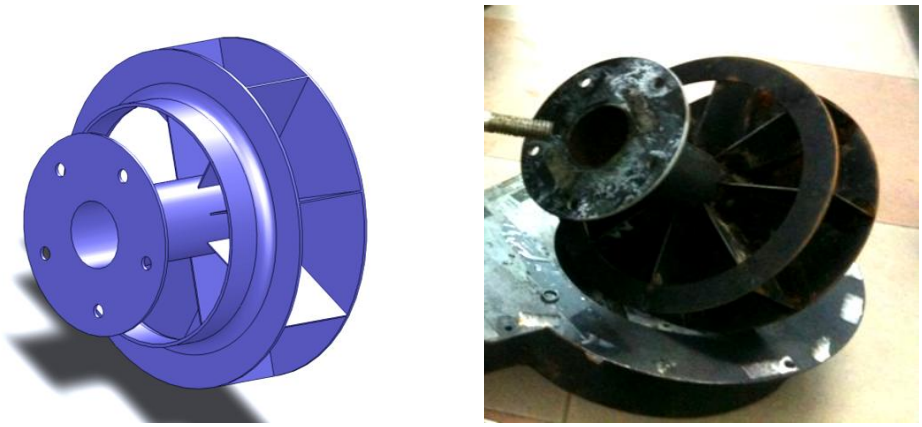

Figure 4.24: Axial-flow impeller with single outlet housing diffuser

The duo bi-directional outlets as shown Figure 4.23 is to a generate reverse thrust. This concept was designed to generate a turning moment when the vehicle has no forward velocity; which later could provide an improvement and maintain iAAV-1 zero radius turn capability particularly on water surface.

4.5.2 Determination of Speed

Figure 4.25: Field test in Titiwangsa Lake

The field test, as shown in Figure 4.25 was conducted in a lake to measure the vehicle speed before and after equipped with the Centripellor. The iAAV-1 was allowed to accelerate for 3 meters until it reached a constant maximum velocity. Timing the next 5 meters, and the corresponding wheel speed was recorded using a tachometer and rotary encoder to the motor. The time arrival was clocked and the vehicle speed was derived from the distance travelled and time taken.

4.5.3 Determination of Mass Flow Rate

The experiment (Figure 4.26) meant to measure the mass flow rate of the Centripellor was conducted in two large tanks. The Centripellor was fully submerged in a controlled volume water tank where the water level was kept constant when the Centripellor is discharging the water to another tank for measurement. Both the tachometer and the rotary encoders were used to measure the rotation of the wheel speed and motor speed respectively. The Centripellor was allowed to discharge the water until the outlet flow was uniformed, measurement tank was put in place, timing starts until the water reaches the indicated line. The corresponding volume and time taken to fill the measurement tank was recorded. The experiment was repeated at different wheel rotational speed.

Figure 4.26: Enclosed experiment to determine the Centripellor outflow rate

4.5.4 Determination of Thrust

Since it was difficult to derive the full scale resistance and measure the outflow water velocity of the iAAV-1, a rather simple experiment as shown in Figure 4.27, was to use a force gauge (Figure 4.28) to measure the generated thrust of the Centripellor in action. However, this can only be done accurately when including both sides of the propeller and a realistic loading distribution as symmetry as possible. As shown in Figure 4.28, the load cell (force sensor) was connected to the force gauge was hooked in between a rigid metal bar and the centerline of iAAV-1. With the iAAV-1 firmly hooked, when the Centripellor was propelled, the rotation wheel speed and maximum thrust was recorded. The experiment was repeated at different rotational wheel speed.

Figure 4.27: Experiment to determine thrust gain

Figure 4.28: The Centripellor thrust is measured using force gauge. The Load cell is hooked firmly in between a rigid metal bar and centerline of iAAV-1

4.6 Summary

In the approach of the naval architect in dealing with propulsion devices for amphibious vehicle, the wheel-based propulsion system was compared favourably because it is a single drive system and it helped to reduce extra payload for the separate thrusters. It was efficient not because of its propulsive force but because the water propulsion mechanism already existed as part of the land maneuvering mechanism. Research findings suggested that an implementation of a wheel pump propeller would improve the controllability and directional stability of iAAV-1. The controllability largely affect the turning ease of an AAV, while the directional stability keeps the AAV stable when operating at high speed, with fewer rudder correction. In order for improvement, an invention called Centripellor was designed using guided propulsive force to improve the thrust of a standard wheel propulsion. The CFD was used to calculate the performance of iAAV-1 at full scale condition. This opened up the possibility to improve the potential flow calculations by giving estimation for the shortcoming invention. Experimental validation was made possible after simulation results shown in Chapter 5 have proven its feasibility. A full scale model of the Centripellor was fabricated and employed on iAAV-1. Field tests and experiment was conducted to prove that the vehicle was more manueverable when equipped with the Centripellor than using conventional wheel-based propulsion.

CHAPTER 5

RESULT AND DISCUSSION

5.1 An Overview

This Chapter discusses the simulations and field tests performed for both iAAV-1 and Centripellor, and is focused especially on their functionalities and performance. On land navigation, iAAV-1 was evaluated for differential drive motor stability using Quartus II simulation, and experiments were conducted to test the zero radius turn accuracy. The Vehicle Design Specifications (VDS) was constructed to provide an overview of the platform performance. Besides, the autonomous system is composed of smaller components integrated together which will be discussed based on the aspects of the control system implementation.

This Chapter continues with the discussion on the Centripellor results based on simulation and various propulsion tests. From the CFD simulation method, design variables using various parameters were evaluated. Simulation convergence and flow visualization developed in the NX will provide qualitative discussion of the concept to date, and recommendations for improvement. The propulsion tests and results in determining the Centripellor performance, as discussed in Chapter 4, were described and compared to the conventional wheel-based propulsion.

5.2 iAAV-1 Platform Assessment

This section will describe the overall performance, design quality, and functionality of iAAV-1 on land navigation. The differential drives system module and zero radius turn module were combined to form a new drive configuration approach for an amphibious vehicle. Tests were conducted to validate the underlying approach, but have pointed to the problems faced and the need for further development.

5.2.1 Differential Drives System Stability

In this section, a real-time simulation for electric differential drives will be presented. Before implementing the electro-mechanical drives and power-electronics system, the two subsystems were tested and simulated to ensure functionalities. Figure 5.1 illustrated the complete control system which consisted of input signals and output signals which allows simulations to be conducted in Quartus II software that was used to develop the UTAR-CRCS. The simulation data were useful in tuning and testing the vehicle controls without having the components installed in the real vehicle. The iAAV-1 control system simulated in Figure 5.1 was made up of multiple functional module blocks with the input signals like the motor command input signal processed through internal logics to send the output signals to the components like the BLDC and servo motors. The system output signals were known based on the design specifications in UTAR-CRCS (Chan et. al., 2010).

To make sure the motor was supplied with desired currents, the outputs signals have to meet the design expectation/specification with a smooth and correct transition between states to show the control system continuity and stability. After the simulation has verified the functionalities of each module, the simulated environment can be performed by replacing the physical system actuators and sensors. The expected signal outputs were used to verify the simulation results, as indicated by the output signals shown in Figure 5.1.

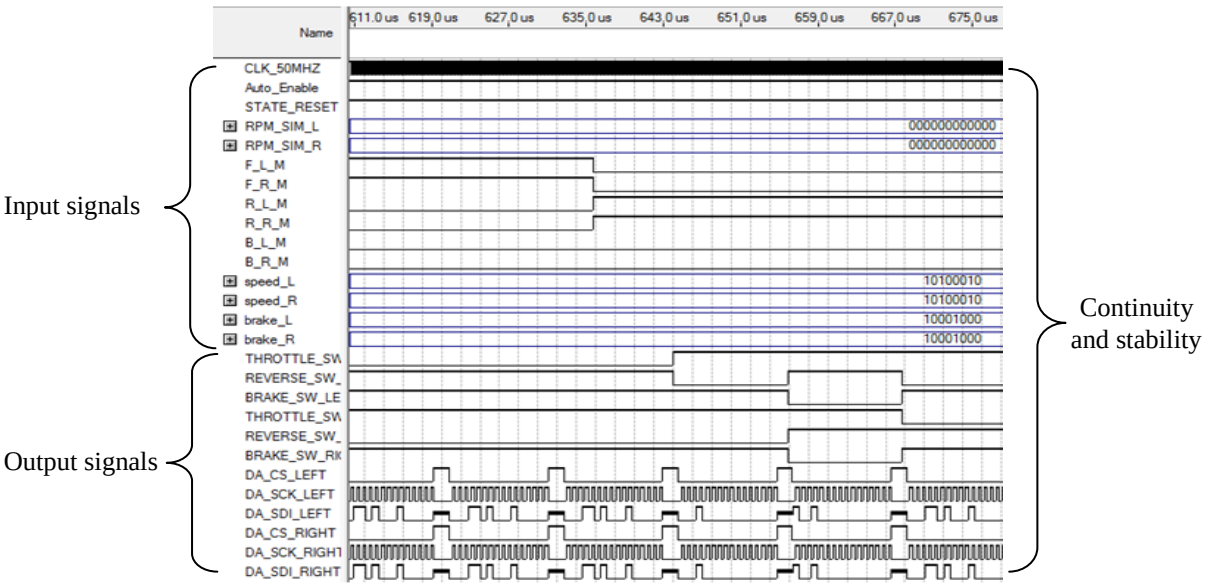

Figure 5.1: Control system level simulation

Once iAAV-1 was constructed, the model was validated against the actual vehicle performance. Two tests were conducted on a level concrete floor to eliminate disturbances due to ground unevenness. Although the rolling friction of coefficient on the floor (0.01 to 0.015) was generally lower than those encountered on the outdoor terrain (>0.30), the resistance was sufficient to test the vehicle dynamics.

The first test was conducted for linear iAAV-1 motion. The objective was to find out how much the vehicle straight line acceleration deviates; both BLDC motor were supposedly supplied with equal amount of current from the control system outputs. In the procedures, iAAV-1 was allowed travel to at different speed for the same distance of 10 meters and subsequently decelerates to rest. At the stop, the final position was recorded and experiment was repeated to obtain a mean deviation from the expected final position. The control system was tuned to give a reasonable match with the expected final positioning recorded by the vehicle. The results are shown in Figure 5.2, whereby the error percentage obtained at a higher speed is increasing, indicating a difference in acceleration on both sides of the wheels.

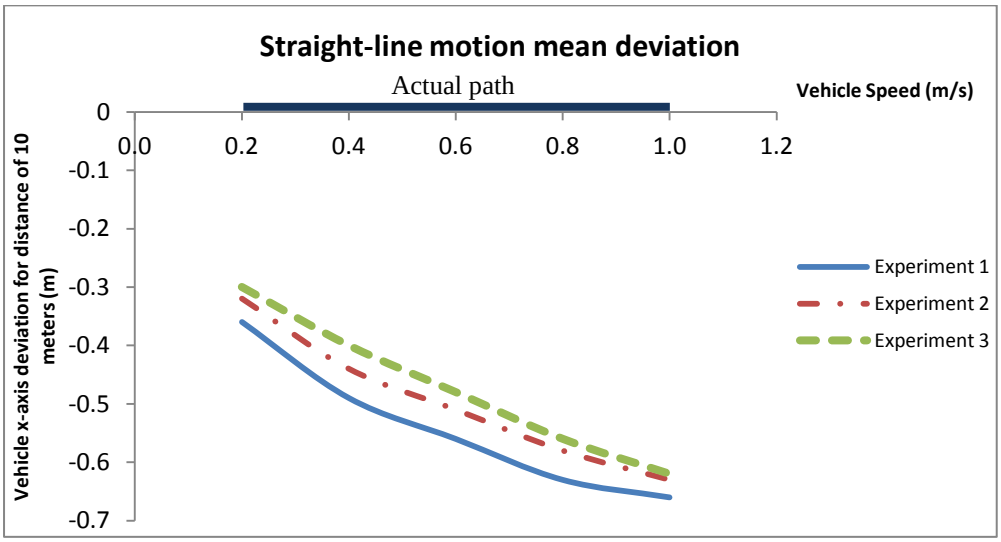

Figure 5.2: Tests conducted for mean deviation of vehicle rest position

From Figure 5.2, the supposedly linear actual path was deviated to the negative x-axis value, towards left of the vehicle direction motion, indicating that the vehicle has a very high tendency to move left in a straight-line acceleration and/or differential turn motion. This could be caused by the

rotational direction of the motors in relation to each other in the vehicle design; the motors have specific forward and reverse direction, causing the left wheel to lag behind the right wheel although the same current was supplied to both the drive wheels. The results were tested on the reverse direction motion and the results appeared in the same manner.

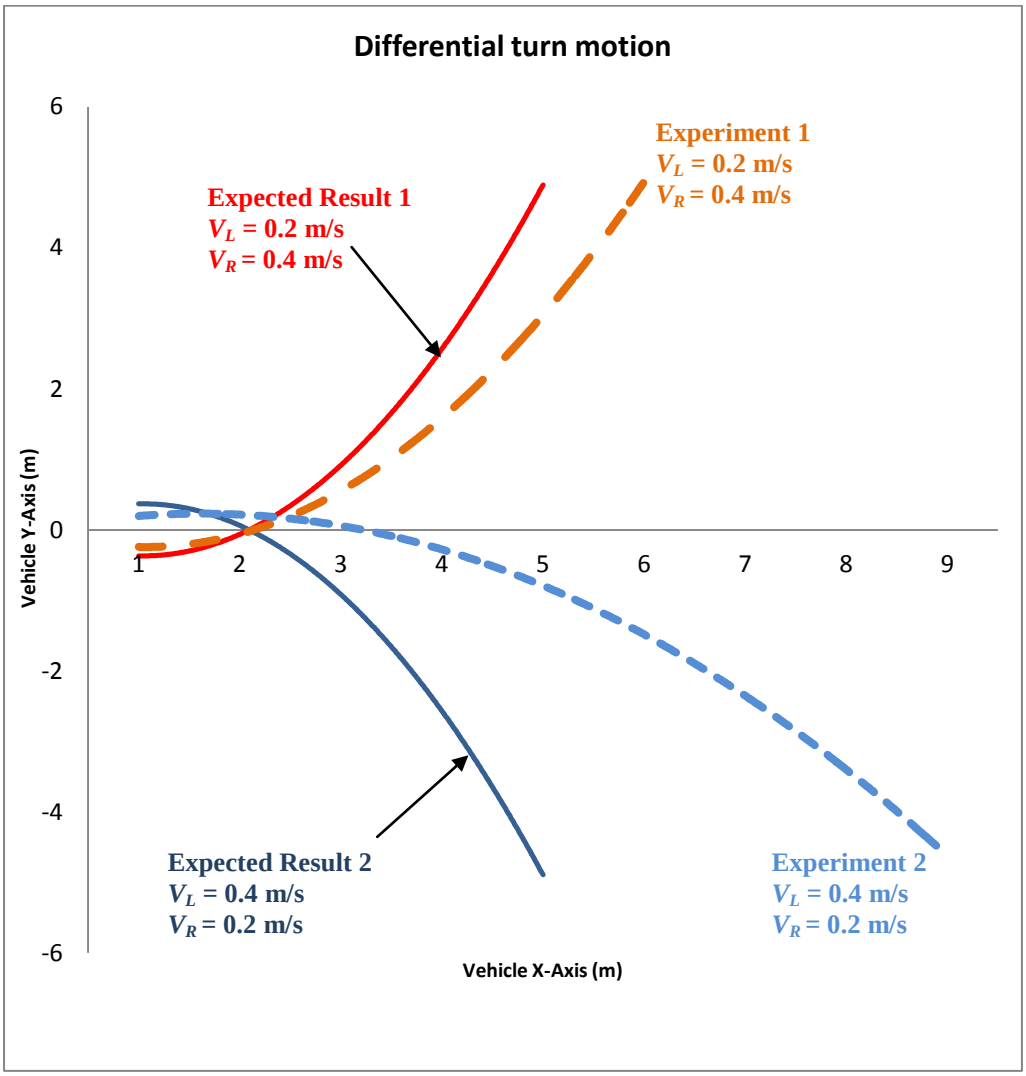

Figure 5.3: Tests conducted for differential turn motion

The second test was conducted for non-linear iAAV-1 motion. The objective was to find out the characteristics of the vehicle motion faults when

the vehicle performed a differential turn. Both motors were now allowed to rotate at different speeds, with two sets of experiment to be conducted. The first set of experiment will be set up with the current supplied to the right wheel (right wheel speed, $V_R \approx 0.4$ m/s) was twice the current supplied to the left wheel (left wheel speed, $V_L \approx 0.2$ m/s). The second set of experiment will be set up with the current supplied to the left wheel (V_L 0.4 m/s) and is twice the current supplied to the right wheel ($V_R \approx 0.4$ m/s). iAAV-1 was allowed to travel towards a maximum radius of 5 meters, and the straight-line distance travelled will be recorded to determine the expected travelled path of the iAAV-1. The results appeared to give the same fault as the linear motion, deviating towards the left of the vehicle. Results were shown in Figure 5.3 along with the expected travelled path

The control feedback system model described in Section 3.4.3 was implemented. Rotary encoders at the motor were used as a speed sensor to give a reasonable match between the intended wheel speed and current supplied to the motor. Tests were repeated and the control system was tuned to provide a reasonable match with the linear motion and non-linear motion of the vehicle. In linear motion, drive wheels were tuned to be driven at same speed as indicated by encoder sensors. As for the more complex non-linear motion, the developed control system in UTAR-CRCS requires a more developed computation, instruments and sensor fault reconstruction model to improve the vehicle kinematic accuracies. This may serve to motivate further development.

5.2.2 Zero Radius Turn Accuracy

The vehicle kinematic model breaks down during movement that require rapid caster rotation. Before the zero radius turn module was developed, the vehicle did not tend to move according to the curvature line because the caster rear wheels were not in position before motion. In other words, the castor rear wheels positioning were affecting the initial momentum at rest prior to the start of the motion, causing the vehicle heading angle to be inaccurate. Therefore, the zero radius turn module design was assembled at the rear wheel for attachment to a sub-frame and electronic drive control system to provide a more flexible steering mechanism in confined areas.

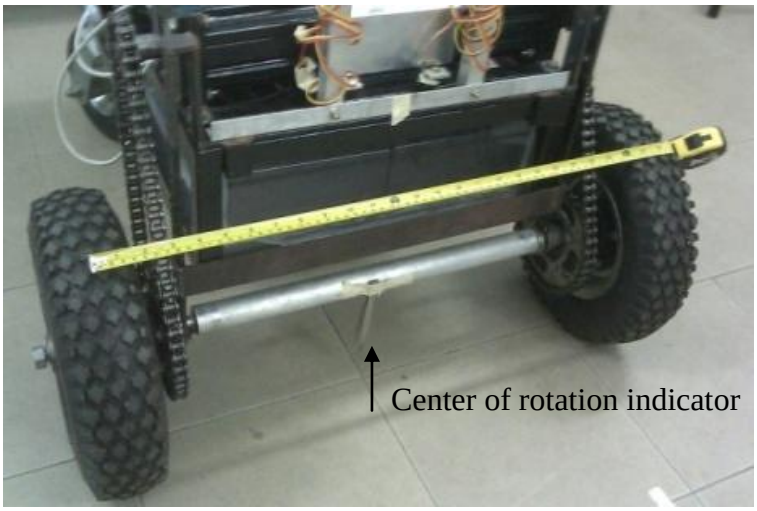

Figure 5.4: Measurement of center of rotation accuracy

The objective of this test was to find out how much the vehicle zero radius turn deviates from its center of rotation at different speed. The zero radius turn requires the servo motors to rotate the caster wheel at angles along the vehicle center of rotation. The caster rear wheels turning angles were

preset. The zero radius turn module also required the frictional torque opposing the caster wheel rotation to be tuned to provide considerable amount of wheel torque. The test was started by recording the vehicle initial center of rotation (x_r, y_r), as shown in Figure 5.4. The vehicle was signalled to make a 360 degree left/right turn, and the subsequent center of rotation at rest position was recorded. The vehicle was allowed to repeat the 360 degree turn with different speed to record the following subsequent center of rotation.

The zero radius turn performance was exceptional, the vehicle center of rotation was recorded with a right and left zero radius turn tolerance of R(±20 mm, ±40 mm) and L(±260 mm, ±350 mm) with respect to the center of rotation of vehicle x-axis and y-axis in the direction motion of vehicle global x-axis. The first test indicated that the left rear wheel was not positioned accurately. The absolute encoder attached to the DC motor was tuned to provide an accurate rear wheel positioning with respect to the speed of rotating differential drive wheels. The final test was a repeat with the tolerance of (±20 mm, ±20 mm) in both turning direction. The overall zero radius turn module performance was very effective and accurate. This module enabled iAAV-1 to perform zero radius turn operation or near zero radius turn operation with very little delay in the rear wheels positioning. Unfortunately, this did not prevent the vehicle from being thrown out of its initial center of rotation when turning at high speed. A speed limit was imposed to the zero radius turn module.

5.2.3 Performance Evaluations

Early attempts were made to select a laboratory aisle way (Figure 5.5 (a)) in a confined area to allow the vehicle to steer from a boundary to boundary, in a perpendicular direction, and reverse course. There was not a known target, only the goal to navigate around the course was predetermined. Later attempts were made to allow the vehicle to traverse on unstructured outdoor terrain (Figure 5.5 (b)) and to test for Centripellor water propulsion in a lake (Figure 5.5 (c)). To improve the wheel-based propulsion system, tests were thoroughly conducted in large water tank (Figure 5.5 (d)) to validate the CFD results.

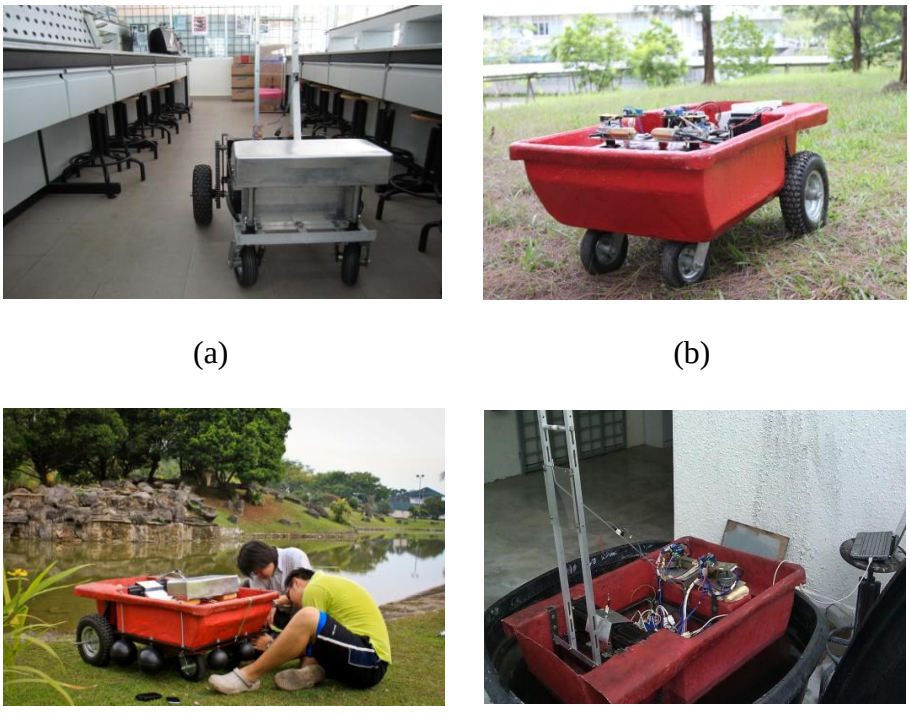

(a) (b)

(c) (d)

Figure 5.5: Field tests (a) laboratory aisle way; (b) tropical outdoor; (c) lake; (d) large tank

The overall performance of iAAV-1 has proved that the platform is rugged, easy to assemble, maintain, and reconstruct during and after the construction of the prototype with various tests conducted on unstructured outdoor terrain. After several modifications, the simple drive chain was both rugged and reliable in running on rough terrain and water environment. The fiber-glass reinforced hull has provided the needed waterproof and buoyancy attachment to operate in water. Under no-load condition, the drive wheels were able to operate up to an approximate 116 km/hr top speed (wheel rotation, $\omega \approx 2000$ RPM) using tachometer for measurement. While the travel speed recorded using motor rotary encoder was between 24.8 km/hr to 29.9 km/hr (accurate field test was too dangerous to conduct). The iAAV-1 batteries performance were also exceptional, iAAV-1 was able to operate more than 8 hours of field tests in Titiwangsa Lake with a calculated specific energy of 35.8Wh/kg and energy density of 8807.8 Wh/m^3. This proved the power electronics components were very efficient and energy saving.

The main problems encountered were due to the weight of iAAV-1. The extra weight was caused by an underestimated and conservative vehicle design. The added weight in the prototype was causing an imbalance when afloat which resulted in the rear caster wheels stalling. The problems were corrected by relocating the batteries to increase its stability. The rear caster wheels were tuned to provide considerable amount of wheel torque to overcome the increased weight. However, given more time and effort to redesign the hardware components, the additional weight can be minimized to reduce the dynamic change on the vehicle.

5.2.4 Vehicle Design Specifications

An optimal design for the iAAV-1 system was sufficiently capable to perform the task and prevent overestimating for economical reasons. Each module was carefully researched and implemented on the prototype so that iAAV-1 has the simplicity and capability to be reconstructed quickly without making major modification. Listed in Table 5.1 is the developed iAAV-1 platform specifications:

Table 5.1: The iAAV-1 specifications

Descriptions	*Specifications*
General Performance	
Land Cruising Speed	30 km/hr (maximum)
Water Cruising Speed	4.4 km/hr (maximum)
Weight	65 kg
Capacity	15 kg
General Dimensions	Modular
Length x Width x Height	(900L x 500W x 1200H) mm
Prime Mover	Electric System
Motor	Twin Brushless DC
Output	1600 W
Horsepower	2 HP
Driveline	Differential Chain Drive
Transmission	2.4 G_R Chain Drive
Primary Steering	Differential Steer
Secondary Steering	Zero Radius Turn
Front and Rear Axles	Separate on common axles
Brakes	Regenerative Braking
Connections	Independent Axle Mount
Wheels	Chain Sprocket and Wheel Hub
Tyres	80W x 80H x 300D mm
Chassis	Metal and aluminium frame
Hull/Body	Fibreglass Reinforced
Energy Supply Compartment	SLA type, 17Ah, 24V ~ 48 VDC

5.2.5 Autonomous Implementation

The FPGA technology was used as the control system because the FPGA device provided a compact and energy saving system when compared with other control systems that consisted of multiple CPUs or a combination of multiple CPUs with multiple processing devices such as micro-controllers and digital signal processors. Although FPGA device did not out-perform the modern computers in terms of speed and hardware/software resources availability, FPGA device occupied little space (size needed: 15.0 cm × 3.0 cm × 15.0 cm), which contributed in reducing iAAV-1 weight significantly (FPGA weight = 0.28 kg), and draws only a maximum power of 2.5 W. These highlighted advantages enabled the realization of compact autonomous amphibious vehicle system in a confined environment for search and rescue mission.

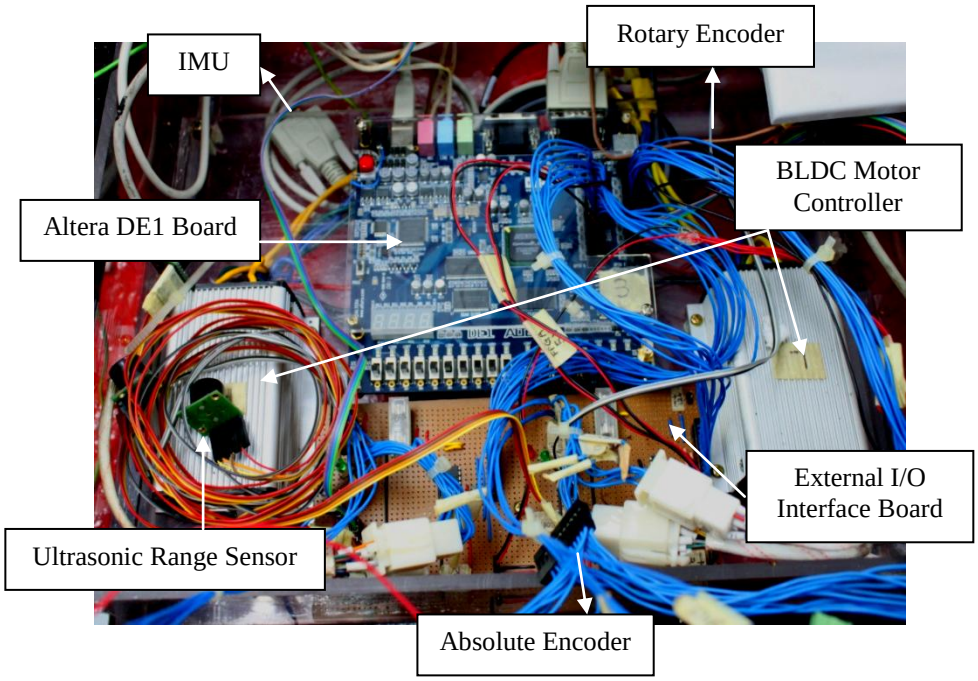

Figure 5.6: The FPGA device with the other components

Achieving autonomy was a major undertaking, requiring numerous tests in the field. These tests were time consuming, and implementation of a high-level of intelligence in the vehicle navigation system can only come at the end of the design cycle. The immediate future does hold promise in the system, communication between multiple modules in UTAR-CRCS parallel processing were deemed sufficient in this implementation (Chan et. al., 2010). FPGA on-chip communication has allowed data to be transmitted in parallel mode instead of serial mode for off-chip communication. Shown in Figure 5.6 is the developed UTAR-CRCS which consists of the FPGA device (Altera DE1 board), low-level sensors, and a custom built I/O board for interfacing with BLDC motor controller.

Additional information from Inertial Measurement Unit (IMU), vision system, and more modules were required for a completely new vehicular design and navigation approach. Fortunately, the vehicle system architecture allows for incremental changes, which was a benefit for using the developed FPGA based real-time control system (UTAR-CRCS) (Chan et. al, 2010). The two speed sensors: rotary encoder and absolute encoder provided reliable data from the wheels under a variation of ground conditions. Collision prevention with multiple ultrasonic(s) was successfully implemented; these sonar range sensors provided accurate signal for obstacle avoidance and preventive accident in various test. The real-time visual guidance system scheme (Teoh et. al., 2010) was designed but has only been tested on image frames. Further development in sensor fusion using FPGA device was needed to help solve navigation problem in an unstructured environment.

5.3 Centripellor Design Tests and Evaluation

The Centripellor will be used as a horizontal propeller in iAAV-1 for water propulsion. Centrifugal pump integrated in wheel propulsions were ideal for the iAAV-1 because they do not require rudders and were driven using the same motors that drive the vehicle on ground. It was necessary to model the invention, enabling appropriate selections to be made. The CFD analysis of the thrusters configuration concluded the model predictions was consistent. The next step will be the construction of a mechanical prototype and mounting on the vehicle for testing.

5.3.1 Variable Evaluation

Figure 5.7: The Centripellor impeller blade height and blade radius

The factors that would affect the Centripellor efficiency were listed in Section 4.3.2. The number of blades was one of the essential parts in the design to disperse the maximum flow rate of the pump. The simulation run in NX indicated that the more blades the impeller has, the higher flow rate the pump disperses. However, the flow rate increases and stop at the peak point after numerous blades were added in. Therefore, six to fifteen blades were

recommended in a centrifugal pump design. In this design, 8 blades were used for Centripellor as the welding work can be difficult to prepare between metal pieces, and the efficiency might not differ much compared to more blades.

A typical pump performance normally described by a graph plotting the variable parameters with respect of flow rates. From NX simulation results, the flow rate of the pump increased as the impeller radius/blade height increased, as shown in the Equation (4.14). Figure 5.8 shows the simulation results generated within the geometrical constraints for impeller radius and blade height, rotating at a constant speed, against the outlet flow rate produced. The blade height was set to just 50 mm to make sure that the pump was not too cumbersome in order not to decrease the iAAV-1 agility when navigating. The radius of impeller was set to 120 mm, will not exceed the vehicle wheel size of 300 mm diameter. The idea of this iAAV-1 is to run from land into watery plains without any mode switching. This was the reason that the pump must be smaller than the size of the wheel so that the pump will not affect the vehicle on land maneuvering.

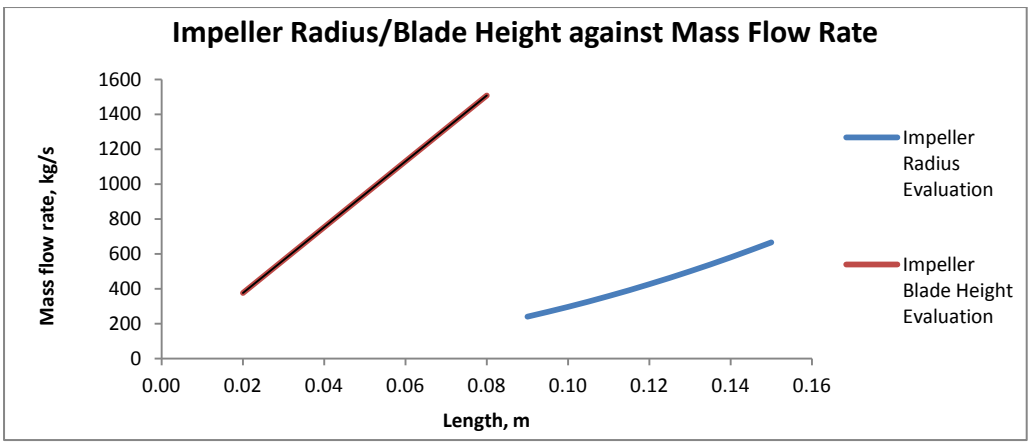

Figure 5.8: Impeller radius/blade height versus outlet flow rate graph

Figure 5.9 shows a comparison of the simulation results generated between the axial (torque flow) impeller and the radial (curvature) impeller. Given the same variable parameters, the graph shows that the axial impeller can deliver 3 times the flow rate of a radial impeller.

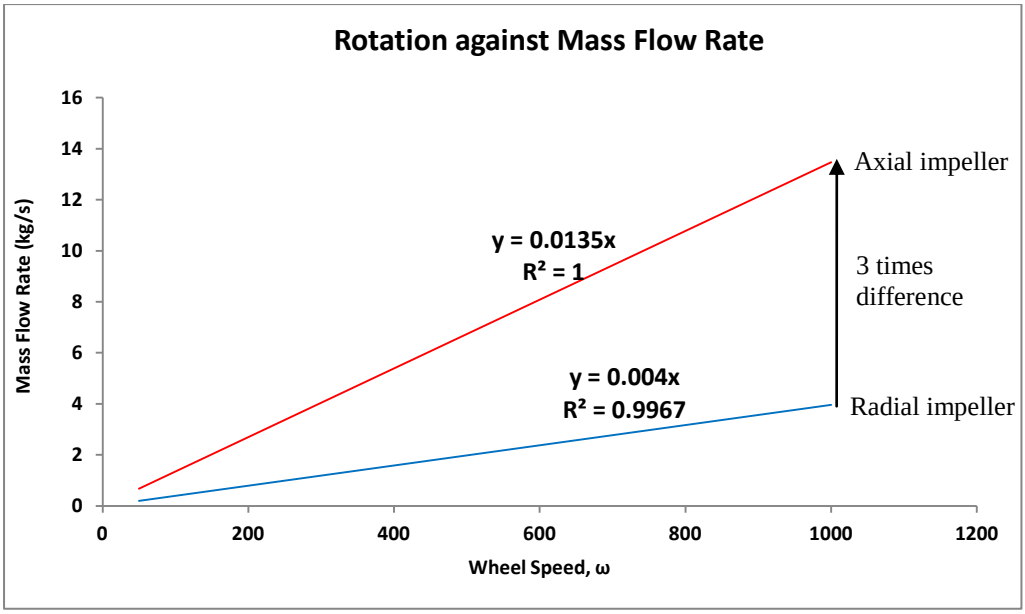

Figure 5.9: Comparison between axial and radial impeller

From the CFD simulation, the implementation of guided vanes design was carried out. From the simulation analysis, the internal pressure was increased which involved a higher efficiency of energy transfer. The efficiency of a centrifugal pump depends upon the hydraulic losses, leakage losses, and friction losses. Guided vanes reduced the losses from the blade passage to the blade exit.

Simulation to evaluate the Centripellor housing variable parameters were carried out to study the effect of parameters on the mass flow rate and outlet average fluid velocity, results are shown in Figure 5.10.

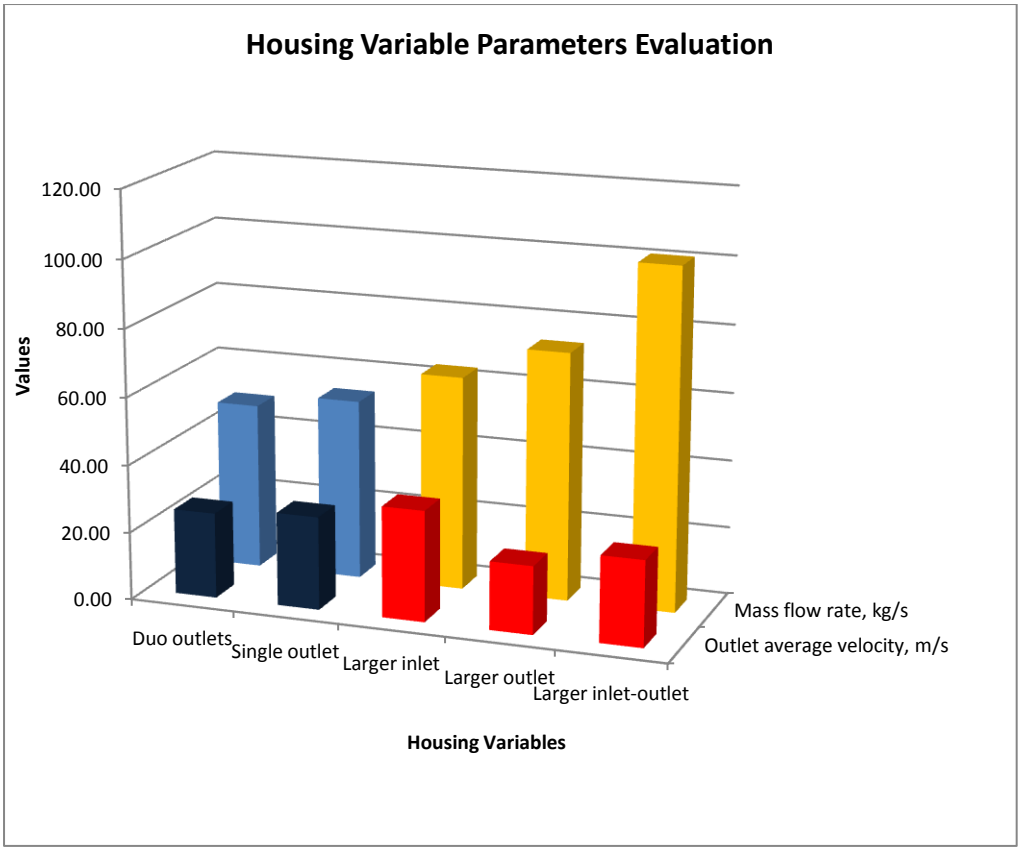

Figure 5.10: Housing variable parameters data comparison

Simulation for bi-directional (duo outlets) the Centripellor shows that it was feasible to be installed in the iAAV-1 and enable the vehicle to navigate through watery plains. Bi-directional housing was considered to enable iAAV-1 to move efficiently in forward and reverse direction. However a bi-directional pump was not as efficient as a single directional pump. This was because the bi-directional impeller blades were not optimum in delivering high flow rate as they were designed to cater for the need to propel the flow rate for both sides without bias. A single direction impeller was designed to optimum the disperse water in one direction. Figure 5.11 shows the activity patterns of the fluid simulated in NX.

Other parameters of the Centripellor housing members were the inlet-outlet size ratio. With the impeller variable parameters remain relatively constant, the cross section areas of the inlet and/or outlet size were varied incrementally to observe the flow rate and obtain an optimum inlet-outlet size ratio for Centripellor. The enlarged inlet size has shown continuous improvement in the efficiency, while the enlarged outlet will have an extended limit before the pressurized pump losses effectiveness.

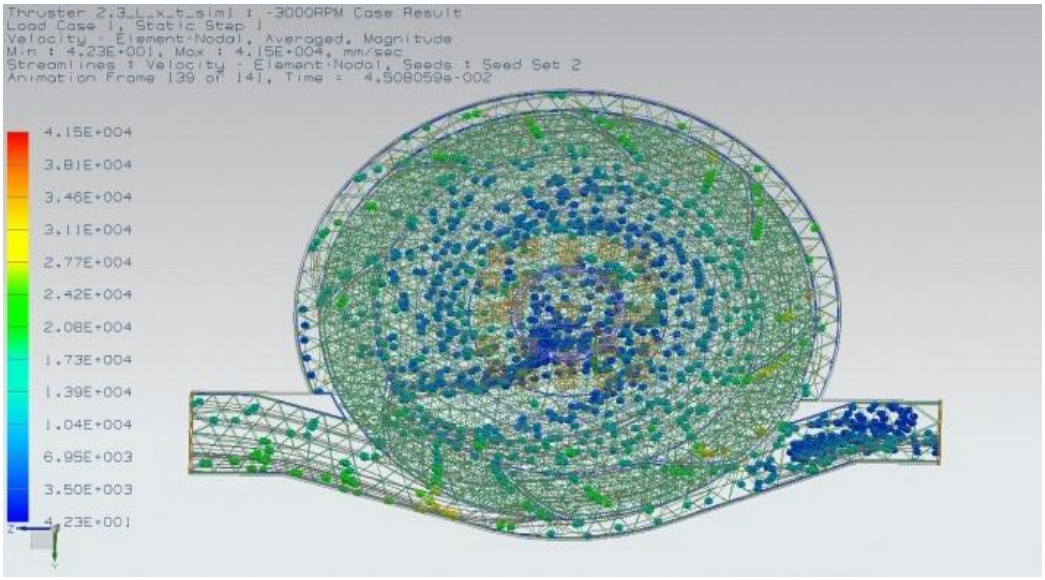

Figure 5.11: Simulations of duo outlets in the Centripellor

The Impeller circumference extension towards housing members were carried out between 0.1 mm to 15 mm gap. The sample size results are shown in Figure 5.12. The efficiency of the Centripellor indicates the hydraulic losses in a minimal close gap in the impeller and housing members, the fluid path through the pump were blocked because of friction. The fluid must change its direction and velocity on its path through the pump.

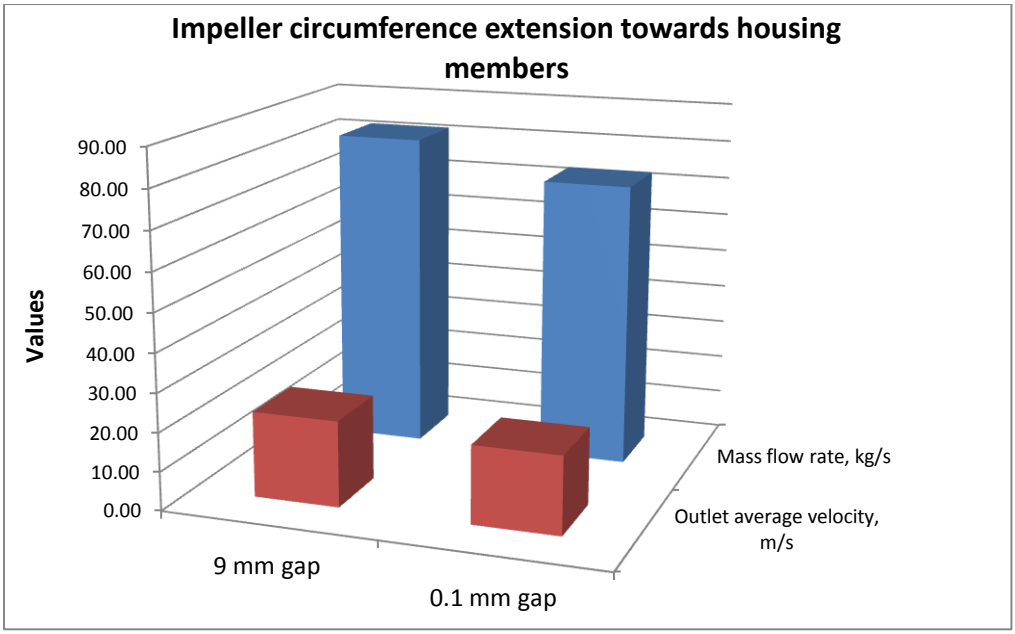

Figure 5.12: Comparison data between 0.1 mm gap and 9 mm gap from impeller circumference extension towards housing members

5.3.2 Simulation Convergence

Shown in Figure 5.13 are two samples of simulations that ran at 250 RPM case. The convergence criteria or stopping criteria were measured by time step, threshold, RMS residuals, iteration limit for both steady state and transient. The iteration in Figure 5.13 (a) shows that a convergence measure cannot be computed accurately because the residuals were unable to approach the flow residual threshold. The iteration in Figure 5.13 (b) shows a good convergence measure for the parameters to which the RMS residuals were heading steadily towards the flow residuals threshold. As such, it is guaranteed that there will be a steady-state converged solution to the iteration, whereby the discretized equation in NX is satisfied.

(a)

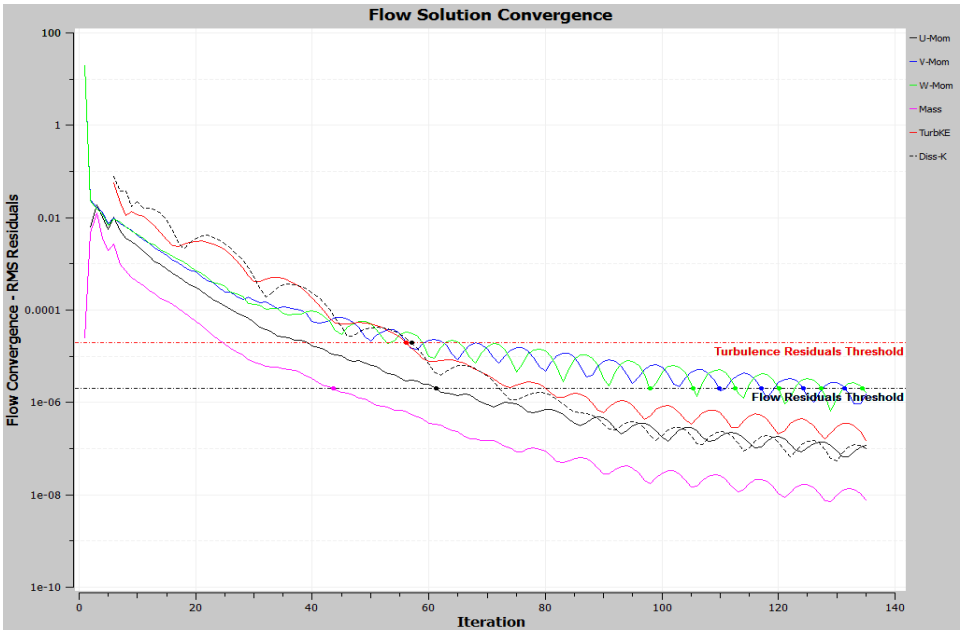

(b)

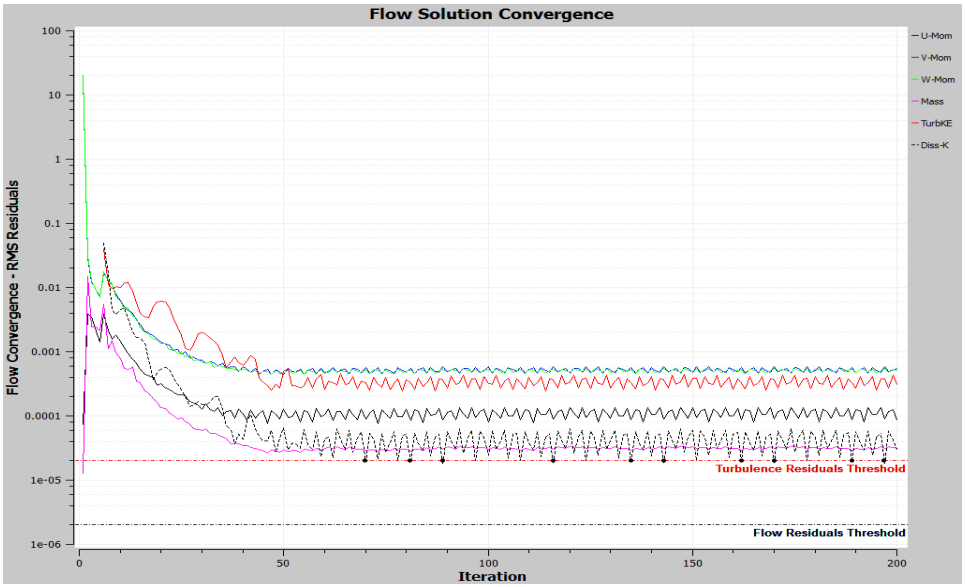

Figure 5.13: Simulation convergence

5.3.3 Flow Visualization

Model velocity-element nodal shown in Figure 5.15 to Figure 5.17 were obtained from the NX simulation to visualize the results of the intended CFD model. Figure 5.15 shows a cut plane section of the Centripellor whereby a 16 straight blades impeller and a tight spacing between the impeller and

housing were simulated. The fluid velocity visualized by different colours indicated that the water outlet flows quickest (red-orange-yellow-green region) at the edge of the impeller tips. Therefore, the circumference of the impeller towards the housing members has to give space for the fluid to swirl by taking the water from the centrifuge inlet and pumped outward towards the impeller tips before directing it to the outlet opening.

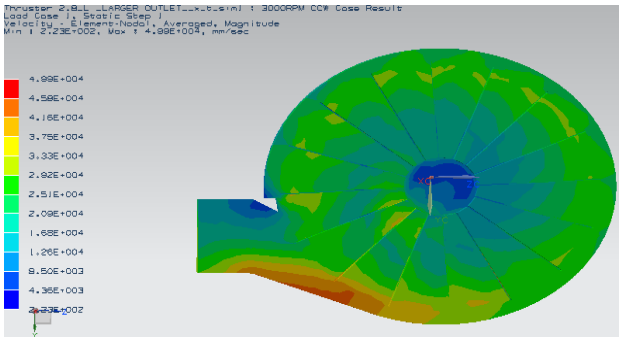

Figure 5.14: The Centripellor cut plane section

Figure 5.16 shows the whole CFD model obtained. From the figure, better aerodynamic guided propulsion housing members can be visualized. However, the design of the housing members remains relatively simple for testing due to the difficulty in prototyping.

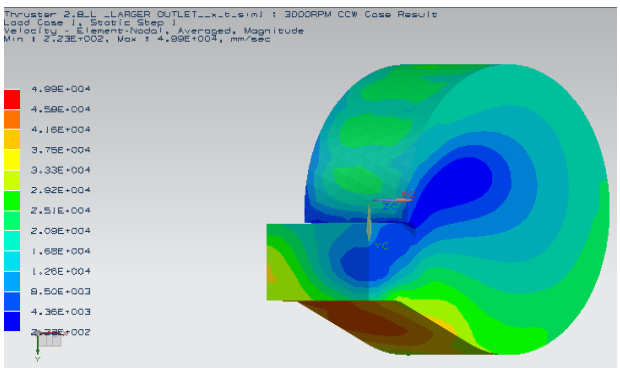

Figure 5.15: CFD model within housing members

Figure 5.17 shows two model of velocity-element nodal of a cut-plane using bubble streamlines to simulate the rotating fluid domain. These were a few amazing post-processing and reporting capabilities in NX. The real-time animated streamlines added interaction provided by flow visualization techniques was very useful for flow visualization in 3D and within the domain of versatile grids/plane associated with CFD simulation. From the bubbles/streamlines, the flow rate was reflected by the scalar properties inherent in the flow field.

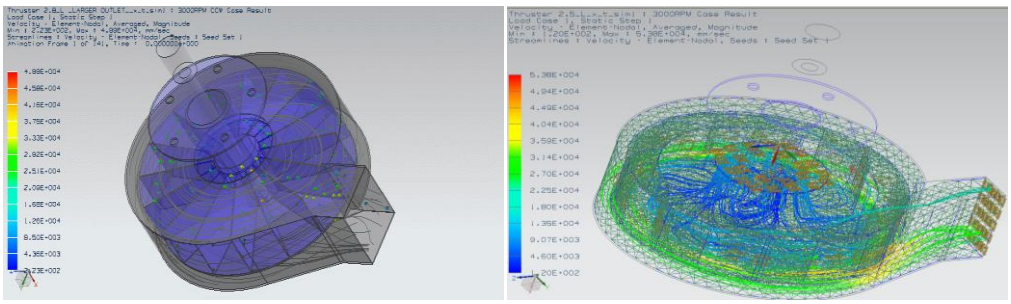

Figure 5.16: Bubbles (left) and streamlines (right) flow visualization in CFD model for the Centripellor

5.3.4 Propulsion Tests

The CFD model cannot predict the model resistance more accurately than the experimental method. Kuiper, 2010, suggested that past and present effort has been devoted to validating the experimental methods with full scale data. The propeller designer has to live with the experimentally found model resistance, thrust deduction and the wake distribution or their numerically calculated model equivalents, to find the propeller thrust.

5.3.4.1 Mass Flow Rate Curves

The accuracy of the simulation analysis was tested by comparing the simulation results with the experiment data. Figure 5.18 shows the comparison results of the mass flow rate obtained. From the figure, the experiment data were taken between a confidence range between 100 RPM to 500 RPM , they are plotted with thicker trend lines.

The errors were taken as the difference between the results of the experimental solution and the CFD simulation for axial impeller and radial impeller were 35 % and 2 % error respectively. Experimental results for axial impeller (as indicated by red colour line) has a performance growth over radial impeller (as indicated by blue colour line) of 2.5 times. Whereas, simulation results for axial impeller (as indicated by dotted purple line) has a performance growth over radial impeller (as indicated by dotted orange colour line) of 3.5 times.

Results have shown that the axial impeller was more superior than the radial impeller in drawing a high rate of mass flow in and out from the Centripellor. The error obtained and comparison method has shown that the simulation data were highly accurate. Unfortunately, the experimental data error in axial impeller produces 35 % less amount of flow rate. This could be caused by the axial blades angle which experienced more resistance in actual solution compared to computational simulation.

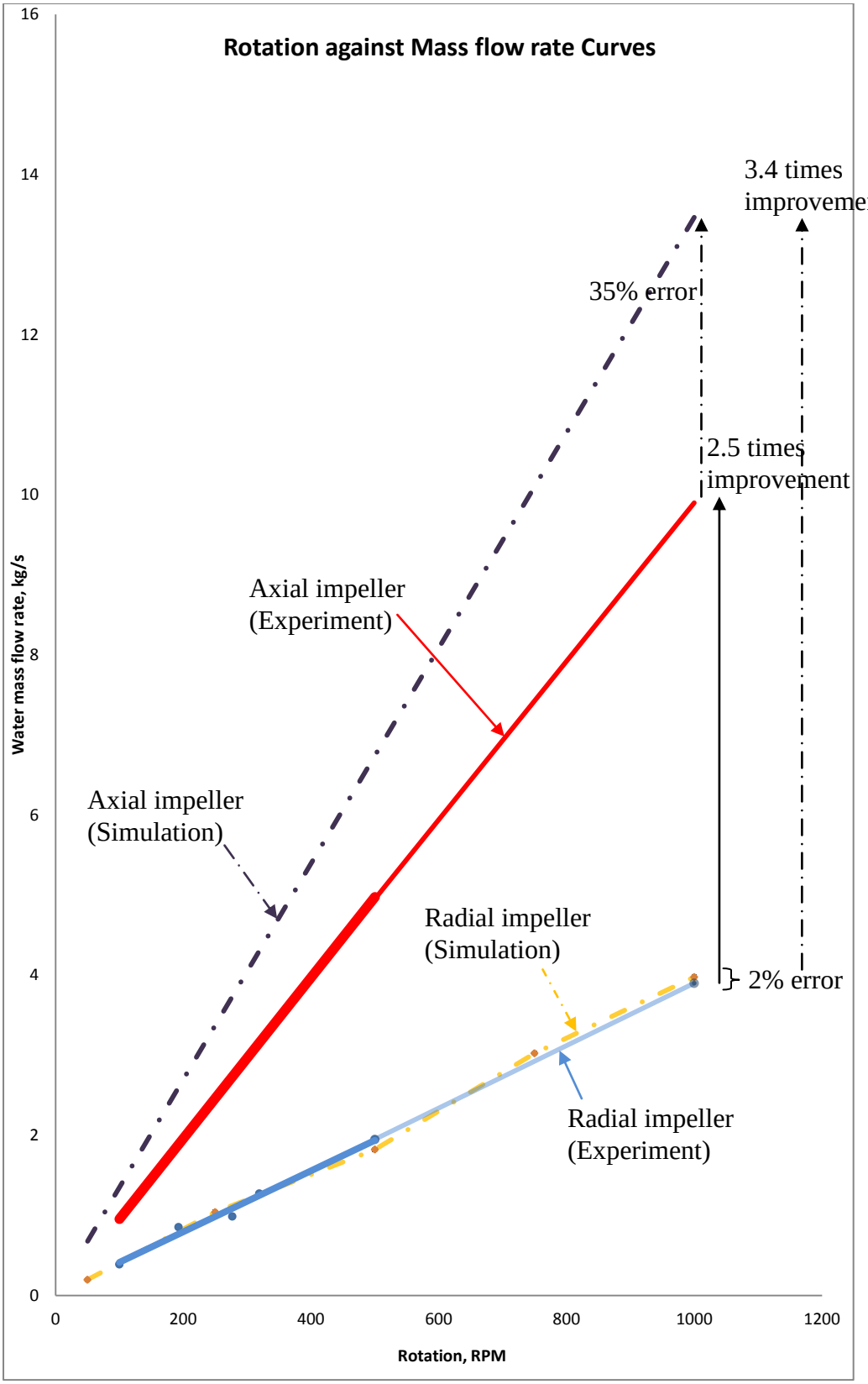

Figure 5.17: Comparison of simulated flow rate for axial and radial impeller versus experiment data

5.3.4.2 Thrust Curves

Figure 5.18 shows the performance of thrust gained by the wheel-based propulsion and the Centripellor. The Centripellor were represented by axial impeller (as indicated by red colour line) and radial impeller (as indicated by blue color line). The wheel-based propulsion was represented by left/right wheel (as indicated by orange/black colour line). The confidence data regions were represented by prefect straight line, where the dotted line were extension for simulation data comparison. The Centripellor recorded a thrust improvement by 20 % for an axial impeller and 5 % for radial impeller. 3 out of 4 experimental curves were plotted with full regression, indicating accurate tests performed and satisfying the governing equation relation $T = \frac{dm}{dt} \cdot v$ and $T \propto \omega^2$, where a second order polynomial equation was obtained.

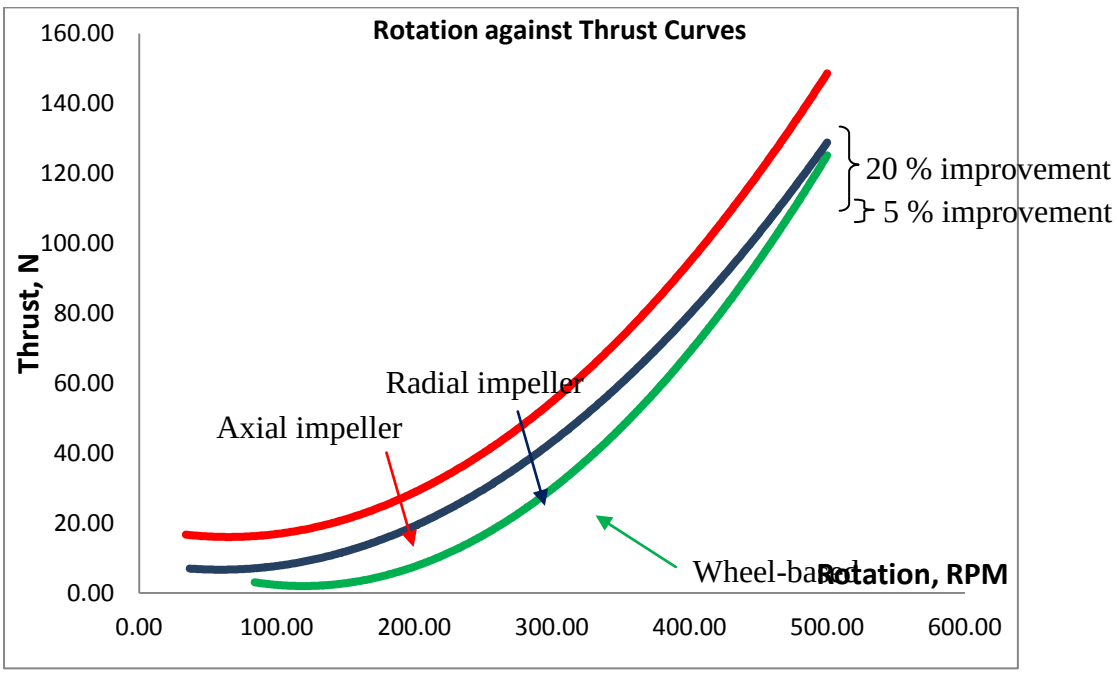

Figure 5.18: Comparison of experimental data between Centripellor and wheel-based propulsion

Figure 5.19 shows the comparison results between the experiment (red line) and the simulation data (yellow region) for axial impeller. In another graph, Figure 5.20 shows the comparison results between the experiment (red line) and the simulation data (blue region) for radial impeller.

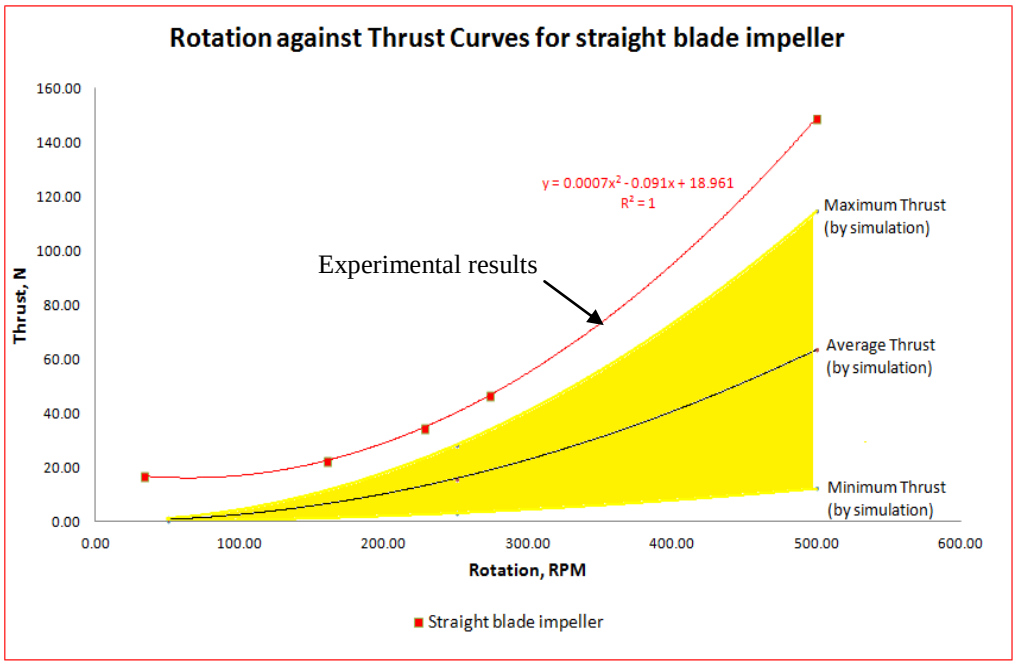

Figure 5.19: Comparison of experiment and simulation data for axial impeller

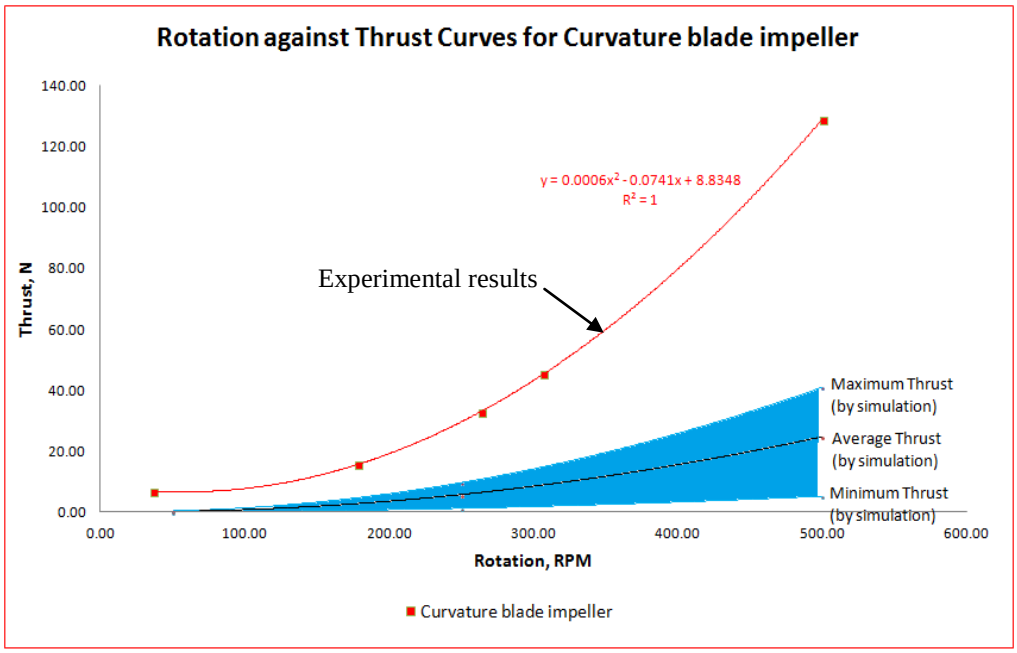

Figure 5.20: Comparison of experiment and simulation data for radial impeller

5.3.5 Water Propulsion Performance

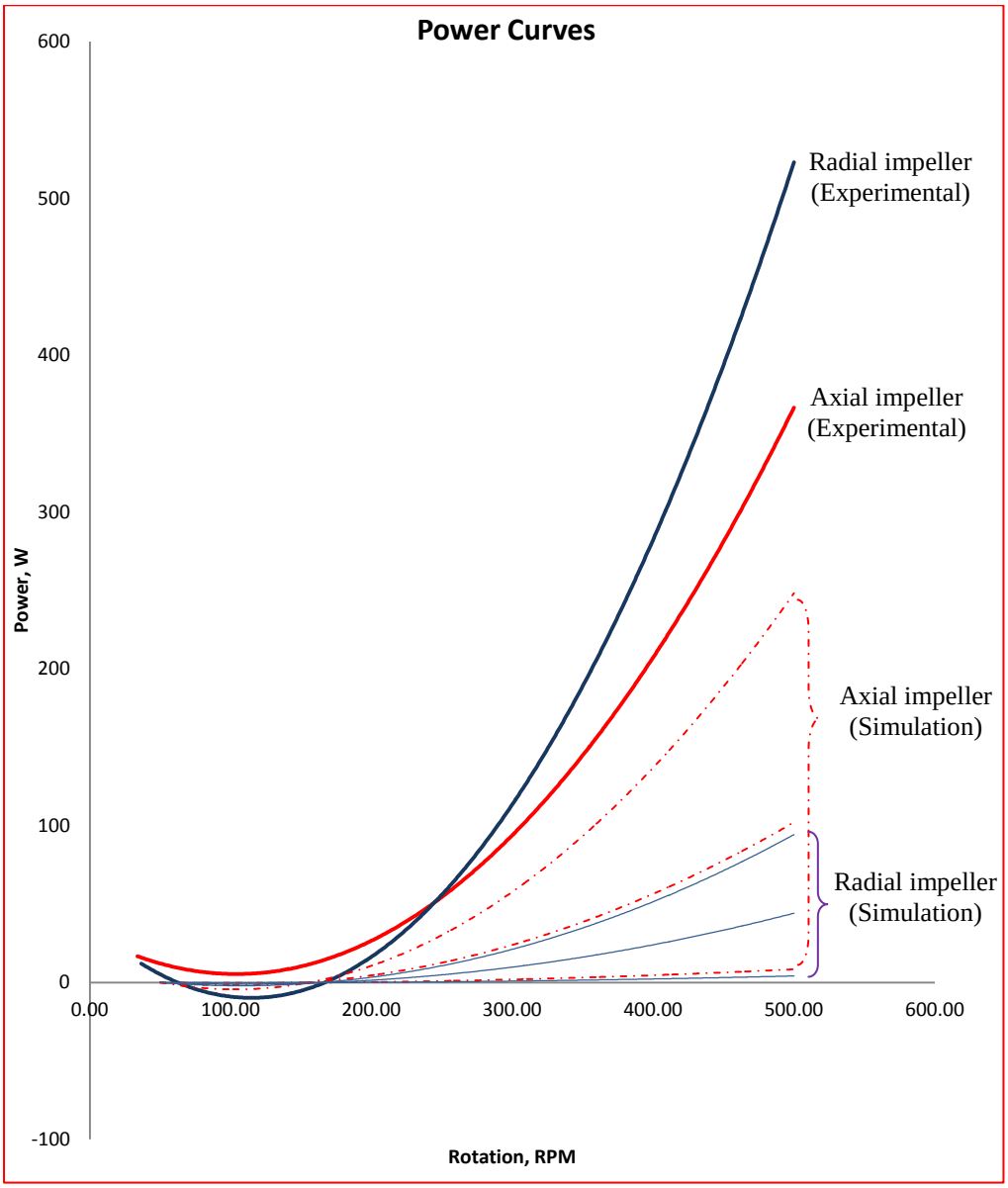

Figure 5.21: Power curves generated for Centripellor

The power curves of the Centripellor simulation results and experiment data are plotted in Figure 5.21. The use of radial impeller produced more power than the axial impeller in the given $P^2 = \frac{T^3}{4\rho A}$ relationship. Two such Centripellor with given the same outlet area. The radial impeller provided

additional 43% power to generate the same amount of flow. The simulation results were plotted below the region of experimental results where the axial impeller covers a wide area with its maximum and minimum curves, while the radial impeller covers the area right below the mean values of axial impeller. This was logical since there were additional wall-reflection forces generated in the large confined tank. The generated guided propulsive thrust was the sum of the force generated from the flow and the force of the wall-reflection; two forces were produced in the experimental procedure.

Experiments at full scale need not be expensive, The Centripellor development yield immediate result in altering and improving the flow. With the auxiliary propulsion device mounted on the iAAV-1, the measured travel speed of 4.4 km/hr in an open lake was 3 times the comparable figure of the conventional wheel-based propulsion at 1.3 km/hr. From Figure 5.18, the thrust developed by the Centripellor within the confident level (normal operating condition) of rotation speed between 50 RPM to 350 RPM was recorded between 16.7 N to 46.5 N. The comparable figure for the conventional wheel-based propulsion was 2.4 to 31.9 N. The effectiveness of the Centripellor generally improved the wheel-based propulsion thrust by 37.5%.

As far as the Centripellor performance was concerned, measurements were generally obtained from the tests. However, tests will hardly be the actual conditions. The sea state, wind condition or unstructured environment will always complicate things for the iAAV-1. Attention has been given to the validation of the Centripellor invention. Focus has been on delivering the first

concept in improving the wheel-based propulsion guided propulsion approach using centrifugal pump. In such a case, some hypotheses were made based on the CFD model simulation results and some corrections were applied to the design. There were corrections ranging from the size and design of the impeller or the housing members of the Centripellor. When that was not effective a redesign was made in which the design process was repeated using computational modelling in the CFD.

A full scale model were tested to reveal the observations made, which in the past, these observations were difficult and expensive because of the cost in prototyping. As a summary for the iAAV-1 water navigation, the practical results obtained confirmed the simulation results generated.

CHAPTER 6

CONCLUSIONS AND FUTURE WORK

6.1 Summary of Research Work

A new and novel approach to design and control the AAV was proposed in this dissertation. The new approach specified the intended environment applications to furnish new control hardware and software for the AAV under tight and confined areas such as in tunnels, tropical areas with riverbanks and muddy swamp, or underneath collapsed structures. This new approach is intended for the new control amphibious vehicle systems to be more flexible, easier to implement, build, and to modify.

6.1.1 Land Navigation

This dissertation presented the initial studies and development of an autonomous amphibious vehicle platform, called iAAV-1 which is performed by the Autonomous Amphibious Vehicle (AAV) team from the UTAR Center of Vehicular Technology. The research claims were completed on and off the iAAV-1 platform from an embodiment design and various modelling and simulation data acquired towards prototyping and testing. The initial results confirmed the feasibility of the preliminary design concept which complied with the following development:

1. Fully developed functioning compact hardware platform.
2. Electrical power transmission.
3. Single drive system to traverse on land and water surface.
4. Flexible maneuvering control and configuration.
5. Remote assistance and autonomous capability.
6. Parallelism using FPGA.
7. Simplicity and capable to reconstruction quickly

6.1.2 Water Navigation

A new Centripellor was developed using the CFD computational data to allow for verification and obtaining of experimental data to confirm the feasibility of the preliminary design concept. The Centripellor achieved the following requirements in its initial studies and development:

1. Guided propulsive forces primary from the wheels.
2. The Centripellor as an auxiliary propulsion device.
3. The iAAV-1 achieved travel speed of 4.4 km/hr (comparable figure of the conventional wheel-based propulsion was 1.3 km/hr).
4. The Centripellor thrust was developed between 16.7 to 46.5 N (comparable figure for the conventional wheel-based propulsion was 2.4 to 31.9 N).
5. Three times improvement on water speed and an increased thrust of 37.5% from a conventional wheel-based propulsion.

6.2 Anticipated Impact

A new approach to build an autonomous amphibious vehicle (iAAV-1) was described in this thesis. The iAAV-1 architecture system and land-water drive system generated information that may help the future development of autonomous application and pave the way for a relatively low-cost autonomous application for industrial as well as academic purposes.

The aim of this iAAV-1 architecture system was to model the precision maneuvering on land and an improved performance on water. The architectural guidelines were based on observations of the environments which the iAAV-1 might need to operate in. Many autonomous mobile vehicles have tried to achieve zero-radius steering by giving flexibility in performing sharp corners using a steering mechanism that employed a pair of independently controlled driving wheels. To date, existing amphibious vehicle is a complicated mechanical assemblage that hinders the potential to perform autonomously. It requires years to generate the program and form a process analyzer. Hence, it requires numerous levels of controlled architecture and a high level of operating expertise. Not only does it complicate the operating method, but also the mounted hardware is bulky and not conducive for a vehicle such as the iAAV-1 to perform its search and rescue mission. Robotics were applied to this steering mechanism because it was easier to operate autonomously and differential directional drive makes more sense for an amphibious vehicle that needs to navigate in water.

6.3 Future Works

The iAAV-1 land navigation can be further improved by:

1. Enhancements of iAAV-1 adaptability on rough terrains. The kinematic equations of the vehicle in interactions with ground need to be derived by taking consideration on the estimation of slip velocities and terrain parameters.
2. Sensor and actuator fault reconstruction modelling on electrical machinery drives. The Sensor fault reconstruction scheme can reconstruct the fault/failure to achieve fault-tolerant-control; maintaining performance even though a fault is happening.
3. To enhance reliability and durability of the vehicle system. The Integration of articulated suspension and mechanical brakes to the vehicle system improves maneuverability on uneven terrain.
4. To extend the system integration. To develop a sensor fusion for high accuracy estimation for both localization and map-building.
5. To determine the cost function of iAAV-1. Generalization of optimization theory by maximizing and minimising a function involving the vehicle reaction time, cost, speed, energy, target achievement, mileage driven, etc.

iAAV-1 water navigation can be further improved by:

1. Enhancing the iAAV-1 adaptability on stream water surface. Tests should be carried out in different water states, as well as determine the dynamics and various constraints, such as the zero radius turn capability on water.
2. Modelling of an improved amphibian naval architects. Hull redesigned to reduce resistance and to improve the water traversing characteristics. If designed properly, the structure design of the iAAV-1 should provide the vehicle with optimum and adequate weight and rigidity.
3. Modelling of the bi-directional Centripellor wheel for equal forward and reverse movement.
4. Modelling of the Centripellor using fiber reinforced material as a close-fitting shell to the tires instead of an extensive closure to the wheel hub. The first prototyping of the Centripellor was a separate piece to the vehicle wheel. An integration between the wheel hub and Centripellor using fiber-glass material can reduce the overall weight and the dimension width of the iAAV-1.
5. Predicting the hydrodynamic resistance of immersed iAAV-1. To determine the iAAV-1 water navigation capability, it is important to find out the vehicle resistance because testing has revealed that the CFD computation analysis differs from the actual resistance.

AUTHOR'S PUBLICATIONS

Tee Y. H., Tan C. S., Tan Y. C., et al., 2010a. A Compact Design of Zero-Radius Turning Steering Autonomous Amphibious Vehicle with Direct Differential Directional Drive – UTAR-AAV. Singapore: IEEE Conference on Robotics, Automation and Mechatronics (CIS-RAM), pg. 176-181.

Tee Y. H., Tan C. S., Tan Y. C., et al., 2010b. Design Considerations of an Autonomous Amphibious Vehicle – UTAR- AAV. Kuala Lumpur: IEEE Conference on SusTainable Utilization and Development in Engineering aNd Technology (STUDENT), pg. 13-18.

REFERENCES

Adams C.D., 1999. Amphibious All Terrain Vehicle. *United States Patent*: No.: 5,993,273, Appl. No.: 09/042,091.

Ashcraft B., 2009. Just Press "Save" - Disaster Search-and-Rescue in Robot-Crazy Japan, *Popular Science* [Online]. Available at: http://www.popsci.com/scitech/article/2009-05/just-press-save-1 [Accessed: 12 May 2011]

Black R., 2009. Japan's Earthquake Rescue Robot, *BBC News* [Online]. Available at http://news.bbc.co.uk/2/hi/science/nature/8069435.stm. [Accessed: 12 May 2011]

Bräunl T., 2008. *Embedded Robotics - Mobile Robot Design and Application with Embedded Systems* (3rd Edition), Driving Robots, pp. 131-156. Perth, Australia: Springer.

Bryham M.J., 2008. Amphibious Vehicle, *United States Patent*: No.: US 7,314,395 B2, Appl. No.: 11/294,537, Sealegs International Limited, Aukland (NZ).

Byrne R.H., Klarer P.R., Pletta J.B., 1992. Techniques for Autonomous Navigation Sandia Report, Sandia National Laboratories, Albuquerque, NM. No.: SAND92-0457.

Carsten J. et. al, 2006. Global Planning on the Mars Exploration Rovers: Software Integration and Surface Testing. *Jet Propulsion Lab Technical Report*.

Chan K.C., Tan C.S., Cheng C.L., Lee K.S., Kho C.L., Fong Y.S. and Teng C.M., 2010. Feasibility Study of FPGA Based Real-Time Controller for Autonomous Vehicle Applications, *IEEE Conference on Sustainable Utilization and Development in Engineering and Technology (STUDENT)*, pp.1-6.

Carlton J., 2007. *Marine Propellers and Propulsion* (2nd Edition), Propulsion system, London, UK: Butterworth Heinemann. pp. 13-29.

Dally W.R., Johnson M.A., Osiecki D.A., 1994. Initial Development of an Amphibious ROV for Use in Big Surf. *Marine Technology Society Journal*, Vol. 28, No. 1, pp. 2-10.

Davis G. & Cornwell, 2005. Amphibious Vehicle, *United States Patent*: No.: US 6,971,931 B2, Appl. No.: 10/692,998.

Dixon. D., 2008. All-Terrain Robotic Omni-Directional Drive Assembly, *United States Patent*: No.: US 2008/01565547 A1, Appl. No.: 11/772,605.

Dolinskaya I. & Smith R., 2008. Obstable-Avoidance Fastest Paths in Anisotropic Media. *University of Michigan Technical Report*.

Ehrlich I.R., Kamm I.O., and Worden G., 1970. Water Performance of Amphibious Vehicles Part I – Drag and Water Speeds. *Journal of Terramechanics*, Vol. 7, No. 2, pp. 61-102, Pergamon Press, Great Britian.

Ehrlich I.R., Sloss D., Hanamoto B., and Nuttall C.J., 1972. The Wheel Pump Propulsion System for Floating Vehicles. *Journal of Terramechanics*, Vol. 8, No. 4, pp. 43-52.

Flom B., 2009. DUKW 21 - Autonomous Navigation - Autonomous Path Planning for an Amphibious Vehicle. *Naval Surface Warfare Center, Carderock Division*: Re. No.: NSWCCD-CISD-2009/008.

Frejek M. and Nokleby S., 2008. Design of a Small-scale Autonomous Amphibious Vehicle. *21st Annual Canadian Conference on Electrical and Computer Engineering (CCECE)*, Niagara Falls, Canada. pp. 781-786.

Gage D.W., 1997. "Introduction" *Mobile Robots XII*, SPIE: Vol. 3210, page vii.

Gizmodo, 2011. Meet the Newest Member of Yokohama's Mechanized Earthquake Rescue Brigade [Online]. Available at: http://uk.gizmodo .com/5161465/meet-the-newest-member-of- yokohamas-mechanized-earthquake-rescue-brigade [Accessed: 20 May 2011]

Global Security, 2004. Military - DUKW in Action [Online]. Available at: from http://www.globalsecurity.org/military/systems/ground/dukw-action.htm [Accessed: 20 May 2011]

Gonzales F., Orme R., Ruppert A., Schaffer J., 2007. DUKW 21 - Amphibious Cargo Transfer from Ship to Shore. *Naval Surface Warfare Center, Carderock Division*: Re. No.: NSWCCD-CISD-2007/003.

Ha Q.P., Tran T.H., Scheding S., Dissanayake G., and Durrant-Whyte H.F., 2005. Control Issues of an Autonomous Vehicle. *22nd International Symposium on Automation and Robotics in Construction (ISARC)*. Ferrara, Italy.

Hart R., 2010. Robotos Could Assist in Quake Search and Rescue, *ABC7 News* [Online]. Available at: http://abclocal.go.com/kgo/story ?section=news/drive_to_discover&id=7224227 [Accessed: 12 May 2011]

Helvacioglu S., Helvacioglue I.H., Tuncer B., 2011. Improving the River Crossing Capability of an Amphibious Vehicle. *Journal of Ocean Engineering*, Elsevier Ltd, Turkey. No. 38, pp. 2201-2207.

Hewitt S.C. & Ketchikan, 2011. Amphibious Vehicle, *United States Patent*: No.: US 7,950,973 B2, Appl. No.: 12/591,265.

Hu H., Gu D., and Brady J.M., 1997. Outdoor Navigation of a Mobile Robot with Multiple Sensors, *Mobile Robots XII*, SPIE: Vol. 3210, pp. 13-24.

Hsu J., 2009. Medic Bot Does Curls to Save Wounded Soldiers, *Popular Science* [Online]. Available at: http://www.popsci.com/military-aviation-amp-space/article/2009-08/bear-medic-bot-does-curls-save-wounded-soldiers [Accessed: 12 May 2011]

IIHS, 2012. Low-speed Vehicles, Insurance Institute for Highway Safety (IIHS) [Online]. Available at: http://www.iihs.org/laws/lowspeed vehicles.aspx [Accessed: 15 June 2012]

Kuiper G., 2010. New Developments and Propeller Design. *Journal of Hydrodynamics*, Vol. 22 (5), pp. 7-16.

Lacroix S., Mallet A., Bonnafous D., Bauzil G., Fleury S., Herrb M., Chatila R., 2002. Autonomous Rover Navigation on Unknown Terrains: Functions and Integration. *The International Journal of Robotics Research*, Vol. 21, No. 10-11, pp. 917-942, Sage Publications, France.

Lee D., 2011. Microsoft Kinect-Powered Roboto to Aid Earthquake Rescue, BBC World Service [Online]. Available at: http://www.bbc .co.uk/news/technology-12559231 [Accessed: 12 May 2011]

Mott R.L., 2006. *Machine Elements in Mechanical Design* (4th Edition). Virginia, US: Prentice Hall.

Munson B.R., Young D.F., Okiishi T.H., 2006. *Fundamentals of Fluid Mechanics* (5th Edition), John Wiley & Sons: Asia. Pumps and Turbines, pp. 684-736.

Nassiraei A.A.F., Ishii K., 2007. Concept of Intelligent Mechanical Design for Autonomous Mobile Robots. *Journal of Bionic Engineering*, Vol. 4, pp. 217-226.

Pohl R., 1998. *Schwimmauto* [Online]. Available at: http://www.schwimmauto.de [Accessed: 12 May 2011]

Popular Science, 1931. Strange Craft at Home on Water or Land, *Popular Science Monthly*. April Vol. 118, pp. 70.

Richmond T., 1905. Awesome Amphibian Cars, *Ooodd* [Online]. Available at: http://www.oooddd.com/97-awesome-amphibian-cars [Accessed: 12 May 2011]

Rymiszewski A.J., 1964. Improving the Water Speed of Wheeled Vehicles. *Journal of Terramechanics*, Elsevier Ltd., US. Vol. 1, No. 1, pp. 75-90.

Tai R., Chan A., Seit R., 2009. Planning of Deep Sewage Tunnels in Hong Kong. *Drainage Services Department*, Government of Hong Kong SAR, China.

Teoh C.W., Tan C.S. and Tan Y.C., 2010. Preliminary Study on Visual Guidance System for Autonomous Vehicle in Rainforest Terrain, *IEEE Conference on Robotics Automation and Mechatronics (RAM)*, pp. 403-408.

The Star, 2009. Ministry sets eyes on 'Sealegs' [Online]. Available at: http://thestar.com.my/news/story.asp?file=/2009/11/21/nation/5156360 &sec=nation [Accessed: 21 Nov 2009]

Tran T.H., Ha Q.P., Grover R., Scheding S., 2007. Modeling of an Autonomous Amphibious Vehicle. *Proceedings of the Australiasian Conference on Robotics and Automation*, pp. 1-7. Canberra, Australia.

Tuvie, 2012. Tuvie design of the future [Online]. Available at: http://www.tuvie.com/future-amphibious-hybrid-concept-vehicle-with-intelligent-wheel-system/ [Accessed: 23 July 2012]

UATM, 2007. DUKW, *U.S. Army Transportation Museum (UATM)* [Online]. Available at: http://www.transchool.eustis.army.mil/museum/dukw. htm [Accessed: 20 May 2011]

Wang V., 2009. Send in the Rescue Robots - Testing emergency-response robots in Disaster City, Texas, *Popular Science* [Online]. Available at: http://www.popsci.com/scitech/article/2009-05/send-rescue-robots [Accessed: 12 May 2011]

Wikipedia, 2009. The Singapore Green Plan [Online]. Available at: http://en. wikipedia.org/wiki/ Singapore_Green_Plan_2012 [Accessed: 12 May 2011]

Wikipedia, 2011a. *Oruktor Amphibolos* [Online]. Available at: http://en.wikipedia.org/wiki/Oliver_Evans [Accessed: 12 May 2011]

Wikipedia, 2011b. *Amphibious ATV* [Online]. Available at: http://en.wikipedia .org/wiki/Amphibious_ATV [Accessed: 12 May 2011]

Wikipedia, 2011c. Water supply and sanitation in Singapore [Online]. Available at: http://en.wikipedia.org/wiki/Water_supply_and_ sanitation_in_Singapore

Wikipedia, 2011d. Amphibious Vehicle [Online]. Available at: http://en. wikipedia.org/wiki/Amphibious_vehicle [Accessed: 12 May 2011]

Wikipedia, 2012. *ARGO* [Online]. Available at: http://en.wikipedia.org/wiki/ARGO [Accessed: 23 July 2012]

Wood S., 2006. Modular Amphibious Research Crawler – Characterization of the Coastal Environment Using a Portable Remotely Operated Crawler. *Sea Technology*, Vol. 47, No. 2.

Zhao J., Gong Q.M., Eisensten Z., 2007. Tunneling Through a Frequently Changing and Mixed Ground: A case history in Singapore. *Tunneling and Underground Space Technology*, Elsevier Ltd.. Lausanne, Switzerland. Vol. 22, pp. 388-400.

BIBLIOGRAPHY

Abe M. and Hendrick J.K., 2001. *A Mechatronics Approach to Advanced Vehicle Control Design*. Inc. H. Aref and J.W. Philips (eds), Mechanics for a New Millennium, pg 147-164. Kluwer Academic Publishers, the Netherlands.

Anousaki G.C., Konstantinos, Kyriakopoulos J., 2007. Simultaneous Localization and Map Building of Skid-Steered Robots –Ensuring Safe Movement in Structured Outdoor Environments. *IEEE Robotics & Automation Magazine*, Vol. 14, No.1, pg. 79-89.

Bagnell J.A., Bradley D. et. al., 2010. Learning for Autonomous Navigation – Advances in Machine Learning for Rough Terrain Mobility. *IEEE Robotics & Automation Magazine*, Vol. 17, No.2, pg. 74-84.

Belta C., Bicchi A. et. al., 2007. Symbolic Planning and Control of Robot Motion – Finding the Missing Pieces of Current Methods and Ideas. *IEEE Robotics & Automation Magazine*, Vol. 14, No.1, pg. 61-70.

Bensalem S., Gallien M. et. al., 2009. Designing Autonomous Robots – Towards a More Dependable Software Architecture. *IEEE Robotics & Automation Magazine*, Vol. 16, No. 1, pg. 67-77.

Boxerbaum A.S., Werk P. et. al., 2005. Design of an Autonomous Amphibious Robot for Surf Zone Operation: Part I Mechanical Design for Multi-Mode Mobility. *International Conference on Advanced Intelligent Mechatronics* (IEEE/ASME), pg. 1459-1464.

Chan K.C., 2011. *Compact Real-Time Control System of Autonomous Vehicle System Using FPGA Platform*. MEngSc (A), University of Tunku Abdul Rahman (UTAR).

Ehrlich I.R., Kamm I.O., and Worden G., 1970. Water Performance of Amphibious Vehicles Part II – Propulsion and Maneuverability. *Journal of Terramechanics*, Vol. 7, No. 3 and 4, pp. 69-99, Pergamon Press, Great Britian.

Le-Anh T., De Koster M.B.M., 2005. A Review of Design and Control of Automated Guided Vehicle Systems. *European Journal of Operational Research*, Elsevier B.V., the Netherlands. Vol. 171, pg. 1-23.

Livatino S., Muscato G. et. al., 2008. Mobile Robotic Teleguide Based on Video Images – Compaison Between Monoscopic and Stereoscopic Visualization. *IEEE Robotics & Automation Magazine*, Vol. 15, No. 4, pg. 58-67.

Martinez S., Cortes J., and Bullo F., 2003. *Motion Planning and Control Problems for Underactuated Robots*. Inc. A. Bicchi, H.I. Christensen, D. Prattichizzo (eds), Control Problems in Robotics, STAR 4, pp. 59-74. Springer-Verlag Berlin Heidelberg.

Mohammed O.A. and Abed N.Y., 2008. Real-time Simulation of Electric Machine Drives with Hardware-in-the-loop. *The International Journal for Computation and Mathematics in Electrical and Electronic*

Engineering, , Emerald Group Publishing Ltd. Miami, Florida, USA. Vol. 27, No. 4, pp. 929-938

Sloss D., 1970. Water Performance Tests of the Wheel Pump Installed on a 1/4-ton Floater/Swimmer. *Davidson Laboratory Report* 1450.

Teoh C.W., Tan C.S. and Tan Y.C., 2010. Ground plane detection for autonomous vehicle in rainforest terrain. *IEEE Conference Sustainable Utilization and Development in Engineering and Technology (STUDENT)*, pp. 7 - 12.

Teoh C.W., 2011. *Near-Range Water Body Detection and Obstacle Detection in Rainforest Terrain / Tropical Terrain*. MEngSc(A), University of Tunku Abdul Rahman (UTAR).

Vis I.F.A., 2004. Survey of Research in the Design and Control of Automated Guided Vehicle Systems. *European Journal of Operational Research*, Elsevier B.V., the Netherlands. Vol. 170, pg. 677-709.

Wassmann W.A., 1973. Bi-Directional Centrifugal Pump. United States Patent, Mansfield, Ohio, US, No.: 3,751,179, Appl. No.: 166,096.

Williams S.B., Newman P. et. al., 2001. Autonomous Underwater Navigation and Control. *Journal Robotica*, Cambridge University Press New York, NY, USA, Vol. 19, No. 5, pg. 481-496.

APPENDIX A

NX 7.5: ADVANCED FLOW

Mass and Momentum Equations

The mass and momentum equations, when expressed in Cartesian coordinates and using the tensorial notation, are:

$$\frac{\partial \rho}{\partial t} + \frac{\partial (\rho U_j)}{\partial x_j} = S_m \tag{A.1}$$

$$\frac{\partial (\rho U_j)}{\partial t} + \frac{\partial (\rho U_i U_j)}{\partial x_i} = -\frac{\partial P}{\partial x_j} + \frac{\partial}{\partial x_i}\left(\mu\left(\frac{\partial U_i}{\partial x_j} + \frac{\partial U_j}{\partial x_i}\right) - \overline{\rho u_i u_j}\right) + S_{U_j} \tag{A.2}$$

In Eqs. (A.1) and (A.2), the Einstein convention is used (i, j, k = 1,2,3), U_j and u_j are the components of the mean and the fluctuating velocity in the x_j direction, P is the pressure, ρ is the density of the fluid, μ is the dynamic viscosity of the fluid, and $-\overline{\rho u_i u_j}$ represents the turbulent (or Reynolds) stresses. S_m and S_{U_j} are the source terms for the mass and momentum equations, respectively. Equation (A.1) expresses the conservation of mass of the fluid and is valid for incompressible and compressible flows. Equation (A.2) represents the conservation of momentum for general flows. The various terms of this equation are in the same order of the equation: the transient term, the convection term, the pressure gradient term, the stress term and the source term. This equation is also valid for both, incompressible, and compressible

flows. The source term S_{U_j} in Eq. (A.2) can represent body forces, or flow resistance forces:

1. For natural convection flows, S_{U_j} includes the buoyancy force. See Buoyancy force for more information.
2. For flows in a rotating frame of reference, it includes Coriolis and centripetal forces. See Centripetal and Coriolis forces for more information.
3. For flows through porous blockages, S_{U_j} contains additional resistance terms.

Energy Equation

In order to describe completely deferent kinds of flows, the equation of conservation of energy must also be implemented. Starting from total energy equation, the high speed form and the low speed form of the energy equation will be derived. The instantaneous total energy equation in tensorial notation is

$$\frac{\partial\left[\rho\left(e+1/2U^2\right)\right]}{\partial t}+\frac{\partial\left[\rho U_i\left(e+1/2U^2\right)\right]}{\partial x_i}= \\ =-\frac{\partial q_i}{\partial x_i}-\frac{\partial PU_i}{\partial x_i}-\frac{\partial}{\partial x_j}\left[U_i\mu\left(\frac{\partial U_i}{\partial x_j}+\frac{\partial U_j}{\partial x_i}\right)\right]+q' \tag{A.3}$$

where e is the internal energy, U, the velocity magnitude, q_i, the heat flux in the direction x_i, and q', a heat generation or heat sink per unit volume.

In Eq. (A.3), the various terms represent, in order: the rate of energy gain per unit volume, the rate of energy input per unit volume due to convection, the rate of energy addition due to conduction and turbulent mixing, the rate at which work is done on the fluid by pressure and viscous forces (dissipation term), and the rate of heat generation by internal sources. The second and fourth terms in the above equation can be combined as:

$$\frac{\partial\left[\rho U_i\left(e+\frac{1}{2}U^2\right)\right]}{\partial x_i}+\frac{\partial PU_i}{\partial x_i}=\frac{\partial}{\partial x_i}\left[\rho U_i\left(e+\frac{1}{2}U^2+\frac{P}{\rho}\right)\right] \tag{A.4}$$

Furthermore, using the definition of the total enthalpy, h_o,

$$h_o=h+\frac{1}{2}U^2=e+\frac{P}{\rho}+\frac{1}{2}U^2 \tag{A.5}$$

and combining with Eq. (A.3) into Eqs. (A.4) and (A.5) gives

$$\frac{\partial(\rho h_o)}{\partial t}+\frac{\partial(\rho U_j h_o)}{\partial x_j}=\frac{\partial P}{\partial t}+\frac{\partial q_j}{\partial x_j}-\frac{\partial}{\partial x_j}\left[U_i\mu\left(\frac{\partial U_i}{\partial x_j}+\frac{\partial U_j}{\partial x_i}\right)\right]+S_h \tag{A.6}$$

where S_h is the energy source term. In Eq. (A.5) h is the static enthalpy of the fluid.

Low Speed Equation

For low speed flows (Mach < 0.3), the energy equation is simplified for robustness and for round-off purposes. For low speed incompressible and compressible flows, the pressure work and dissipation terms in Eq. (A.8) can be neglected. The simplified form of the energy equation has the mechanical energy subtracted from the total energy, and becomes a thermal energy equation.

$$\frac{\partial(\rho h)}{\partial t} + \frac{\partial(\rho U_j h)}{\partial x_j} = \frac{\partial}{\partial x_j}\left(\frac{k}{c_p}\frac{\partial h}{\partial x_j} - \overline{\rho u_j h'}\right) + S_h \tag{A.7}$$

This form of the equation ensures conservation of the thermal energy, and avoids round-off problems. The low speed form of the energy equation is used by default in the flow solver.

High Speed Equations

After modeling the conduction and taking the Reynolds average of Eq. (A.6), Eq. (A.6) becomes:

$$\frac{\partial(\rho h_o)}{\partial t} + \frac{\partial(\rho U_j h_o)}{\partial x_j} = \frac{\partial P}{\partial t} + \frac{\partial}{\partial x_j}\left(\frac{k}{c_p}\frac{\partial h_o}{\partial x_j} - \overline{\rho u_j h'}\right) - \frac{\partial}{\partial x_j}\left(U_i\left[\mu\left(\frac{\partial U_i}{\partial x_j} + \frac{\partial U_j}{\partial x_i}\right) - \overline{\rho u_i u_j}\right]\right) + S_h \tag{A.8}$$

where:

k is the thermal conductivity.

c_p, the specific heat at constant pressure.

h' is the fluctuating static enthalpy.

$-\overline{\rho u_j h'}$ is the turbulent or Reynolds flux.

This equation expresses the conservation of the total energy (i.e. the thermal energy plus the mechanical energy). It is valid for all flow situations, but the user should limit it for high speed flows.

Equation of State

An *equation of state* is a constitutive equation which provides a mathematical relationship between thermodynamic state variables for a given material. With the mass, momentum, and energy equations, it completes the mathematical representation of your fluid model. The following state variables need to be defined:

1. Density, ρ
2. Dynamic viscosity, μ
3. Specific heat a constant pressure, c_p
4. Conductivity, k
5. Specific enthalpy, h (Notes: You define all of these material variables except the specific enthalpy in NX.)

These material variables can vary with temperature or pressure or both.

The flow solver uses the state variables differently depending if your fluid is a gas or a liquid.

(Note:

The flow solver differentiates between a liquid and a gas as follows:

1. If the gas constant, R_s, is defined, the fluid material is a gas.
2. If the gas constant, R_s, is *not* defined, the fluid material is a liquid.)

Equation of State for Liquids

When your fluid is a liquid, the density ρ and the specific heat cp are assumed constant. The flow solver calculates the specific enthalpy, *h*, from the energy equation Eq. (A.6), and uses the following equation to calculate the temperature T.

$$h = cpT \tag{A.9}$$

Non-Newtonian Fluids – In non-Newtonian fluids, the shear stress of the fluid is not proportional to the rate of deformation, therefore viscosity is no longer constant. An additional model is required to model viscosity, you can use one of the following models according to the behavior of the fluid:

1. Power-Law model
2. Herschel-Bulkley model
3. Carreau model

Power-Law Model

Equation (A.10) presents the fluid viscosity, μ, of a Power-Law fluid defined in NX Flow.

$$\mu = K\dot{\gamma}^{n-1}e^{T_0/T} \tag{A.10}$$

with

$$\mu_{\min} < \mu < \mu_{\max} \tag{A.11}$$

where:

K is the consistency index.

$\dot{\gamma}$ is the shear rate.

n is the power law index.

T_0 is the reference temperature.

T is the fluid temperature.

μ_{min} is the minimum viscosity limit.

μ_{max} is the maximum viscosity limit.

Herschel-Bulkley Model

Equations (A.12) and (A.13) present how the fluid viscosity, μ, of a Herschel-Bulkley fluid is modelled in NX Flow.

$$\mu = K\dot{\gamma}^{n-1} + \frac{\sigma_0}{\dot{\gamma}} \qquad \dot{\gamma} > \frac{\sigma_{\text{int}}}{\mu_0} \tag{A.12}$$

$$\mu = \mu_0 \qquad 0 < \dot{\gamma} < \frac{\sigma_{\text{int}}}{\mu_0} \tag{A.13}$$

where:

K is the consistency index.

$\dot{\gamma}$ is the shear rate.

n is the power law index.

σ_0 is the yield stress.

σ_{int} is the intersection value for which Equations 2-37 and 2-38 are equal.

μ_0 is the yield viscosity or plastic viscosity.

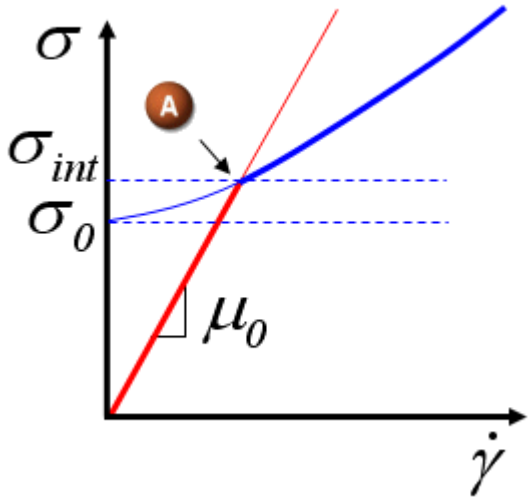

Figure A.1: Herschel-Bulkley model

To smooth convergence, a fluid define with Herschel-Bulkley model, will behave like a Newtonian fluid until the local shear stress reaches intersect, shown in Figure A.1 as a red curve. The yield viscosity, μ_0, is a mathematical artefact introduced to improve convergence of the Herschel-Bulkley model when the stress is less than the yield stress. The blue curve in Figure A.1 shows the Non-Newtonian Herschel-Bulkley behavior.

Carreau model

Equation (A.14) presents the fluid viscosity, μ, of a Carreau fluid defined in NX Flow.

$$\mu = \mu_\infty + (\mu_0 - \mu_\infty)\left[1 + \left(\lambda\dot{\gamma}e^{T_0/T}\right)^2\right]^{\left(\frac{n-1}{2}\right)} \tag{A.14}$$

where:

λ is the time constant.

$\dot{\gamma}$ is the shear rate.

n is the power law index.

T_0 is the reference temperature.

T is the fluid temperature.

μ_∞ is the infinite-shear viscosity.

μ_0 is the zero-shear viscosity.

ASSUMPTIONS

The derivation of the near-wall relations for turbulent flows mentioned in Section Ideal gas law depends on several assumptions presented in this section. We will assume that the flow close to the wall is in the x direction.

Fully developed flow. This means that all streamwise derivatives vanish, i.e. $\frac{\partial()}{\partial x} = 0$, and that the flow is parallel to the wall.

Constant shear layer flow. This is equivalent to requiring that there is no pressure gradient or other momentum source term.

$$-\overline{\rho u' v'} = \tau_w \tag{A.15}$$

Boussinesq or eddy viscosity assumption. This states that the Reynolds stress can be expressed as the product of an effective eddy viscosity and the mean flow strain rate.

Combining the Boussinesq approximation to Eq. (A.15) above gives

$$\tau_w = \mu_t \frac{dU}{dy} \tag{A.16}$$

Prandtl mixing length hypothesis. Prandtl argued that the eddy viscosity could be expressed as the product of a turbulence length, l_t, and a velocity scale, V_t, i.e.

$$\mu_t = \rho V_t l_t \tag{A.17}$$

and that

$$l_t = \kappa y \tag{A.18}$$

$$V_t = l_t \frac{dU}{dy} \tag{A.19}$$

where κ is the von Karman constant. Combining Eqs. (A.17) to (A.19) gives

$$\mu_t = \rho \kappa^2 y^2 \frac{dU}{dy} \tag{A.20}$$

Substituting Eq.(A.20) into (A.16) yields

$$\tau_w = \rho \kappa^2 y^2 \left(\frac{dU}{dy}\right)^2 \tag{A.21}$$

Rearranging gives

$$\frac{dU}{dy} = \left(\frac{\tau_w}{\rho}\right)^{1/2} \frac{1}{\kappa y} \tag{A.22}$$

The integration of Eq. (A.22) yields the famous log-law. However, before that, several other useful relations can be found.

Substituting Eq. (A.22) into (A.20) gives

$$\mu_t = \rho \kappa y \left(\frac{\tau_w}{\rho}\right)^{1/2} \tag{A.23}$$

The production of turbulence kinetic energy, k, is

$$P_k = \tau_w \frac{dU}{dy} \tag{A.24}$$

So using Eq. (A.22) again

$$P_k = \rho \left(\frac{\tau_w}{\rho}\right)^{3/2} \frac{1}{\kappa y} \tag{A.25}$$

Local equilibrium assumption. In a turbulent boundary layer satisfying assumptions (A.15 to (A.18), the largest terms in the turbulence kinetic energy equation are the production and dissipation terms, which tend to be of similar magnitude, but of opposite sign. So a further assumption is made that production equals dissipation

$$P_k = \rho\varepsilon \tag{A.26}$$

so that

$$\varepsilon = \left(\frac{\tau_w}{\rho}\right)^{3/2} \frac{1}{\kappa y} \tag{A.27}$$

Launder and Spalding's eddy viscosity. In the k-ε model, it is assumed that

$$\mu_t = C_\mu k^2 / \varepsilon \tag{A.28}$$

where C_μ is a constant. This is a general expression for μ_t valid everywhere, including in the near-wall region. Equating Eqs. (A.28) and (A.23) gives

$$\rho C_\mu \frac{k^2}{\varepsilon} = \rho k y \left(\frac{\tau_w}{\rho}\right)^{1/2} \tag{A.29}$$

Substitute Eq.(A.27) for ε and simplify

$$k = \frac{1}{C_\mu^{1/2}} \left(\frac{\tau_w}{\rho} \right) \tag{A.30}$$

Note that the equations for μt, P_k, ε and k (Eqs. (A.23), (A.25), (A.27) and (A.30) respectively) were all derived without recourse to the log-law, they do not involve any unresolved velocity scales and they are all explicit in terms of τ/ρ. The actual logarithmic relation follows from Eq. (A.20). Integrating it gives

$$U = \left(\frac{\tau_w}{\rho} \right)^{1/2} \frac{1}{\kappa} \log \left(\frac{y}{y^*} E \right) \tag{A.31}$$

where y^* is a length scale and E is a dimensionless constant (E/y^* is the constant of integration). This can be rearranged to

$$\tau_w = \frac{\rho U^2}{\left(\frac{1}{\kappa} \log(y^+ E) \right)^2} \tag{A.32}$$

where

$$y^+ = \frac{y}{y^*} = y \frac{\rho}{\mu} u^* \tag{A.33}$$

so that a velocity scale, u^*, is used instead of the length scale.

Once a velocity scale is selected, the constants K and E in Eq. (A.32) can be matched with experimental data. Traditionally, and quite reasonably, the choice for the velocity scale has been

$$u_* = \left(\frac{\tau_w}{\rho} \right)^{\frac{1}{2}} \tag{A.34}$$

With this value, constants of K = 0.41 and E = 8.43 correlate well to a range of boundary layer flows for smooth walls, usually to the degree that the assumptions (A.15) to (A.20) hold. In other words, if velocity measurements, U, where made for a large number of flows, then the dimensionless velocity u +/- = u/u* would approximately follow the same logarithmic prole:

$$u^+ \equiv \frac{U}{u^*} \approx \frac{1}{\kappa} \log (y^+ E) \tag{A.35}$$

These relations can be used to compute a wall shear without resolving the details of the near-wall region. The algorithm proceeds by taking a near-wall velocity (computed from the Finite Volume equations for the conservation of momentum) and then solving for the other dependent variables.

Further Considerations for the k-ε Model

The near wall velocity gradient can be written as:

$$\frac{dU}{dy} = \frac{\tau_w}{\mu} \frac{du^+}{dy^+} \tag{A.36}$$

which, using Equation (A.34) becomes

$$\frac{dU}{dy} = \frac{\tau_w}{\mu} \frac{1}{\kappa y^+} \tag{A.37}$$

The near wall production used in the k-ε is obtained by combining Equations (A.25) and (A.37), which gives

$$P_k = \frac{\tau_w^2}{\mu}\frac{1}{\kappa y^+} \tag{A.38}$$

The definition for the velocity scale u^* given by Eq. (A.34) is not suitable for regions of flow separation, reattachment and stagnation points where $\tau\omega$ goes to zero. For the k-ε model, an alternative is to make use of (A.30) as follows:

$$u^* = \left(\frac{\tau_w}{\rho}\right)^{1/2} = C_\mu^{1/4} k^{1/2} \tag{A.39}$$

From Eq. (A.37) and (A.38), combined with the assumption of equilibrium (Eq. A.25), the near wall dissipation is given by

$$\varepsilon = \frac{\rho C_\mu k^2}{\mu}\frac{1}{\kappa y^+ f_\varepsilon} \tag{A.40}$$

The factor f is a damping factor used to model the influence of the wall on the dissipation level. It is defined as:

$$f_\varepsilon = 1 - \exp\left(-\frac{y^+}{3.8 C_\mu^{1/4}}\right) \tag{A.41}$$

This influence of f on the near wall dissipation is significant only if the near wall node is at $y+<5$.

APPENDIX B

Manufacturer Specifications

Table 1: Common Rechargeable Batteries Specifications

Types	Nickel-metal Hydride (NiMH)	Sealed Lead-acid (SLA)	Lithium-ion (Li-ion)	Nickel-cadium (NiCd)	Lithium-ion Polymer (LiPo)
specific energy (W·h/kg)	60 – 120	30 – 40	100 – 250	40 – 60	130 – 200
energy density (W·h/L)	140 – 300	60 – 75	250 – 620	50 – 150	300
specific power (W/kg)	250 – 1000	180	250 – 340	150	>3000
Charge/discharge efficiency (%)	66	50 – 92	80 – 90	70 – 90	99.8
Energy/consumer-price (W·h/USD)	2.75	**7 – 18**	2.5	~2 – ~3	2.8 – 5
Self-discharge rate (%/month)	30	3 – 20	8 – 31	10	5
Cycle durability (cycles)	500 – 1000	500 – 800	400 – 1200	2000	500 – 1000
Nominal cell voltage (V)	1.2	2.105	3.6/3.7	1.2	3.7
Life (years)	n/a	**5 – 8**	2 – 3	n/a	2 – 3

Table 2: Manufacturer DC brushless 800 W motor specification

Model	Voltage	No-Load		Rated Parameters			Peak Torque	Weight	Length	Efficiency
		RPM	Current	RPM	Torque	Current				
	VDC	rpm	A	rpm	N.m	A	N.m	Kg	mm	%
90BLDC090	48	2860	1.4	2500	3.0	15.6	7	5.0	141	>85

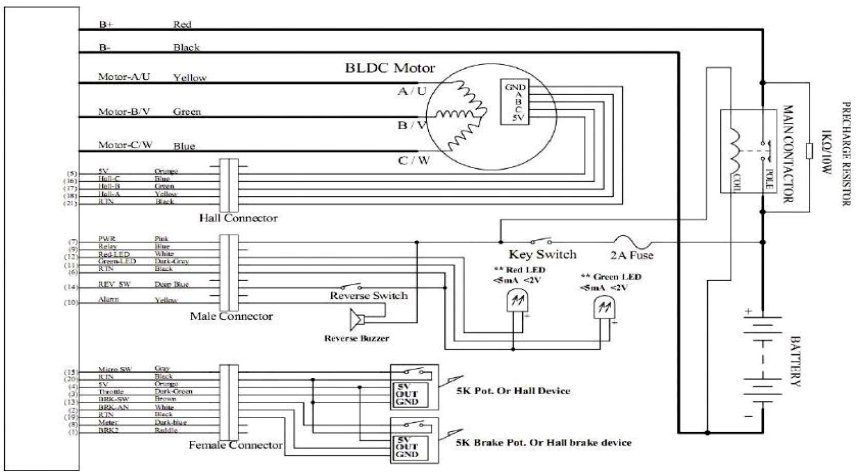

Figure 1: BLDC motor and controller wiring schematic